Study of Gas Bubbles Stabilized by Surfactants for Use as Ultrasound Contrast Agents and Drug Carriers

A Thesis

Submitted to the Faculty

of

Drexel University

by

Boriphat Methachan

in partial fulfillment of the

requirements for the degree of

Doctor of Philosophy

June 2012

Acknowledgments

First, I would like to thank Dr. Wheatley for her advice, guidance, and support. I cannot imagine how I could have finished this thesis without her understanding and encouragement.

I also would like to thank my committee members: Dr. Fred Allen, Dr. Frank Ferrone, Dr. Uri Hershberg, and Dr. Yinghui Zhoung for taking their time to review my thesis.

For *in vivo* tumor perfusion study, I would like to thank University of Pennsylvania team: Dr. Sydney Evans, Dr. Cameron Koch, Dr. Chandra Sehgal, Susan Schultz, and Lee Shuman. The team's effort contributed greatly to the success of experiment providing important insights and understanding.

I also would like to thank my colleagues at Drexel University for their help, feedback, and suggestions. Many thanks to my past and present lab members: Odelia Mualem Burstein, Seunglee Kwon, Kelleny Oum, Carl Solise, John Eisenbrey, Nicola Francis, Michael Cochran, Nutte Tarn Teraphongphom, and Reva Street. Also, special thanks to Lauren Jablonoski for her help with SEM.

Finally, I would like to thank my family and friends for their patient and enduring support, and especially Dr. Richard Waters for his work on this manuscript.

Table of Contents

List of Tables

List of Figures

Abstract

Study of Gas Bubbles Stabilized by Surfactants for Use as
Ultrasound Contrast Agents and Drug Carriers

Boriphat Methachan
Margaret A. Wheatley, PhD

It has been well established that the vasculature in a tumor is more 'leaky' than that in normal tissue. The cutoff pore size is in the range of 380 and 780 nm depending on the tumor model and stage. It would be useful to fabricate an ultrasound contrast agent (UCA) that is smaller than the cut off pore size of a tumor allowing it to flow into the tumor. This would facilitate better perfusion yielding better tumor imaging and lead to a new and more effective way to deliver the chemotherapeutic drug for cancer treatment,.

One of UCAs fabricated our lab was gas bubbles stabilized by surfactants. Specifically, perfluorocarbon (PFC) gas bubbles have been stabilized by the mixture of two surfactants. Two surfactant stabilized agents were developed: 1) a PFC gas bubble contrast agent, ST68, stabilized with Span60 and Tween 80 with a mean diameter of 1.88±0.16 μm and 2) SE61, with a Span60, d-α tocopheryl polyethylene glycol 1000 succinate, or TPGS shell and comprised of gas bubbles with a mean diameter of 1.31±0.20 μm. These agents provided 20-30 dB ultrasound enhancements and the stability was dependent on the particle size that stabilized the bubbles.

A new model was proposed to explain a previously unexplained observation, i.e., the fact that only combinations of solid Span with Tween (a liquid) can form microbubbles, liquid Spans do not. Various studies were conducted which indicate that the bubbles stabilized by solid particles is a realistic possibility. These included the

behaviors of the bubbles as they dried, the fact that larger Span particles produced more robust bubbles and preliminary scanning electron microscopic evidence.

A substantial number of nanobubbles were fabricated for SE61 compared with ST68. These nanobubbles still retained good echogenicity, but they were less stable (1.75±0.24 min) as compared to the microbubble (16.45±1.56 min).

ST68 with a bubble diameter ranging from 955 nm to 2.67 μm and SE61 with bubble sizes ranging from 342 nm to 900 nm were used to see if the smaller sized bubbles would yield better ultrasound imaging for tumor perfusion deeper into the tumor bed. Power-Doppler ultrasound imaging was used *in vivo* to analyze the tumor perfusion for both agents in an animal (rat) study. Tumor coverage and time were plotted and analyzed by comparing parameters in wash-in and wash-out phases. The results showed that both agents gave good tumor coverage. However, SE61 provided better perfusion imaging than ST68 and took longer to clear out of the tumor. It should be noted that Delta-projection is better in portraying the vasculature of the tumor as compared to Power-Doppler.

By using Nile Red, a hydrophobic fluorescent solvatochromic probe, we showed that a hydrophobic drug could intercalate into the hydrophobic portion of the surfactants in the bubble shell to make drug delivery possible. The subsequent experiments showed that Paclitaxel, a promising anti-tumor agent with poor water solubility, intercalated into the bubbles at the concentration around 3.8 μg/ml. This concentration was close to 100 times higher than the suggested effective concentration from other studies.

1. INTRODUCTION

Cancer is caused by uncontrolled growth and spreading of abnormal cells, and if the spread is not controlled, it can result in death. A total of 577,190 Americans are expected to die of cancer and about 1,638,910 new cancer cases will be diagnosed in 2012. [1] The estimation of overall costs of cancer by The National Institutes of Health was $228.1 billions in 2008. Cancer killed 7.6 million people around the world in 2008 and the number is expected to rise to 17.5 million by 2050. Available treatments are surgery, radiotherapy, chemotherapy, hormone therapy, and immunotherapy. [2] For the most effective result, early and precise detection are the most important factors.

The long term-goal of this study is to develop a surfactant-stabilized diagnostic ultrasound contrast agents that can also act as a targeted drug carrier for cancer therapy. The advantage of this combination makes it possible for real time diagnostic imaging and ultrasound-triggered drug release. As a function of the focused ultrasound, not only specific site imaging can be performed but also the drug can be delivered directly to the cancer cells to improve drug dosage compared with systemic administration. The result of this will be to reduce drug toxicity and undesired side effects that are caused by a typical treatment, thereby measurably improving the efficacy of treatment and the quality of life for the cancer patient.

There are four specific aims for this study.

Specific Aim 1: Development and testing of a new model to elucidate the mechanism of stabilization of the gas bubbles by the surfactants.

Previously, a mixed surfactants model had been proposed for the structure of the agent shell. [3] This model, however, cannot adequately explain why the microbubbles can be stabilized, neither can stability be inspection of the Hydrophilic-Lipophilic Balance (HLB) of the constituent molecules. From this study, it was noticed that stability only occur when mixing at least one solid surfactant with another surfactant. The hypothesis of the particle-stabilized foams will be examined in order to explain this unresolved question. The key parameters that play an important role in the surfactant-stabilized gas bubbles, were determined. The results were analyzed to test for a fit with the suggestion that the bubbles are stabilized in accordance with the "particle-stabilized foams" theory. The importance of the correct model will be useful for further study and expanding the therapeutic applications of the surfactant-stabilized gas bubbles.

Specific Aim 2: Investigate the method for increasing the proportion of the nano-sized bubble component relative to population created using the standard method.

The difference between blood vessels that develop to supply a tumor and normal physiological vessels is the tendency to be 'leaky'. These gaps in the vessel walls have been reported between 380 and 780 nm depending on the tumor model and stage. However, the previous study in our lab for the surfactant- based contrast agents mostly dealt with microbubbles. [3-8] The nanobubbles were fabricated in conjunction with the microbubbles and were then separated by buoyancy and characterized. [9, 10] In this specific aim, the method of increasing the proportion of nano-sized contrast agent was investigated with a view to elucidating the contribution of each component, and use of a

new surfactant combination which may lead to a method of increasing the proportion of the nano component.

Specific Aim 3: *In-vivo* tumor perfusion study comparing the agents with different nanobubble populations.

With success in fabricating agent with increased nano-sized bubble population, the agents were tested *in vivo* to see if the agent that consisted of smaller bubbles would be better in ultrasound imaging and tumor perfusion. Our hypothesis is the smaller bubbles will provide better tumor perfusion. In this specific aim, the two agents that have different size distributions were compared with respect to the tumor perfusion imaging in two modes of ultrasound imaging: Power Doppler and B-mode for Δ-projection. The tumor perfusion was calculated from the percentage area of flow plot and a first-pass kinetics gamma-variate function was used to calculate the perfusion ratio.

Specific Aim 4: Develop a method to intercalate a hydrophobic drug into the agents.

Because the long-term goal of this study is using the UCA as a drug carrier for ultrasound triggered drug release, the studies in this specific aim were tested to see if it was possible to load drugs into the bubble shell. The hydrophobic dye, Nile Red, was used as a hydrophobic drug model. The hypothesis is that the hydrophobic portions of the amphipathic molecules that make up the shell of the agents could be sites to intercalate a hydrophobic drug. The success in loading Nile Red led to testing the loading of Paclitaxel. The drug-loaded agents were tested for their echogenicity and the amount

of Paclitaxel loading was measured. The success of the Paclitaxel loading portends the possibility of drug delivery using surfactant stabilized bubbles as drug carriers.

2. BACKGROUND AND LITERATURE REVIEW

In this chapter the background of this study will be discussed in conjunction with a review of the literature which bears on key components of the study. These components include ultrasound, ultrasound contrast agents, foam and bubble stability, and ultrasound used in drug delivery.

2.1 Ultrasound

Ultrasound is simply sound waves that are comprised of waves of compression and decompression passing through a medium (e.g. air or water), traveling at a fixed velocity. The frequencies of diagnostic ultrasound are in the range of 1 - 15 MHz. The diagnostic applications of ultrasound imaging have been expanding and offer many advantages over other imaging modalities. These advantages include safety, portability, acquisition of real time images, and relatively low cost.

Ultrasound imaging works by a transducer transmitting acoustic waves through a body. Some of the waves reflect back to the transducer due to differences in acoustic impedance. Images are then generated from the reflected waves. The acoustic impedance (z) depends on density of the medium (ρ) and the speed of sound in the medium (c). The acoustic impedance can be defined as: [11]

$$z = \rho \times c \qquad \text{Eq 2.1}$$

The reflection occurs when an ultrasound wave passes from one medium to a second medium. A reflection coefficient (R) is a measure of the degree of reflection,

which R = 1 denotes 100% wave reflection, while R = 0 denotes 100% transmission of the wave. The reflection coefficient R equals: [11]

$$R = \frac{Z_2 - Z_1}{Z_2 + Z_1} \qquad \text{Eq 2.2}$$

There are several modes of ultrasound imaging. Some of these modes are:

A-mode: A-mode (amplitude mode) is the simplest mode. It is an amplitude modulation scan that gives the information in a one dimensional form. A single transducer scans a line through the body with the reflections plotted on screen as a function of depth.

B-mode: B-mode (brightness mode) or grey scale is when a linear array of transducers simultaneously scan a plane through the body that can be viewed as a two-dimensional image on screen.

Doppler mode: The image of this mode can be constructed by means of the Doppler Effect in measuring and visualizing blood flow.

Harmonic mode: In this mode, a fundamental frequency is emitted and a harmonic overtone is detected to improve resolution.

2.2 Ultrasound Contrast Agents

The ultrasound technique is limited in its ability to distinguish between diseased and normal tissue. It is similarly limited in distinguishing between two soft tissue boundaries. However, with the utilization of contrast agents such soft tissue boundaries as the myocardium and tumors can be distinguished. [12]

Ultrasound contrast agents are used to enhance the backscattered signal, improving resolution. In general, contrast agents are comprised of stabilized gas bubbles.

There are several micron-range contrast agents both in clinical use and in development Table 2.1 shows some examples of microbubble contrast agents. [13, 14]

Table 2.1 Microbubble contrast agents

Name	Shell	Gas
Albunex	Albumin	Air
Definity	Lipid/surfactant	Octafluoropropane
Echovist	Galactose	Air
Echogen	Sucrose	Dodecafluoropentane
Imagent	Lipid/surfactant	Perfluorohexane/nitrogen
Levovist	Galactose	Air
Optison	Albumin	Octafluoropropane
Sonazoid	Lipid/surfactant	Perfluorobutane
Sonovue	Lipid	Sulfur hexafluoride

Due to the high acoustic impedance mismatch between gases and blood or soft tissue, the acoustic backscatter of microbubbles is greater than the backscatter of blood and the majority of other tissues and organs. This property makes microbubbles useful as contrast agents for ultrasound imaging.

Stabilized gas bubbles based on surfactant-shells have been developed. [3, 4] These gas bubbles are meeting with essential clinical requirements, which are that they are non toxic, biocompatible, less than 8 μm in diameter in order to traverse the capillaries in the pulmonary bed, and stable enough to perfuse the tissue and last the duration of imaging. [15] A mixture of two non-ionic surfactants, Span and Tween, was used to stabilize gas bubbles. Both surfactants are fatty acid esters of sorbitan, which have a hydrophobic tail group, for example monolaurate (C11: Span 20 and Tween 20), monopalmitate (C15: Span 40 and Tween 40), monostearate (C17: Span 60 and Tween 60), and monooleate (C17: Span 80 and Tween 80). All chains are fully saturated except for the oleate chains which contain a single cis-double-bond. The difference between Tween and Span is that Tween has the hydrophilic sorbitan head group modified with polyethyleneoxide groups (Figure 2.1) and this greatly increases the polarity that makes the molecule more water-soluble. It should be noted that the stable microbubbles are successful only in the combination between solid Span (Span 40 and Span 60) and almost all types of Tween. The trioleate series of Span 85 and Tween 85 do not stabilize bubbles in any combination, which is not unexpected since the three oleate fatty acid chains that they possess are extremely bulky (Table 2.2). [4] Also, different combinations of surfactant and different gases affect the backscatter from the microbubbles. [6]

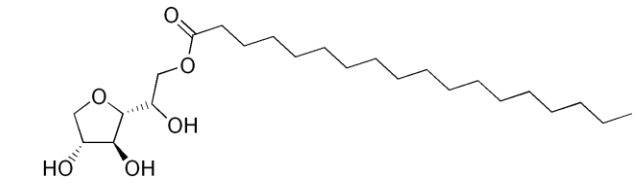

(a)

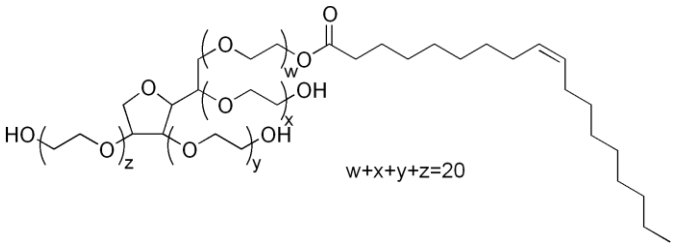

(b)

Figure 2.1 Molecular structure of Span 60 (a) and Tween 80 (b) [6]

Table 2.2 The stability of microbubbles, which were stabilized with different combination of Span and Tween [6]

	Span60 (solid) 4.7[a]	Span40 (solid) 6.7	Span20 (liquid) 8.6	Span80 (liquid) 4.3	Span85 (liquid) 1.8
Tween20 (liquid) 16.7[a]	Y	Y	N	N	N
Tween40 (liquid) 15.6	Y	Y	N	N	N
Tween60 (liquid) 14.9	Y	Y	N	N	N
Tween65 (solid) 10.5	Y	Y	N	N	N
Tween80 (liquid) 15.0	Y	Y	N	N	N
Tween85 (liquid) 11.0	N	N	N	N	N

Y: microbubbles were formed, N: microbubbles were not formed.
[a] HLB values.

The previous model for microbubbles stabilized by Span 60 and Tween 80 is shown in Figure 2.2 [3, 4], and was developed using a Langmuir trough. The model suggested that the stability of the bubble is due to the fact that the bulky head of Tween is stabilized by the presence of Span in the shell which causes the reduction of the repulsive force in Tween molecules by hydrophobic attraction between the tail groups. This model, however, cannot explain why the microbubbles are stable only with solid Span. One explanation proposed in this work could be the additional stability due to the presence of nano-sized particles of Span. Understanding particle-stabilized foams might help us to understand the stability of these particular contrast agent microbubbles.

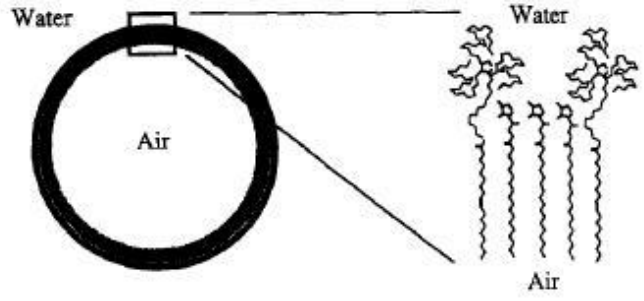

Figure 2.2 The previous proposed model for microbubbles stabilized by Span 60 and Tween 80 [6]

2.3 Foam and Bubble Stability

Foams can be considered thermodynamically unstable. However, kinetic mechanisms involved with breakdown can be so slow that the foams can be thought of as having metastability. Depending on the system, some foam can breakdown within an hour but in some case, the foams have been stable for more than 3 weeks. [16-24] The primary processes for instability in foams are drainage and coalescence. [25] Water

drainage is most significant in foam stability. This is caused by gravity-induced movement due to the density differences between gas and water. Coalescence comes about by the binding of two or more foam bubbles, where the interfacial film drains and is eventually ruptured forming a single larger bubble.

Another important form of foam instability is disproportionation. This is a process that occurs when the gas molecules diffuse between bubbles. The diffusion flux generally results in the growth of larger gas bubbles and the shrinking of the smaller bubbles due to the increasing of Laplace pressure of the smaller bubbles. [26, 27] The Laplace pressure is a pressure difference between inside and outside the bubble and can be calculated by:

$$\Delta P = P_{inside} - P_{outside} = \frac{2\gamma}{R} \qquad \text{Eq 2.3}$$

where γ is the surface tension and R is the bubble radius.

It is normally necessary to add some component to help stabilize foams. In air-water system, foaming agents are required to first produce the conditions that will create foams and also stabilize them. Without the foaming agent, 'clean' air bubbles passed through water will burst immediately on drainage of water in a thin film [28]. The foaming agents can be surfactants, polymers or larger proteins. Surfactants adsorbed to an air-water interface stabilize foam by reducing the free energy involved with producing a high surface area, resulting in reduced interfacial surface tension. Polymers and proteins facilitate stability largely through electric and steric repulsion. [25]

2.4 Particles-stabilized Foams

There is a theory that attempts to explain how particles can act as surfactants in stabilizing foams and emulsions, labeled "particle-stabilized foam" theory. [25, 29, 30] The solid particles can function in the same ways as surfactants but some behaviors are different. For example, particles do not always assemble the same way that surfactant molecules do when they form micelles, and, hence the solubilization phenomena (i.e. the ability of dilute surfactant solutions to solubilized water-insoluble substances to form stable systems [31]) is absent in the particle case. When the spherical particles adsorb to interfaces (Figure 2.3), the contact angle θ which the particle makes with the interface is important. [29] For hydrophilic particle, the contact angle measured into the aqueous phase is normally less than 90^o and the larger fraction of the particle resides in the water. By analogy with surfactants, the monolayer will curve to make the larger area of the particle surface remain on the external side, giving rise to air or oil-in-water emulsions for $\theta<90^o$. There will be an opposite effects for hydrophobic particles, which are suitable for water-in-air or water-in-oil emulsions with a contact angle which is greater than 90^o. Our system involves oil (PFC) in water emulsion, and would therefore suggest the presence of hydrophilic particles, which is not the case with Span. An alternative situation must therefore exist.

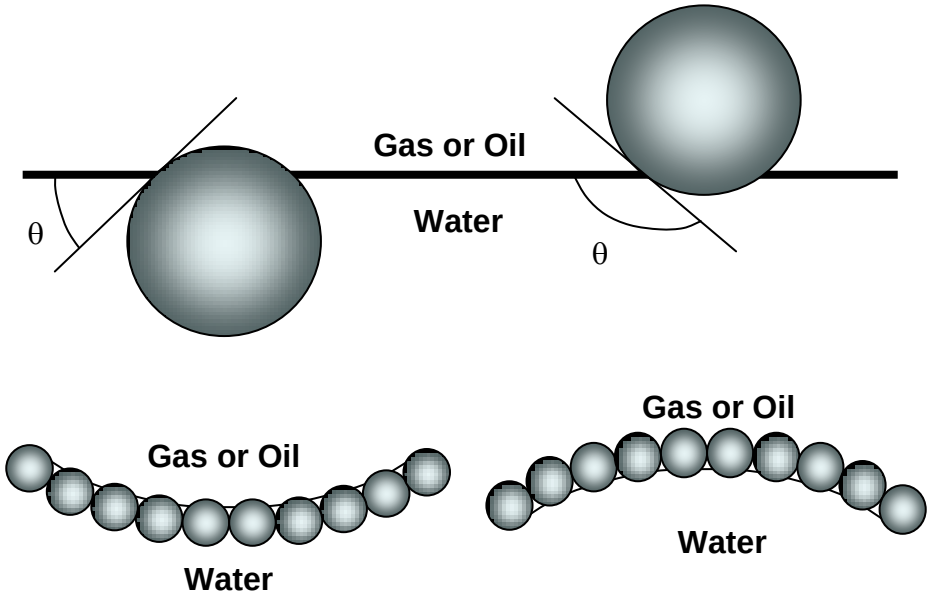

Figure 2.3 Position of a small spherical particle at the interface for a contact angle (measure through the aqueous phase) less than 90^o (left), solid-stabilized aqueous foam or o/w emulsions may form. For $\theta > 90^o$ (right), solid –stabilized aerosols or w/o emulsions may form. (Adapted from [29])

The physical reason for the better efficiency of particles over surfactants in stabilizing foams is their attachment energy which can be up to several thousand *kT* per particle, where *k* is the Boltzmann constant and *T* is the absolute temperature, compared to only a few *kT* per surfactant molecule. [32] Because of this high energy attachment at the interface, the particle adsorption can be considered as irreversible. [33] The required energy to remove the particle from its equilibrium position at the interface to the bulk liquid phases is [34]

$$\Delta G_{remove} = \pi r^2 \sigma (1 \pm \cos\theta)^2 \qquad \text{Eq 2.4}$$

where *r* is the radius of the spherical solid particle; σ is the interfacial energy; θ is the

contact angle; sign'+' refers to particle removal into gas phase, while sign '-' refers to the removal into the liquid phase. Equation 2.4, however, does not say anything about the stability of the thin liquid layer between bubbles which are stabilized by particles. To answer this question, the maximum capillary pressure was introduced and can be calculated from [34]

$$P_c^{\max} = p\frac{2\sigma}{R}(\cos\theta + z) \qquad \text{Eq 2.5}$$

where p and z are the parameters for different particle arrangements, which are shown in Figure 2.4 [34]. For example in the case of a close-packed bilayer, if $\theta<90^o$, p = 4.27 and z = 0.405 but for $90^o \leq \theta < 129.3^o$, p = 2.73 and z = 0.633. With equation 2.4 and 2.5, Kaptay can make the calculations that agree with the experimentally observed optimum contact angle interval. [34]

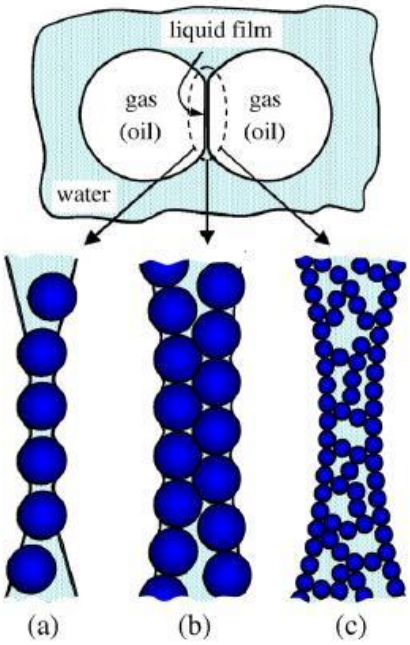

Figure 2.4 Possible mechanisms of liquid film stabilized by: (a) a monolayer of particles; (b) a bilayer of close-packed particles and (c) a network of particle aggregated inside the film. [35]

Another approach to particle-stabilized foams is by changing the hydrophilicity and wetting properties of the solid particles so as to favor their attachment at the gas-liquid interface. One possibility is mixing the colloid particles with amphiphilic molecules or surfactant. [30] This scenario should fit well in our study using the hydrophobic particles of Span mixed with Tween. The model and picture of this type of the system are shown in Figure 2.5 and 2.6.

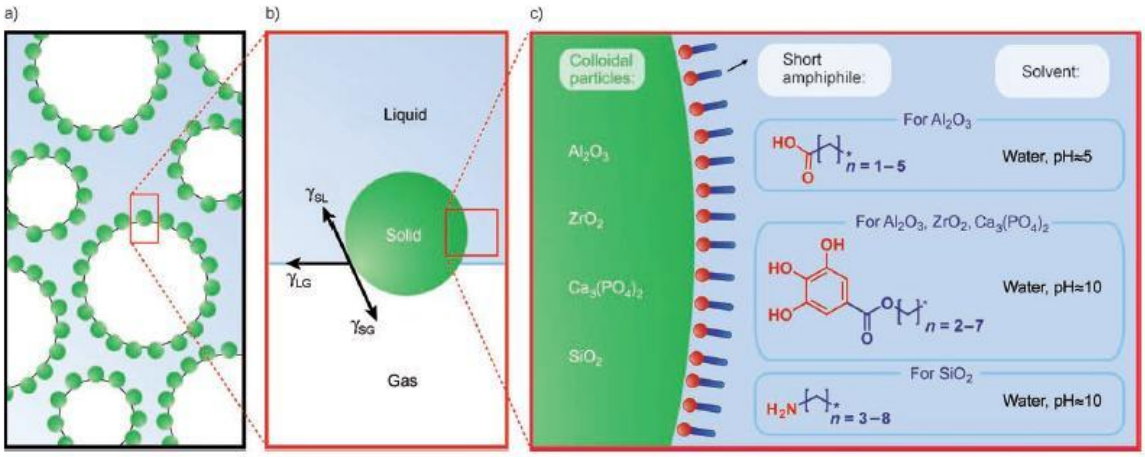

Figure 2.5 Possible approaches to attach colloidal particles at gas–liquid interfaces by tuning their surface-wetting properties. a) Schematic illustration of the stabilization of gas bubbles with colloidal particles (the particle size is exaggerated for clarity). b) The adsorption of partially lyophobic particles at the gas–liquid interface, c) The approaches used to tune the wetting properties of originally hydrophilic particles to illustrate the universality of the foaming method developed. The same principles can be easily extended to other types of particles, by using different surface modifiers as well as liquid and gaseous phases. [30]

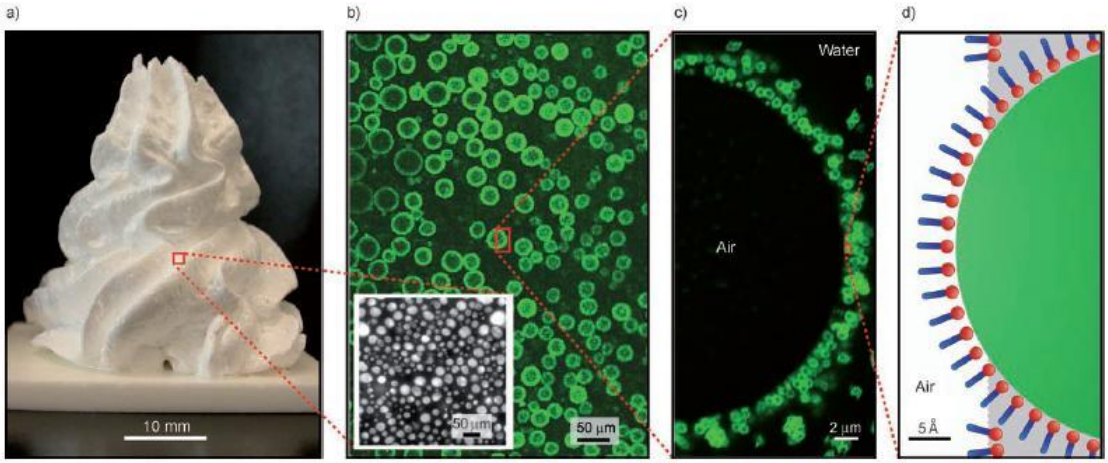

Figure 2.6 Hierarchical features of the particle-stabilized foams containing short amphiphilic molecules. High-volume macroscopic foams (a) with bubble sizes within the range 10–50 mm (b) are formed through the adsorption of submicrometer-sized colloidal particles at the air–liquid interface (c). Particles attach at the air–water interface as a result of the surface hydrophobicity imparted by the adsorbed amphiphilic molecules, as indicated schematically in (d). The confocal images shown in (b) and (c) were obtained after dilution of concentrated foams (inset in b) containing fluorescently labeled silica particles and hexylamine as amphiphile. [30]

2.5 Ultrasound and Drug Delivery

The goal of controlled drug delivery is to improve the efficiency of drug treatment in the region of the disease and reducing undesirable side effects in the healthy tissues. For this reason, many studies are investigating the application of an external trigger to locally release drugs. Ultrasound waves have advantages as a controlling field for drug delivery since they can be focused at a given site.

Ultrasound is widely applied in medicine and allows easy focusing and penetration deep into the body. There is some discussion that the effect of ultrasound alone has been shown to increase cell membrane permeability. [36] The presence of ultrasound energy provides highly efficient ways of perturbing cell membranes and increasing their permeability. With the added ability of microbubbles to act as cavitation nuclei, the subsequent bubble collapse increases cell membrane permeability, and the net result is that the use of microbubbles with ultrasound has a significant additive effect.

[36] Normally, pharmaceutical drug carrier particles are too large to cross the endothelial layer and escape from the blood stream. The destruction of microbubbles has been shown to increase vessel permeability and create conditions to help overcome the endothelial lining barrier in the targeted tissue. [37] However, there is some size limitation for the drug carrier to release into specific targeting sites. The nano-sized bubbles, therefore, will be produced to overcome this limitation.

New vasculature is needed to supply the rapidly dividing cells of a tumor with nutrients during tumor development, and the growth process for new vessels is known as angiogenesis. [38] One consistent difference between tumor blood vessels and normal physiological vessels is the tendency to be 'leaky'. [39] It has been reported that the pore cutoff size of several tumor models rages between 380 and 780 nm [40, 41], but some studies suggested the pore cutoff size lies around 400 nm. [42] Therefore, if we want the carriers to exit the blood stream, it is important to develop drug carriers that are smaller than these suggested pore cutoff sizes. Nanoparticles can deliver anti-cancer drugs through these pores by targeting specific cancer tissue or cells, while protecting the drug from inactivation during transport.

There are extensive studies on polymeric drug-loaded nanoparticles. [43] One study shows that combining ultrasound with nanoparticles increasing drug susceptibility of cancer cells. [44] A mixture of nanoparticles stabilized by biodegradable block copolymers and their micelles as drug-loaded carriers for ultrasound targeted chemotherapy has been achieved. [45] The main idea is that the micelles and nanobubbles can go through defective endothelial gaps to the tumor and coalescence into larger, highly echogenic microbubbles in the tumor tissue. With the tumor-directed

ultrasound, the microbubbles cavitate and collapse resulting in a release of the drug and enhanced intracellular drug uptake by the tumor cells. This system, however, has some disadvantages. It is suggested that the bubbles are getting irreversibly bigger when heated to the physiological temperature (i.e. 37°C) because the vaporization of Perfluoropentane which they contain. [45]

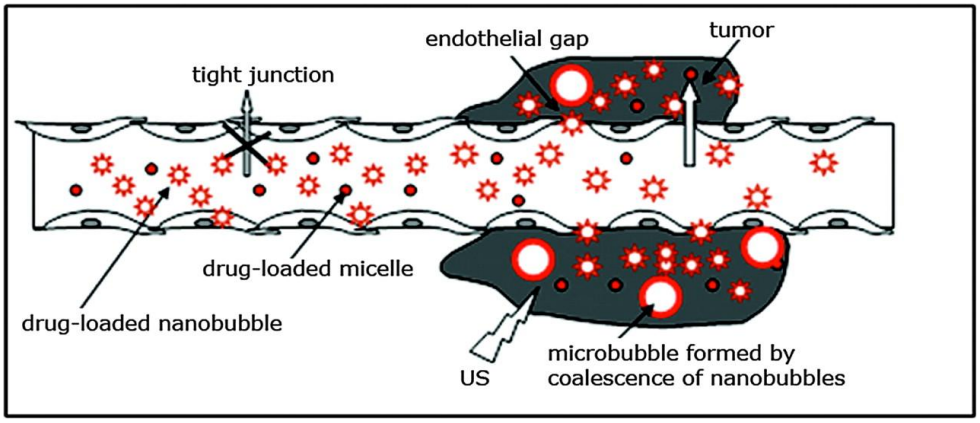

Figure 2.7 Schematic representation of a drug targeting though the defective tumor microvasculature using an echogenic drug delivery system. The system consists of polymeric micells (small circle, nanobubbles (stars) and microbubbles (large circles). [45]

2.6 Nile Red

A hydrophobic dye, Nile Red, (molecular weight MW: 318.375) is a popular fluorescent probe in biological and medical research used to localize and quantify lipids, to stain proteins, and to detect ligand-binding to enzymes. It is also used as a florescent dye probe for the study of micelles. [46-48] Nile Red has fluorescence that is strongly dependent on the polarity of its environment. [49] In DMSO, Nile red has Abs/Em = 552/636 nm. In cholesterol ester droplets or hydrocarbon solvents, Nile red fluoresces yellow-gold (528 nm), while in ethanol or phosphatidylcholine vesicles, the dye fluoresces red (>610 nm). [50] In aqueous media, it is relatively insoluble and

fluorescence is strongly quenched. Chiefly because the color of the observed fluorescence is directly dependent on the hydrophobicity of the surrounding and it is highly hydrophobic, Nile Red will be chosen as a model for a highly hydrophobic drug Paclitaxel (MW = 853.9) that can intercalate into the hydrophobic shell of our contrast agent.

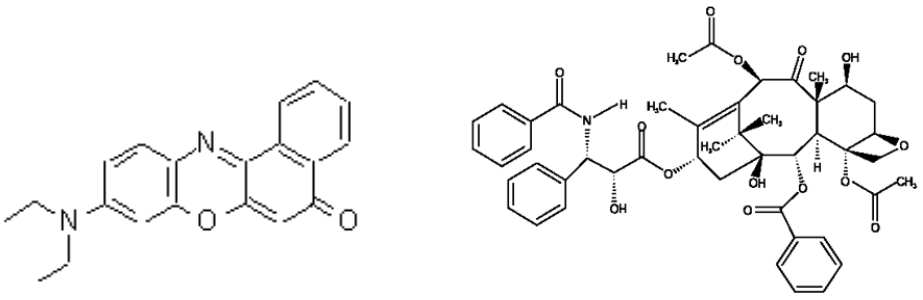

(a) (b)

Figure 2.8 Molecular structure of (a) Nile Red and (b) Paclitaxel

2.7 Paclitaxel (Taxel®)

Paclitaxel is a promising anticancer drug with special effects against a wide spectrum of cancers, including breast, ovarian, lung, colon, head and neck cancer, multiple myeloma, melanoma, and Kaposi's sarcoma. [2] It was approved by Food and Drug Administration for the treatment of ovarian cancer in 1992, advanced breast cancer in 1994 and early-stage breast cancer in 1999. Because of its highly lipophilic nature, it is insoluble in water, and this leads to one of the main limitations of Paclitaxel, is it is difficult to administer to the patient. A commercially available dosage form is the solution of Paclitaxel in Cremophor EL (polyethoxylated castor oil) and dehydrated alcohol. [2, 51, 52] Although it has been used to administer other drugs, the amount of

the Cremophor required to deliver Paclitaxel is significantly higher than those other drugs, and this leads to increased patient toxicity and can lead to hypersensitivity reactions in certain individuals. Since Paclitaxel is one of the most commercially successful anticancer drugs, it will be important to develop a better dosage form to avoid the toxic Cremophor, and this may have enormous clinical and commercial value.

There are many alternative Paclitaxel administration suggestions [52, 53] but one interesting suggestion is Paclitaxel-loaded microspheres. It has been shown that acoustically active lipospheres, the microbubbles surrounded by a shell of oil and lipid, can be used as Paclitaxel delivery vehicles. [54] Because of its highly hydrophobicity, Paclitaxel will be chosen for loading into our contrast agent.

2.8 Vitamin E TPGS (d-α-tocopheryl polyethylene glycol 1000 succinate)

TPGS is a water-soluble form of natural source vitamin E. It is very stable and does not hydrolyze under normal conditions. TPGS can be prepared by esterifying the acid group of d-alpha-tocopheryl acid succinate with polyethylene glycol 1000. The molecular structure of TPGS is shown in Figure 2.9. It can be used as an emulsifier, drug solubilizer, absorption enhancer, and as a vehicle for lipid-base drug-delivery formulations.

TPGS has found wide utility in pharmaceutical formulations including improving drug bioavailability, emulsion vehicle, reducing drug sensitivity on skin or tissues, and water-soluble source of vitamin E. There are some studies that show the possibility of PLGA nanoparticles containing vitamin E TPGS to control and release Paclitaxel. [53, 55] These studies also show that the biodegradable polymers containing TPGS give

higher Paclitaxel encapsulation efficiency. For these reason, and the structural similarity to Tween, TPGS is chosen for investigation as a possible co-surfactant in our bubbles, with the aim to produce a significant nano population through closer packing of the head groups.

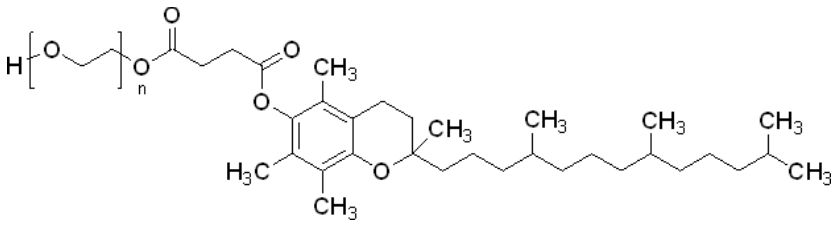

Figure 2.9 Molecular structure of d-α-tocopheryl polyethylene glycol 1000 succinate (TPGS)

3. MATERIALS AND METHODS

3.1 Materials

3.1.1 Surfactants

There are three non-ionic surfactants used in this study. Span60 (sorbitan monostearate), and Tween80 (polyoxyethylene-sorbitan monooleate) were purchased from Sigma (St. Louis, MO). Vitamin E TPGS (d-a Tocopheryl polyethylene glycol 1000 succinate) NF grade was purchased from Eastman (Kingport, TN). All surfactants were used without further purification.

3.2.2. Other Chemicals

PFC gas (octafluoropropane) was purchased from American Gas Group (Toledo, OH). Paclitaxel was purchased from LC Laboratories (Woburn, MA) and used without purification. Acetonitrile HPLC Grade and Ethyl Acetate HPLC Grade were purchased from Fisher Scientific (Fair Lawn, New Jersey). All other chemicals were purchased from Sigma-Aldrich (St. Louis, MO).

3.2 Methods

3.2.1 Microbubble Contrast Agent Fabrication

Ultrasound contrast agents were fabricated by a procedure that modified the procedure of previous studies. [9, 10] The Standard Operating Procedure (SOP) for preparing the surfactant stabilized UAC is explained in the appendix A.1 for ST68 and A.2 for SE61. Briefly, the desired amount of Span 60 with Tween 80 for ST68 and Span

60 with TPGS for SE61 and Sodium Chloride were added into 50 ml PBS. The mixture was heated with a constant stirring until all chemicals were dissolved. The solution was then sterilized for 35 min at which point it was cooled to room temperature with constant stirring. To generate the bubbles, the cooled solution (held in an ice bath) was sonicated at 110 W for 3 min (Misonix Inc. CL4 tapped horn probe with 0.5" tip, Farmingdale, NY) in the presence of PFC gas to be entrapped. The bubbles were then washed three times with cold (4 ^{o}C) 50 ml PBS in a cold (4 ^{o}C) 125 ml separation funnel. The solution is allowed to separate into three distinct layers (35 min for ST68 and one hour for SE61) and the bottom layer consisting of unused surfactants is discarded with each wash. After the last wash, the microbubbles at the middle layer were collected.

3.2.2 Drug Loading UCA Fabrication

The Paclitaxel loaded UCA was fabricated followed the SOP for fabricating UAC with minor modifications. Paclitaxel was added to the mixture before sonication, after it cooled down to room temperature after the sterilization step. The mixture was heated and boiled with constant stirring for 30 min and cooled to room temperature. After that, sonication and washing in the standard procedure were continued.

3.2.3 Characterization of UCA

3.2.3.1 Size Distribution

Particle and bubble sized distributions were done by using a Malvern Nano ZetaSizer (Worcestershire, United Kingdom). For the particle size, the amount of 50 μL solution was diluted with 950 μL PBS before the measurement. For bubble size

distribution, 0.2 ml of the bubbles were added to 10 ml volume metric flask, then 10 ml volume was made up by cold (4^oC) PBS, which was used for an acoustic testing. All volume values were quoted back to the original volume after preparation and before dilution.

3.2.3.2 Acoustic Testing of UCA *in vitro*

A one-dimensional pulsed A-mode US set-up (Figure 3.1) with a single element, broadband, 12.7 mm element diameter, 50.8 mm spherically focused transducers with center frequencies 5 MHz (Panametrics, Inc., Waltham, MA) was used for *in vitro* acoustic testing. [9, 56] A transducer does not emit at a single frequency, but at a broad range of frequencies. The difference between the highest and the lowest frequency emitted from the transducer is known as the bandwidth. The -6 dB bandwidth of the transducers was 92%. The transducer was inserted in a water bath filled with deionized water, (37°C) and focused through transparent poly-acrylic window of a custom-made sample vessel. A pulser/receiver (model 5072 PR, Panametrics, Inc., Waltham, MA) was used to pulse the transducers at a pulse repetition frequency (PRF) of 100Hz. The received signals were amplified to 40 dB and fed to the digital oscilloscope (Lecroy 9350A, Lecroy, Chestnut Ridge, NY). Data acquisition and processing was done using LabView 7 (National Instruments, Austin, TX, USA), which the programming was developed in our lab. Backscattering enhancement was measured as a function of UCA dosage and used to gauge the agent's ability to provide enhancement. Enhancement in dB is defined as: [5]

$$\sum E = 20log_{10}\left[\frac{rms[S_{UCA}(t)]}{rms[S_0(t)]}\right] \qquad \text{Eq3.1}$$

where ΣE is backscattering enhancement, $S_{UCA}(t)$ is the rms readings of 60 readings with UCA, and $S_0(t)$ is the rms readings of 60 readings prior to UCA injection. The bubbles were added into the sample chamber using an automatic pipette, and stirred with a magnetic stirrer throughout the readings. The reference (PBS) is taken as an average of six values. Readings with buffer alone indicate that this method does not introduce unwanted air bubbles into the sample chamber. Enhancement and attenuation were calculated as a function of dose and time.

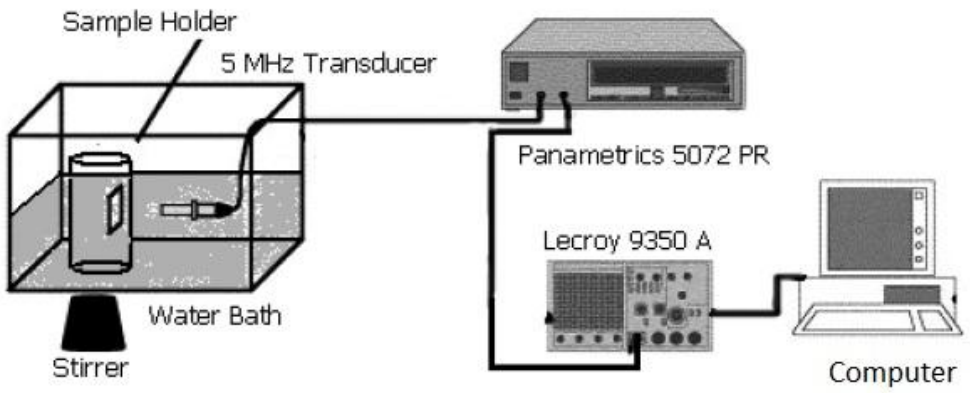

Figure 3.1 A schematic of *in vitro* acoustic set up for testing ultrasound enhancement and stability of UCA [56]

There are two curves which may be constructed from the acoustic set up. First, the enhancement curve shows the echogenicity (dB of impinging sound that is reflected back to the transducer) of the bubbles as a function of dose. For each dose, the diluted sample of the bubbles from the size distribution measurement was added into 50 ml of 37^{o}C PBS in the custom-made vessel then calculated and reported in the unit of μl of the original concentration of bubbles per liter of PBS (μl/L). All of the dose response results are

reported on fresh samples, and are not cumulative. Second, the stability curve shows the testing of the stability of the bubbles over time, under constant insonation. A dose on the linear rise of enhancement response curve must be chosen to conduct an accurate stability measurement.

3.2.3.3 Scanning Electron Microscopy of UCA

The morphology of the bubbles shell was imaged using an environmental scanning electron microscope (SEM) (FEI XL30, Hillsboro, OR). The bubble solution was dropped on to a stub and allowed to dry in cold temperature (4^{o}C). The dry bubble was then sputter coated with platinum-palladium for 40 seconds using a Denton Desk-II sputtering system (Denton Corp, NJ.) prior to imaging. Images were taken at varying magnifications at an accelerating voltage of 5 kV to avoid shell melt down. All SEM imaging and sample preparation was done at the Drexel University Materials Characterization Facility with assistance from Lauren Jablonowski.

3.2.3.4 Turbidity Measurement for the Amount of Fabricated Nanobubbles

Because no direct measurement of the numbers per ml of fabricated nanobubbles was possible, a turbidity measurement was used. The more turbidity, the greater the amount of nanobubbles in the solution. The turbidity was measured by the absorbance at a wavelength of 610 nm and the value was reported as a relative value compare with the turbidity of the nanobubbles fabricated by the standard conditions. The amount of 5 μL of the bubble solution was diluted with 195 μL of cold (4^{o}C) PBS in Non-sterile Polystyrene, Flat bottom, medium binding costar 96 well corning flat transparent plates

(Corning, NY). The absorbance was measured by Tecan infinite M 200 (Research Triangle Park, NC) instrument.

3.2.3.5 Quantitative Measurement Amount of Paclitaxel by HPLC

The amount of Paclitaxel loaded into the UCA was analyzed by the High Performance Liquid Chromatography (HPLC). The loaded Paclitaxel was extracted before the HPLC analysis. The equal volume 2.5 ml of Paclitaxel loaded bubbles and Ethyl Acetate were added into a 50 ml centrifugal tube. The mixture was then mixed by vortex mixing for 1 min, then centrifuged using a Beckman Coulter AllegraTM 21 centrifuge with relative centrifugal force at 8528 g for 15 min. After the centrifugation, 1.5 ml of the upper layer of Ethyl Acetate was taken, added to a glass bottle, and then evaporated in the fume hood. The extracted Paclitaxel was dissolved by adding 1.5 ml Acetonitrile. To make sure that Paclitaxel was completely dissolved in Acetonitrile, the glass bottle was sealed with parafilm, then shaken for 24 hours. The solution was passed through a 0.2 μm syringe filtered before HPLC analysis.

The Waters HPLC system (Waters Corporation, Milford, MA) was used for Paclitaxel concentration analysis with a reverse phase Inertsil ® ODS Column (250mm x 4.6mm, 5μm particle size, GL Science). The mobile phase was 60% Acetonitrile HPLC Grade to 40% 0.2 μm filtered DI water at the flow rate of 1 ml/min. The column effluent was detected with UV detection at 227 nm. [50, 57-59]

3.2.4 *In vivo* Tumor Imaging

3.2.4.1 Tumor Imaging

The tumors in this study were 9L gliomas which were implanted by tying tumor pieces to the epigastric vein in Fisher 344 rats (Charles River Laboratories, Wilmington, MA). The tumors were imaged after growing to 10 to 20 mm in at least one dimension (approximately 3 to 8 weeks). General anesthesia was induced and maintained with isoflurane and oxygen in each rat, and the hair coat overlaying the tumor was removed by clipping and by the application of a depilatory cream. The tumors were imaged with broadband high-frequency ultrasound transducer at 7 to 15 MHz (Phillips ALT 5000; Phillips Ultrasound, Bothell, WA), which was mounted on a stand and fixed in a position aligned along the longest axis of the tumor. The ultrasound contrast agents were injected via a 26-gauge tail-vein catheter. Because the rat weight was around 250 g and the desired dose of the agents was 0.1 ml/kg, the agents were diluted four times before the injection of 0.1 ml of diluted agents.

There were two modes of imaging in this study, power Doppler and Δ-projection. For a short time before, and then after the injection, the images were immediately acquired. The depth and field of view for each mouse was adjusted such that the tumor occupied the maximum area in the image. To minimize bubble destruction and to ensure high-quality images, the power Doppler was performed at an MI of 0.8, and the ultrasound scanner was externally gated at 0.5 frame/s. Δ-projection images were constructed from gray-scale images to demonstrate tumor perfusion. All images were recorded on videotape and digitized for analysis of a percentage area of flow (PAF), which was equal to the percentage of the area of interest covered by the agent.

3.2.4.2 Image Analysis

The data set consisted of images acquired before and after contrast injections. For the power Doppler imaging, a region representing the tumor was outlined in the pre-contrast image and superimposed on the post-contrast images. A lookup table for the color levels was constructed by using the color palette on the Doppler scans. The color lookup table was used to identify colored pixels within the tumor. The percentage area of flow for power Doppler (PAF_D) for each power Doppler image was determined by the percentage ratio of pixels enhanced by the contrast agent to the total number of pixels in the tumor cross-section. [60]

For Δ-projection analysis, B-mode images of the data set were used. A region representing the tumor was outlined in the first pre-contrast image of the data set. Sequential projection images of the tumor region were reconstructed from the serial contrast-enhanced images by tracing the running maximum change in enhancement. A threshold gray-level difference was applied to the area enhanced by the inflow of contrast agent from the surrounding tissue. In summary, the procedure consisted of increasing the gray-level difference stepwise until the Δ-projection showed the expected absence of enhancement. This approach mapped the pixels of blood vessels that were enhanced by contrast agent. For each image in the time series of the projection images, the percentage area of flow for Δ-projection (PAF_Δ) was determined by taking the percentage ratio of pixels enhanced by contrast agent to the total number of pixels in the cross-section. [60]

The PAF was plotted with time and various parameters were compared between the two agents corresponding to the plotting (Figure 3.2). A first-pass kinetics gamma-

variate function was used to calculate the perfusion ratio of both agents. [61, 62] The tumor perfusion calculation details are described in appendix B.

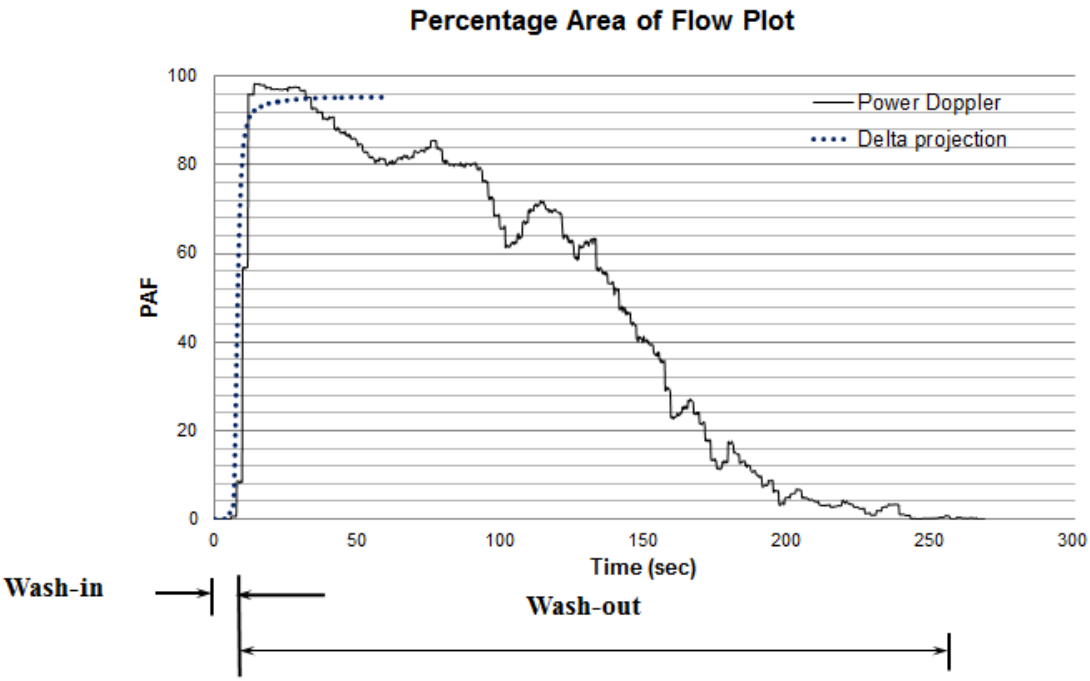

Figure 3.2 Example of regions utilized in the percent area plot of Power Doppler and Δ-projection

3.2.5 Statistical Analysis

The results were shown as means with the error bars displayed as standard error about the mean (SEAM). Statistical analyses were performed using SPSS version 19 (IBM, USA). The parameters were compared by a paired-samples two-tailed student *t* test. The level of significance was set to $p<0.05$

4. RESULTS AND DISCUSSION

4.1 A New Model for the Gas Bubbles Stabilized by Surfactants

The microbubbles stabilized by surfactant had been developed in our lab with an extensive study on mixing Span 60 and Tween 80 at the total surfactant concentration at 85.1mM and the molar percentage of Span 60 to Tween 80 at 80:20 in 1X PBS with the addition of 0.51M of NaCl. This first generation agent is named ST68. Octafluoropropane gas yielded the best stability under ultrasound compared with Sulfur Hexafluoride and air. [6] ST44 consisting of Span 40 Tween 40 has also been prepared and studied. [6, 63]

It has been observed that stable microbubbles can be formed only with a solid Span, i.e. Span 40 and Span 60, mixed with Tween. Neither the mixture of Span 80, a liquid form, with Tween nor Tween alone purged with PFC gas produced stable microbubbles, an observation in agreement with the study of Singhal who used air. [4] For this reason, the potential exists that the stability of the mixed surfactant gas bubbles can be modeled as solid particle-stabilized bubbles, not a mixture of dissolved surfactants.

4.1.1 Differences between Surfactant Stabilized Foam and Particles-stabilized Foam

In order to see the effect of Span and Tween ratios on the mixed surfactant system, mixtures of Span 60 and Tween 80, with a total initial concentration of 85.1 mM, were produced in the molar ratios of 20:80, 40:60, 60:40, and 80:20 Span:Tween. After autoclaving and cooling down to room temperature with constant stirring, the solutions of

pure Tween and at low molar percentages of Span and Tween mixtures (i.e. 10:90 and 20:80) were clear compared with solution using higher percentages (e.g. higher than 30:80), which had a milky appearance. (Figure 4.1) Size analysis of the pure Tween 80 and a low percentage of Span 60 and Tween 80 solutions all showed exactly the same size distribution (mean diameter of between 8-10 nm), which is in the micelle range, compared with the mean diameter of higher percentages of Span 60 and Tween 80 that produced particles with mean diameters close to 60 nm (data not shown). In the case of low Span and Tween percentages, we hypothesize that the Tween in the mixture has increased the solubility of Span by formation of mixed micelles. This scenario agrees with a study by Eiser *et al.* [22], which showed increasing solubilization of a hydrophobic component (e.g. fat particles) in the presence of a water-soluble surfactant. In the case of the high Span 60 and Tween 80 ratios, we surmise that there was not enough Tween 80 to form mixed micelles with Span 60, and Tween 80 adsorbed onto the Span 60 particles, stabilizing the Span 60 particles while the solution cooled down to room temperature after the sterilization. In this way, small particles of Span 60 were formed by preventing the aggregation of Span 60 particles, and the solutions appeared cloudy. For the cooling of solutions of pure Span 60, the particles agglomerated and precipitated out, which can be seen by the naked eye.

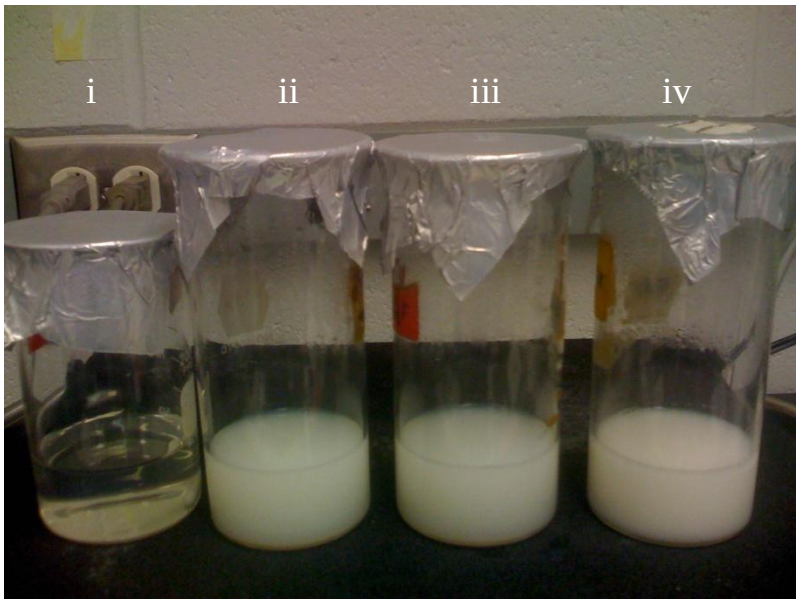

Figure 4.1: The solution of mixture of Span 60 and Tween 80, the initial concentration of 85.1 mM, in the molar percentage of (i) 20:80, (ii) 40:60, (iii) 60:40, and (iv) 80:20, which is a standard ratio for ST68

The hypothesis of the bubbles stabilized by the particles of Span with Tween also can be investigated by observing the dried foams (Figure 4.2). The dry foams can be seen in test tubes for pure Span 60 and the mixture of Span 60 and Tween 80 at molar percentage of 80:20 but not for pure Tween 80 and the mixture of Span 60 and Tween 80 at a molar percentage of 20:80. These results resemble those in the study of Zhang *et al*. [23], which describes this unique characteristic of dried foam resulting from particle-stabilized foam.

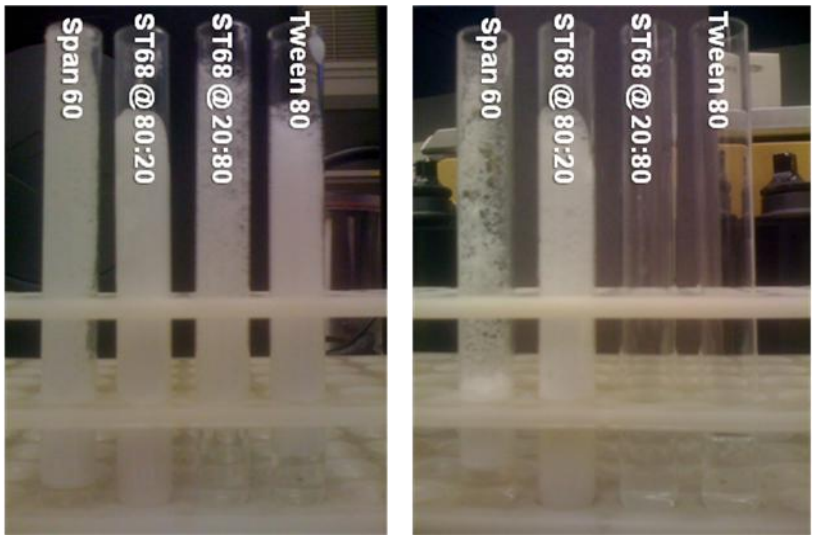

(a) (b)

Figure 4.2: a) Foam and bubble of pure Span 60, mixture of Span 60 and Tween 80 at 80:20 and 20:80 and pure Tween 80, respectively, in test tube after sonication. b) Dry foam of pure surfactant and the mixtures

4.1.2 The Effect of Particle Size on the Stability of Microbubbles

It has been observed by Fujii et al. that the particle size affects the stability of the resulting particle-stabilized foam. [17] To explore this possibility on ST68, we followed up on an observation that was made during fabrication, that the particles are formed during the cool down period after autoclaving.

The constant amount of 2 m mole of Span 60 was mixed with the different amount of Tween 80 at 0.1, 0.5 and 1 m mole in 50 ml PBS with 1.5 g of NaCl to determine if the surfactant ratio had any effect on particle size. The particle sizes after autoclave and cool down to room temperature with constant stirring are shown in Figure 4.3. The results showed that the particle size was smaller when the amount of Tween 80 increased with the same amount Span 60.

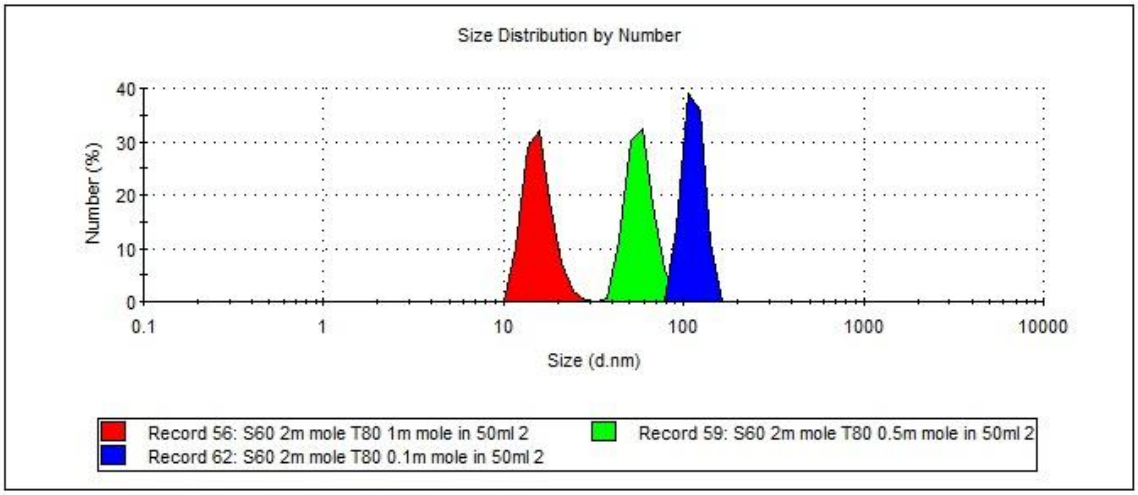

Figure 4.3: Particle size after autoclave and cool down to room temperature of the mixture of 2m mole Span 60 with different amount of Tween 80 at 0.1, 0.5 and 1 m mole in 50 ml PBS

ST68 agent was prepared with these samples and the mean diameters of the resulting bubbles from the mixtures are shown in Figure 4.4. There is no statistically significant difference when mixing the same amount of Span 60 at 2 m mole with different amount of Tween 80 at 0.1, 0.5 and 1 m mole in 50 ml PBS. The mean diameter of the bubbles was close to 2 μm. It should be noted that for the mixture of Tween 80 at 0.1 m mole, which gave the largest particle size with mean diameters close to 100 nm, there was the smallest yield of microbubbles, less than 0.5 ml after collecting the middle layer at the third wash compared with 5-10 ml for other particle sizes. Further decreasing the Tween 80 lower than 0.1 m mole, which should have lead to the bigger particle, was not a suitable condition to fabricate the microbubbles for contrast agent because the size of the bubbles were bigger than 8 μm after the third wash.

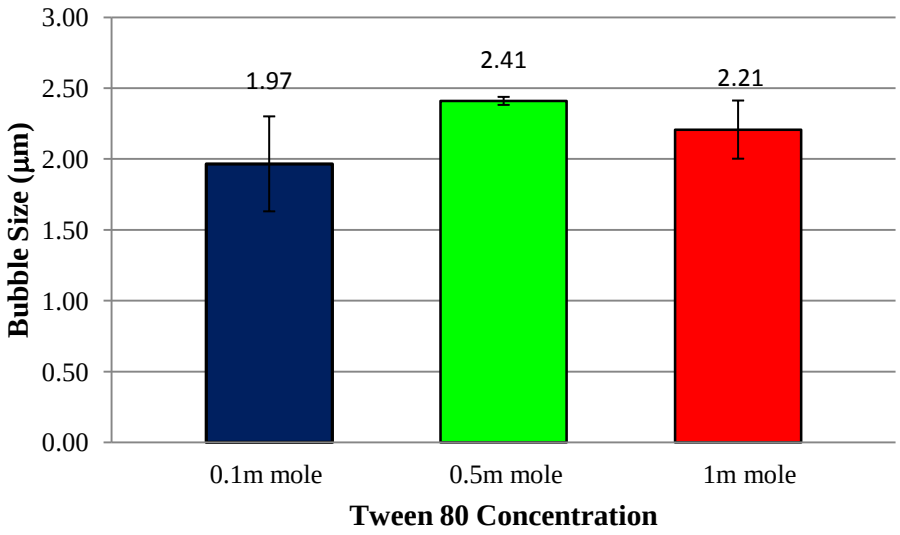

Figure 4.4: Mean diameter of the bubbles fabricated from the mixture of 2m mole Span 60 with different amount of Tween 80 at 0.1, 0.5 and 1 m mole in 50 ml PBS (n=3, error bar=SEAM).

All of the agents fabricated from the mixtures gave a very good acoustic enhancement (Figure 4.5). The enhancement ranged between 25 dB to 30 dB. There was no statistically significant difference for maximum enhancement between these microbubbles. However, the enhancement response curve of the microbubbles that were fabricated from 0.1 m mole of Tween 80 was different from the other two curves, in which it is taking a lot of agent to reach maximum enhancement.

The *in vitro* stability under ultrasound of the agents is shown in Figure 4.6. The microbubbles fabricated from 0.1 m mole of Tween 80 were the most stable with the half life of 18.42 min, compared with 7.41 and 6.02 min for 0.5 and 1 m mole of Tween 80, respectively. This half life of microbubbles fabricated from 0.1 m mole of Tween 80 was statistically significant different from microbubbles fabricated from 0.5 m mole ($p=0.001$, $n=3$) and 1 m mole ($p=0.001$, $n=3$) of Tween 80. There was no statistically significant difference from microbubbles fabricated from 0.5 m mole and 1 m mole of Tween 80. These stability results showed that the stability of the microbubbles related to the size of

the particles. The bigger the particles, the more stable were the microbubbles. This stability of the bubbles can be explained by the energy to remove the particles from the interface (equation 2.4). [34] When the bubbles are exposed to the ultrasound, they will expand and contract due to compression and rarefaction of the sound waves. When the bubbles contract, the Laplace pressure increases (equation 2.3). This pressure can force the particle from the interface into the solution and make the bubbles unstable. From the equation 2.4, the energy required to remove the particles is higher when the particle is bigger. This could explain why the microbubbles fabricated from 0.1 m mole of Tween 80, which consists of the biggest particle, is the most stable compared with other two conditions, one of them is the same ratio of 80:20 (2 m mole Span 60 to 0.5 m mole of Tween 80). These results agree with Fujii et al., which showed that the stability of the bubble is depended on particle size.

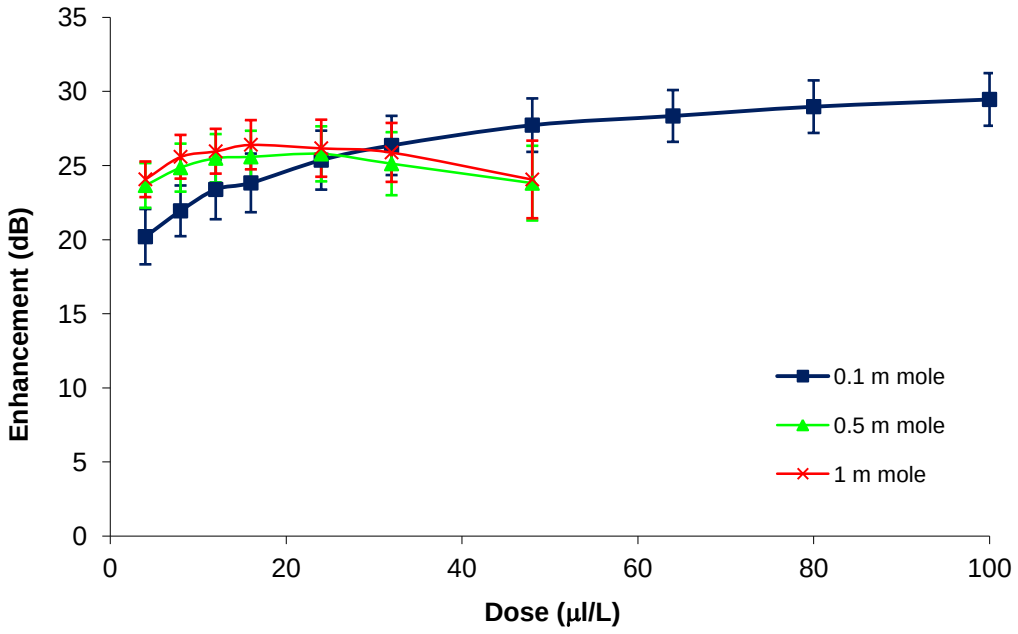

Figure 4.5: *In vitro* ultrasound enhancement of the bubble fabricated from the mixture of 2m mole Span 60 with different amount of Tween 80 at 0.1, 0.5 and 1 m mole in 50 ml PBS (n=3, error bar=SEAM).

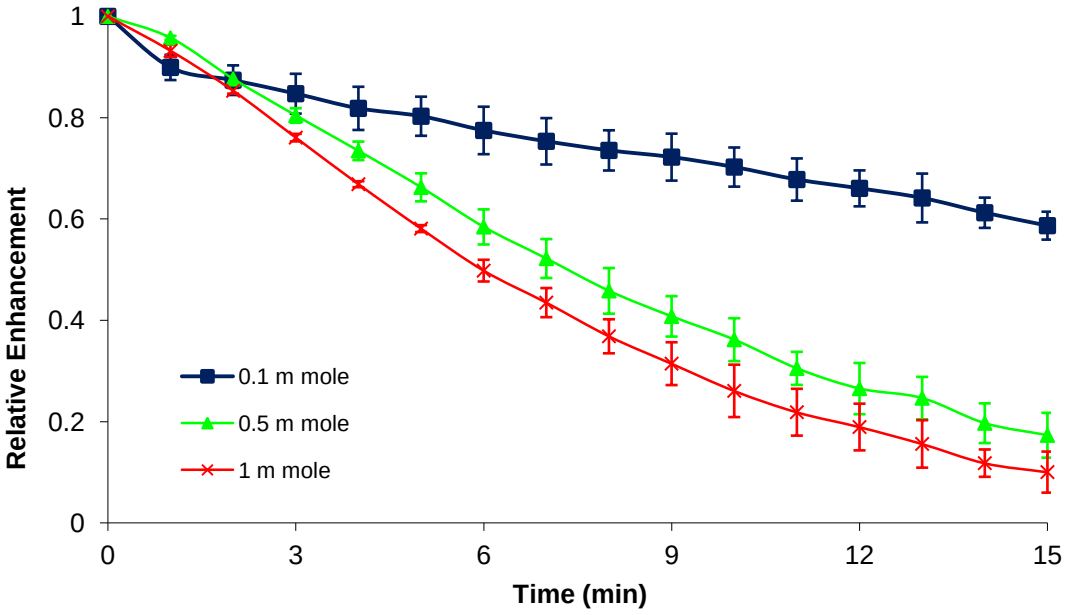

Figure 4.6: *In vitro* stability of the bubble fabricated from the mixture of 2m mole Span 60 with different amount of Tween 80 at 0.1, 0.5 and 1 m mole in 50 ml PBS (n=3, error bar=SEAM).

4.2 Development and Characterization of a New Microbubble Formulation

A newly develop agent was fabricated by directly replacing Tween 80 with TPGS. TPGS was selected for study because, like Tween, it has a restively bulky head group with attached polyoxyethylene -(CH_2CH_2O)- groups and a hydrophobic tail (Figure 2.9). It is also well known as a pharmaceutical ingredient, *which enhances the absorption, bioavailability and effectiveness of bioactive compounds.* TPGS was also chosen because we wanted to use these agents as drug carriers for the ultimate goal of this study, and there are many studies [53-55, 64-66] which show TPGS increasing the amount of drug encapsulation. This new agent was named SE61.

Mean diameter of the new and original ST68 agents are shown in Table 4.1 with SE61 having a slightly smaller diameter than ST68. However, there is no statistical significant between both agents. Both agents were comprised of bubbles where 100% of

bubble population was smaller than 8 μm, which is ideal for the agent to pass the capillary beds.

Table 4.1 Mean diameter of ST68 and SE61

Agents	**Mean diameter (μm)**
ST68	1.88±0.16
SE61	1.31±0.20

The acoustic properties of SE61 compared ST68 are shown in Figure 4.7. SE61 had a statistically significant ($p = 0.011$, $n=3$) higher *in vitro* maximum enhancement than ST68 (Figure 4.3a). The maximum enhancement of SE61 was 30.22±0.74 dB and it was 22.16±0.70 dB for ST68. However, it should be noted that ST68 gave a maximum enhancement at a lower dose at 32 μl/L compared with 120 μl/L for SE61, suggesting that it is more concentrated sample.

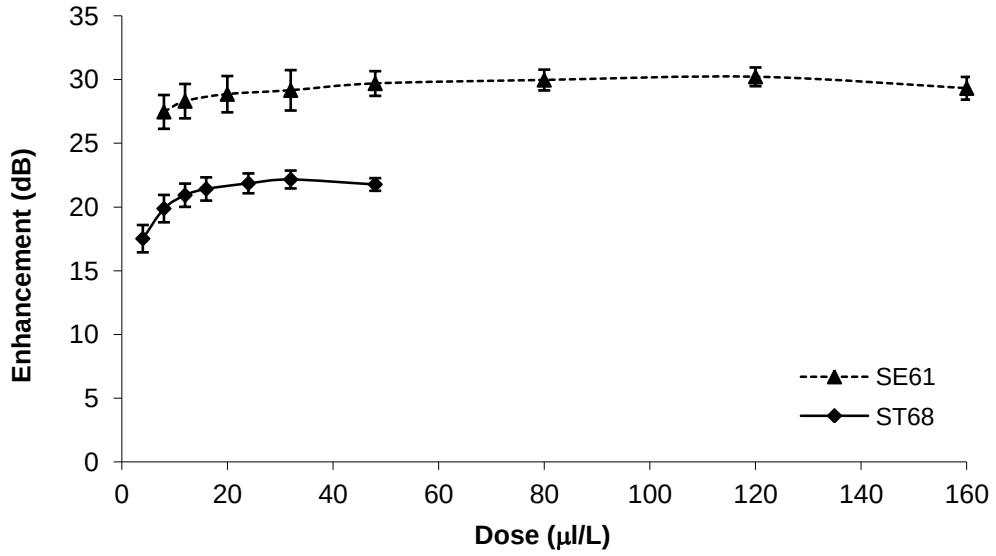

(a)

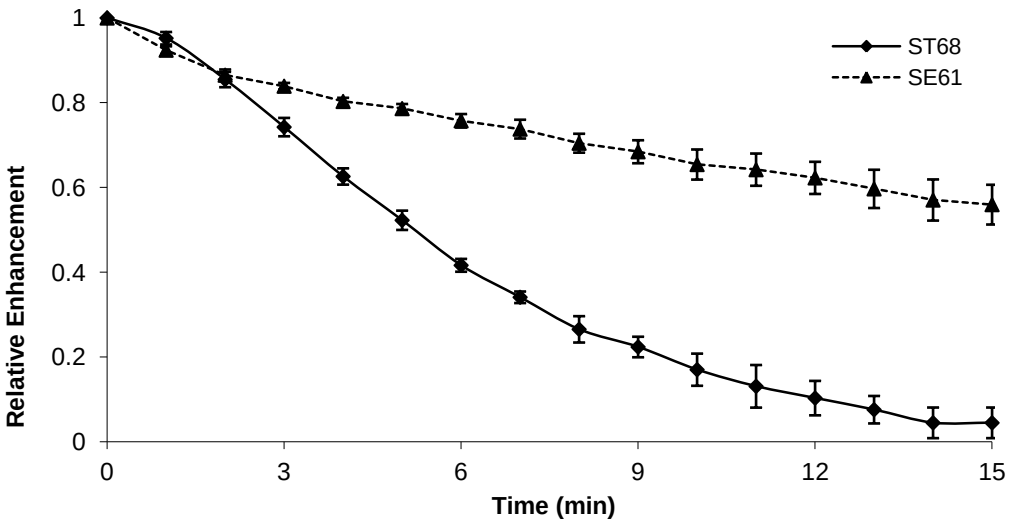

(b)

Figure 4.7: *In vitro* ultrasound enhancement (a) and stability (b) of ST68 and SE61 at 37^{o}C (n=3, error bar=SEAM).

SE61 was also statically significant (p = 0.023, n=3) and more stable under ultrasound than ST61 (Figure 4.3b). The half life of SE61 was 16.45±1.56 min compared with 5.20±0.20 min for ST68.

4.2.1 The Morphology of the Microbubbles

A light microscope and SEM of SE61 are shown in Figure 4.8 and Figure 4.9, respectively. The light microscope assured that the population of the agent was comprised of bubbles smaller than 8 μm. However, the morphology of the bubble could not clearly be seen under the light microscope due to the limitation of the light microscope.

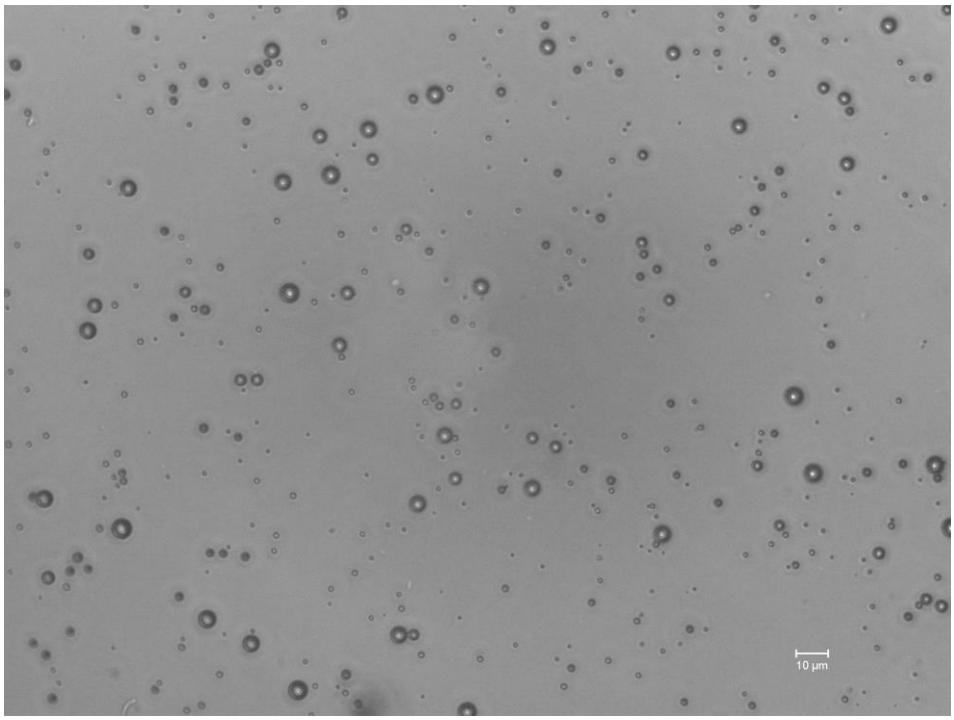

Figure 4.8: SE61 under light microscopy. The numerous small bubbles appearing as dark points in the background Bar = 10 μm

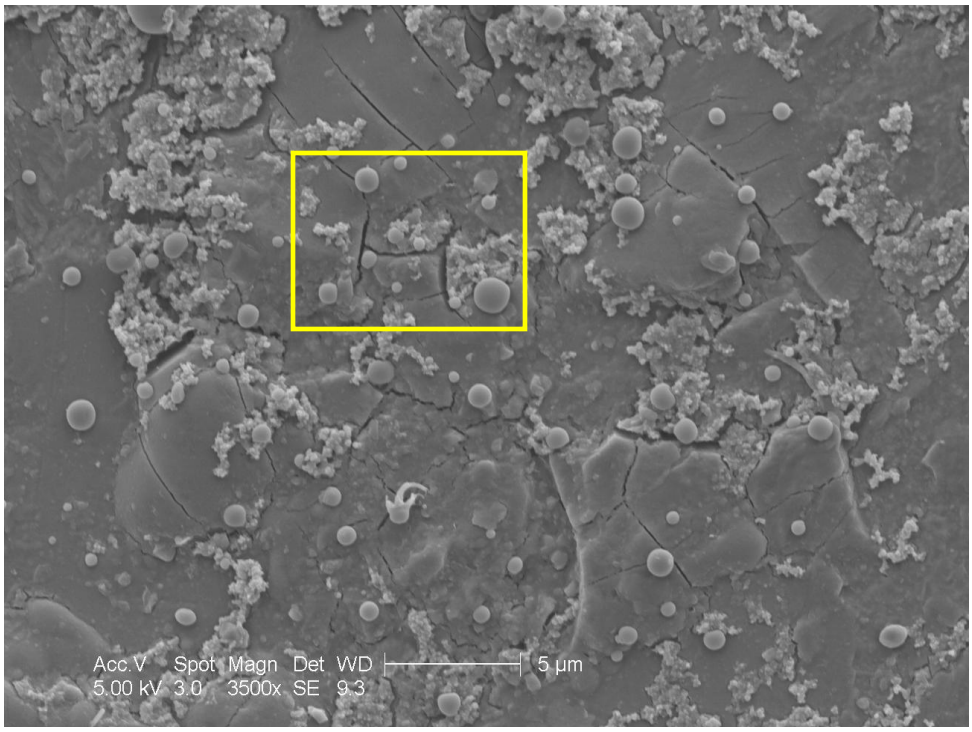

(a)

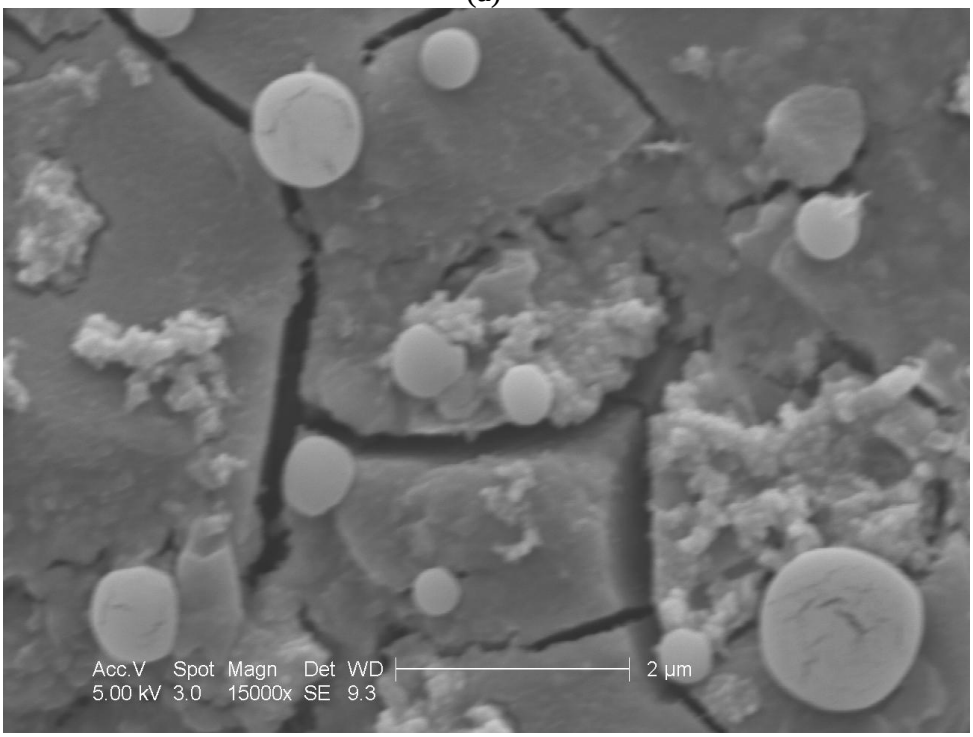

(b)

Figure 4.9: SEM of SE61. The bubble was Pd/Pt sputter coating for 40 seconds. The higher resolution of the yellow square area in Figure (a) is shown in Figure (b)

The sample of SE61 was diluted and dried on the stub in 4^{o}C before imaging by SEM. The SEM showed that SE61 fabricated by the standard procedure consists of the micron-sized and nano-sized bubbles. During preparation the bubbles in the SE61 mixture took a very long time to rise, which indicated to us that the sample contained a large number of nano bubbles which due to their lower buoyancy, took far longer to rise than the micron sized bubbles. The SEM gave the first positive evidence that the nanobubbles could be fabricated by the standard procedure and suggested the need for further study to find a method to increase the nanobubble population by modifying the standard procedure.

The SEM, however, did not show us that the bubbles shell contains particles as hoped. It showed the bubbles had smooth surfaces. This might be because the particles that stabilized the bubbles were too small, ranging from 50 nm to around 100 nm, and could not be clearly seen after the sputter coating for SEM. Further studies on increasing the size of particles to support the particle stabilized model were conducted.

4.2.2 The Effect of the Method of Making Particles and of Different Surfactant on the Stability of Microbubbles

The SEM images of the bubbles from previous studies could not confirm the existence of particles in the stabilized bubbles due to the possibility that the particles are too small to be detected after the sputter coating and do not show up when imaged by the SEM. In the original study, there was another way to prepare the mixture before the sonication. [4] Span 60 can be ground into smaller particles in a pestle and mortar with a

small amount of PBS and NaCl crystals before adding another surfactant. The mixture was then stirred without heating.

Dynamic light scattering of the particles of ground Span 60 mixed with TPGS is shown in Figure 4.10. The mean diameter of 380 nm of the majority of the particles, which was 87% smaller than 530nm, was mixed with big particles. The particles can be seen in the SEM imaging, which shows that most of the particles were smaller than 500 nm (Figure 4.11). The SEM imaging of the microbubbles fabricated from this mixture is shown in Figure 4.12. It can be seen that upon drying, particles are still visible. Certain areas appear with particles grouped together in spherical arrangements.

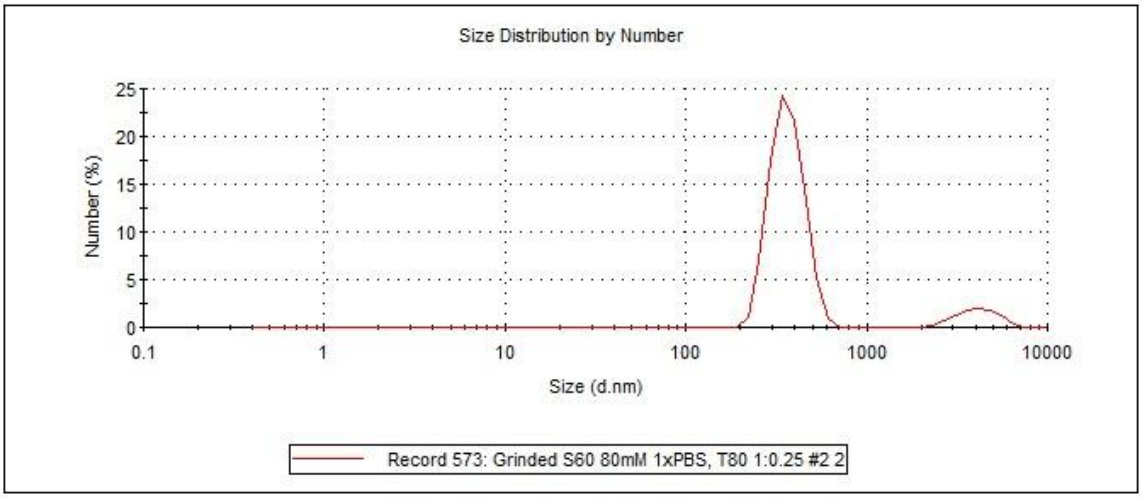

Figure 4.10: Particle distribution of ground Span 60 mixed with TPGS

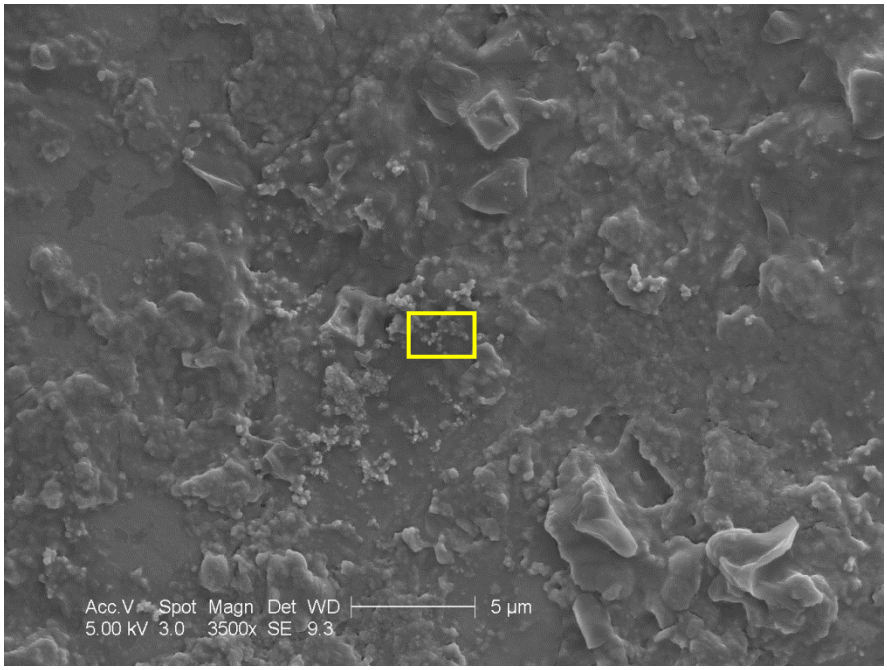

(a)

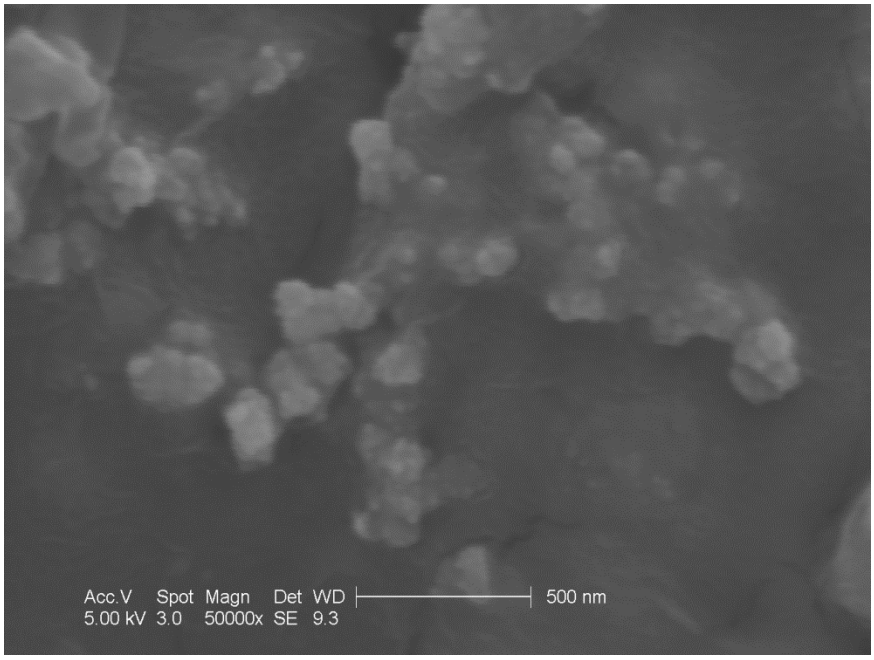

(b)

Figure 4.11: SEM imaging of ground Span 60 mixed with TPGS. Higher magnification of the square in picture (a) is shown in picture (b)

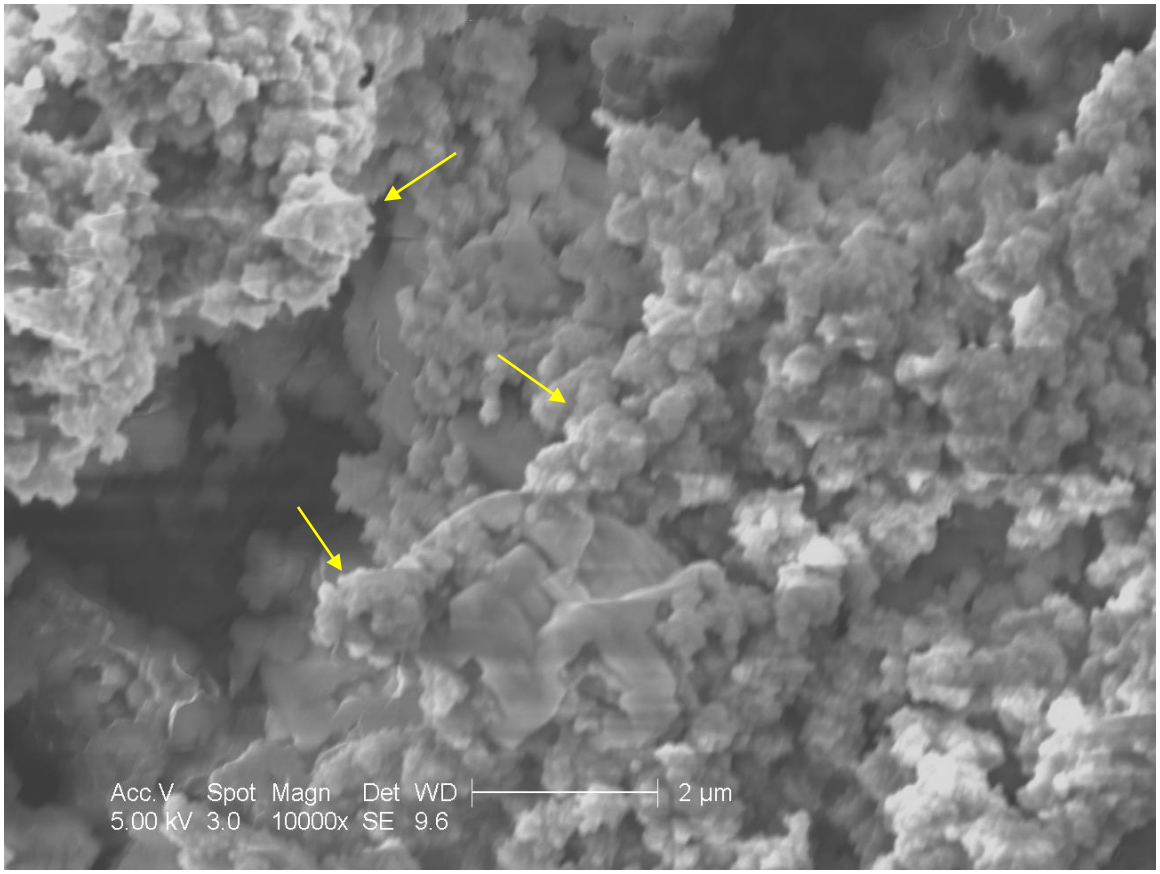

Figure 4.12: SEM imaging of the bubble fabricated from ground Span 60 mixed with TPGS. The arrows are the possible examples of the microbubbles that stabilized by particles.

Further study was conducted to compare: i) the effect of Tween 80 and TPGS adsorbed onto ground Span 60 particle and ii) for TPGS, a comparison of bubble properties using either the ground or heating method of fabrication.

The microbubbles with diameter mostly in a range of 2-3 µm could be fabricated from the mixture of Span 60 to Tween 80 and TPGS between the molar ratios of 1:0.125 to 1:1, including ground Span 60 without another surfactant (Figure 4.13). It should be noted that the microbubbles could not be fabricated from heated Span 60 alone. There was no statistically significant difference in the size of microbubbles among all conditions.

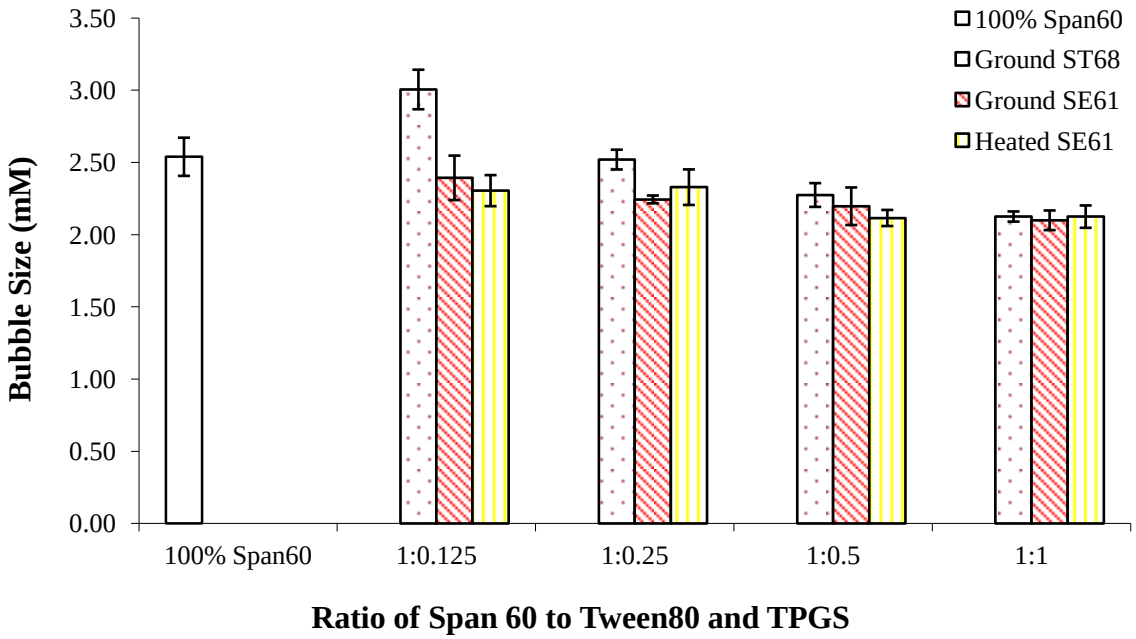

Figure 4.13: Size of microbubble fabricated from ground Span 60 with Tween 80 (ground ST68) and TPGS (ground SE61) and heated Span 60 with TPGS (heated SE61) (n=3, error bar=SEAM)

The amount of microbubbles fabricated from all conditions were recorded and shown in Figure 4.14. For the ground fabrication method, there was no statistically significant difference between ST68 and SE61 at any given surfactant ratio. The amount of microbubbles was at the highest at the ratio of 1:0.25 (molar percent ratio of 80:20) for both ST68 and SE61. There was no statistically significant difference between the ratio of 1:0.125, 1:0.25 and 100% Span 60, but there was statistically significant difference between the ratio of 1.0.25 and 1:0.5 ($p=0.009$ for ST68 and $p=0.004$ for SE61, $n=3$).

These results show the same trend as the previous study, in which the highest yield was when the ratio of Span 60 and Tween 80 was in between 60:40 and 80:20. Binks et al. [21] showed that at very low surfactant concentration of the adsorbed surfactant (compared to our conditions that the ratio of Span 60 to Tween 80 or TPGS are at 1:0.125 and 1:0.25) the foamability, which refers to the ability of surfactants or

particles to produce foam, is dependent on the partially coated particles due to the lack of availability of free surfactants. This is may be explain why there is not statistical significant among 100% ground Span 60 and the ratio of 1:0.125 and 1:0.25 for ground Span 60 with Tween 80 and TPGS. However, at higher concentration of the adsorbed surfactant, there are more free surfactants in the solution. We know that the bubbles that are stabilized by free surfactant, i.e. Tween or TPGS alone, are bigger than 8 μm. This reason can explain why the yield of microbubbles was less at the ratio of 1:0.5 and 1:1.

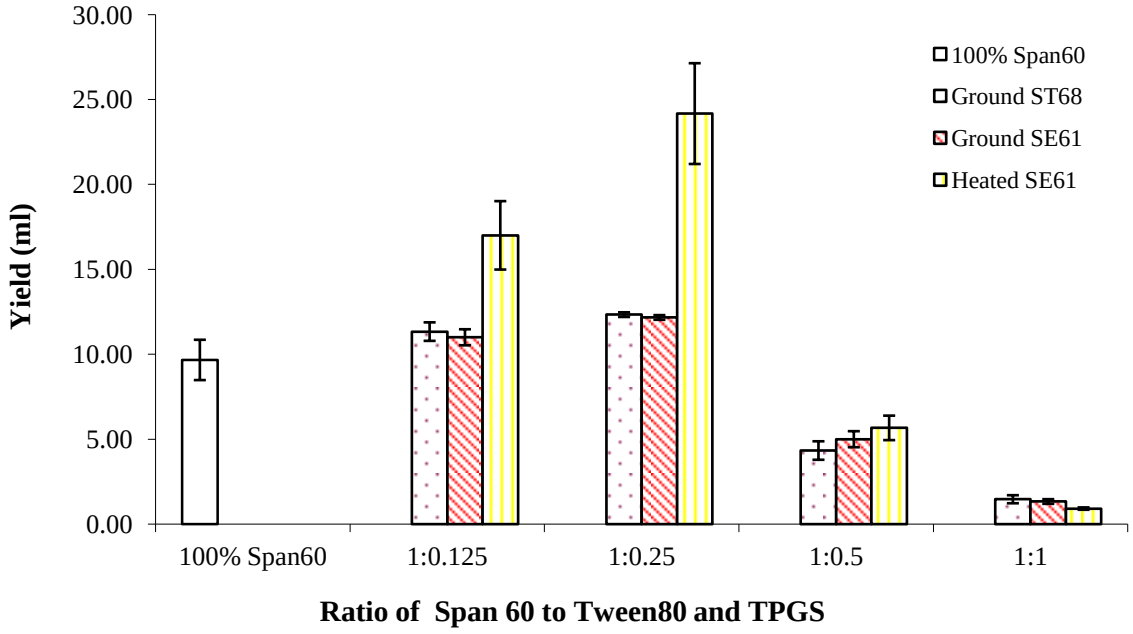

Figure 4.14: Amount of microbubble fabricated ground Span 60 with Tween 80 (ground ST68) and TPGS (ground SE61) and heated Span 60 with TPGS (heated SE61) (n=3, error bar=SEAM)

For the heated fabrication method with TPGS, the amount of microbubbles show the same trend as the ground Span 60 method with the highest amount of microbubbles produced at the ratio of 1:0.25. There was no statistically significant difference between the ratio of 1:0.125, 1:0.25, but there was a statistically significant difference between the

ratio of 1.0.25 and 1:0.5 ($p=0.021$ for $n=3$). There was no statistically significant difference for SE61 fabricated by the ground or heated methods at any given surfactant ratio.

The difference in yield obtained by the heating method can be explained by the size of the particles. Fujii et al. [17] showed that at the same surface morphology of the particle, size of the bubble is depended on the size of particles. The less mean diameter of the particles, the smaller mean diameter of the bubbles. However, if the particles are too small, these particle are efficient at preventing bubble coalescence during foaming. We know from section 4.1.2 that the particles are smaller when the ratio of Span 60 and Tween 80 is higher, this should explain why it is higher yield at the ratio 1:0.25 than 1:0.125. The mean size of particle at 1:0.125 and 1:0.25 were around 60-100 nm compared with 20-30 nm at the ratio of 1:0.5 and 1:1. It is possible that the bubbles from high ratio may not stable enough to survive three time washing steps in separation funnel.

The *in vitro* maximum enhancement of microbubbles is shown in Figure 4.15. There was no statistically significant difference for the maximum enhancement for all conditions, except for the 100% Span 60 compared with all other conditions.

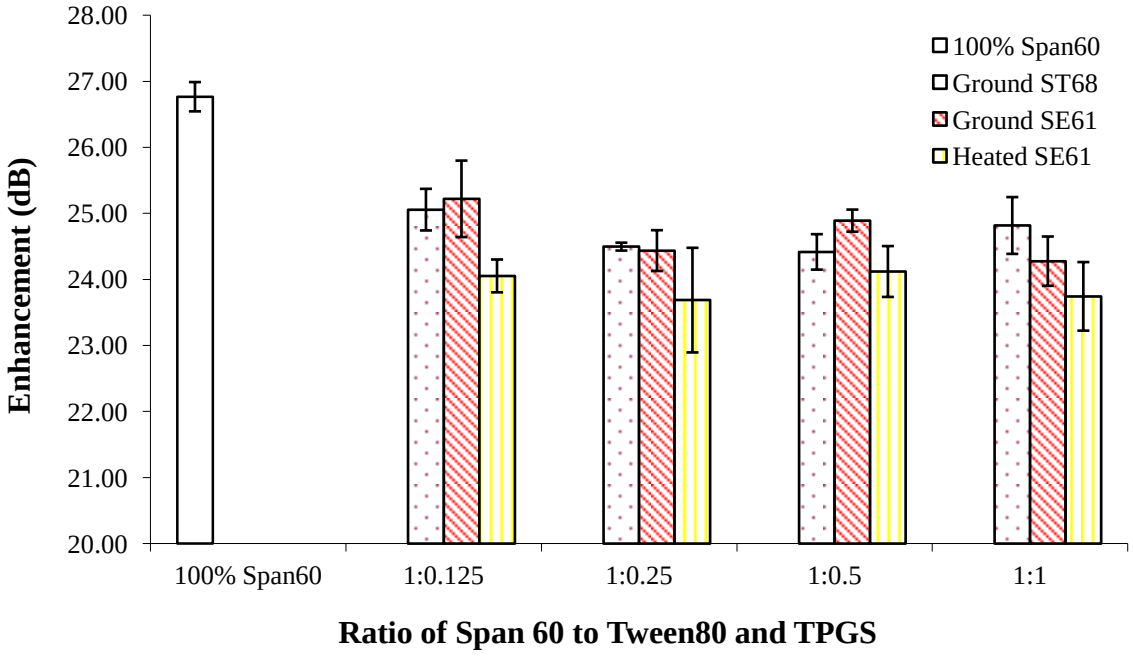

Figure 4.15: *In vitro* maximum enhancement of microbubble fabricated from ground Span 60 with Tween 80 (ground ST68) and TPGS (ground SE61) and heated Span 60 with TPGS (heated SE61) (n=3, error bar=SEAM)

The *in vitro* half life of microbubbles under ultrasound is shown in Figure 4.16. There was no statistically significant difference for the half life for all conditions, except for ground SE61 at the ratio of 1:0.25 to 1:0.5 ($p=0.018$, $n=3$) and 1:0.25 to 1:1 ($p=0.037$, $n=3$). It should be noted that for the heated SE61, the half life showed the same trend as ST68 in the study in section 4.1.4, which was the stability of the microbubbles under ultrasound decreased when increasing the molar ratio of Span 60 to another surfactant component.

As mentioned before with Binks et al. work [21], it is possible that there is a different mechanism between the lower ratio (1:0.125 and 1:0.25) and the higher ratio (1:0.5 and 1:1). This could explain why there is a statistically significant difference between the lower ratio and higher ratio.

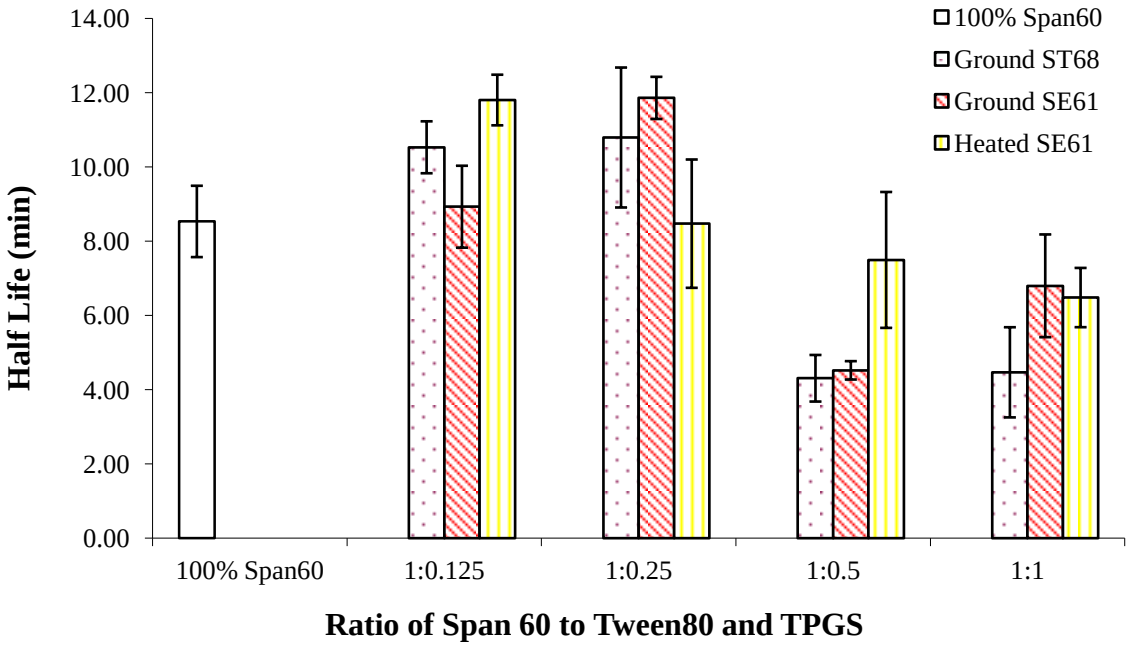

Figure 4.16: : *In vitro* half life of microbubble fabricated from ground Span 60 with Tween 80 (ground ST68) and TPGS (ground SE61) and heated Span 60 with TPGS (heated SE61) (n=3, error bar=SEAM)

4.2.3 Conclusion on Particle Stabilized Model for ST68 and SE61

The microbubbles with mean diameter around 2 μm can be fabricated by mixing Span 60 with Tween 80 (named ST68) and Span 60 with TPGS (named SE61). The size of the particles could be controlled by the ratio of the surfactant. The SEM imaging of microbubbles fabricated by the particle size in a range of 200-500nm shows that these microbubbles were dry to a collection of particles. The size of particles also dictates the stability of microbubbles under ultrasound, which can be explained by the particle stabilized foam theory.

4.3 Investigations into the Nano-sized Contrast Agent

During the investigation of the potential of TPGS to substitute for Tween 80, it was noted that the bottom layer while doing the washing step using the heated SE61, was more turbid compared with ST68 when following the standard procedure. In addition, it took far longer for the layer to clear to collection of the bubbles in the middle layer due to buoyancy. This should suggest it was possible that there were more nanobubbles produced when alternating the surfactant component from Tween 80 to TPGS.

4.3.1 The Properties of the Bottom Layer in the Third Wash of SE61

First, it should be confirmed that the increased turbidity of the bottom layer was due to an increased number of nanobubbles, not the unused surfactants. These nanobubbles can be collected by following the standard procedure (appendix A.2) except at the end of the third washing step, the very bottom layer containing settled Span particles, 50-75 ml, was discarded. Unused surfactant particles should be discarded in this step. After that, 10 ml of solution just underneath the middle layer of microbubbles was collected for further analysis. This layer should contain nano bubbles that were rising at a slower rate than the micro bubbles.

The number size distributions of the collected solution (in green color) compare with the particle before sonication (in red color) are shown in Figure 4.17. The size distribution showed that the majority of nanobubbles were mixed with a small amount of microbubbles. More than 95% of the bubbles were smaller than 615 nm, with a mean diameter of 286 nm, compared with 46 nm for the particles.

The acoustic properties were tested to ensure that the population with mean diameter of 286 nm was nanobubbles not unused surfactant particles since the unused surfactant would not give a high ultrasound enhancement.

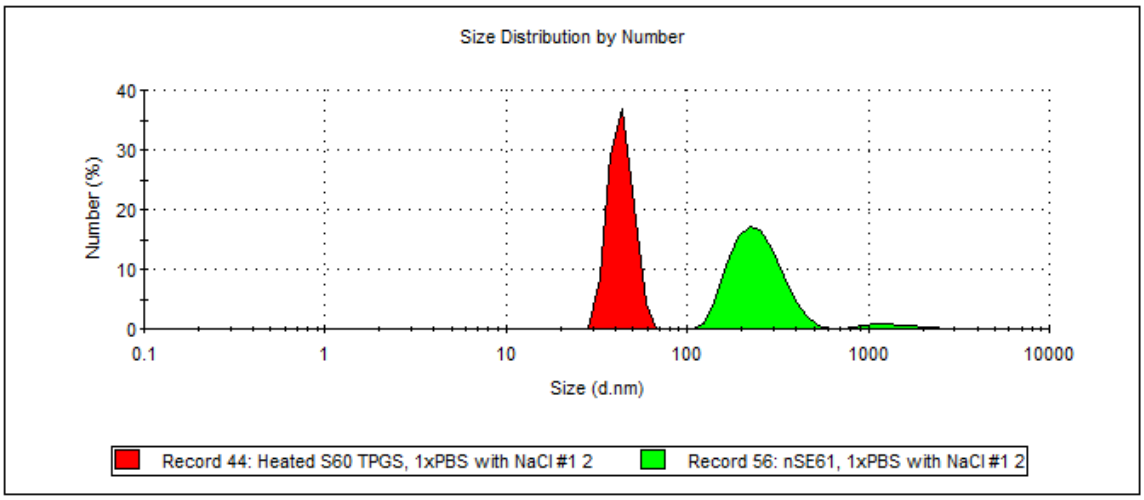

Figure 4.17: Number size distribution of 10ml of the solution just underneath the middle layer of microbubbles

From Figure 4.18a, the maximum enhancement of these nanobubbles was 21.63±1.36 dB. The *in vitro* stability (Figure 4.19b) was very low. The nanobubbles had the half life only 1.75±0.24 min compared with 16.45±1.56 min for SE61 microbubbles. This suggests that these results are dominated by nano bubbles not co-collected microbubbles. The difference in stability between the nanobubble and microbubbles could be explained by the difference in Laplace pressure. Since the nanobubbles would have higher Laplace pressure, it would be less stable compared with the microbubbles. These nanobubbles of SE61 were named nSE61.

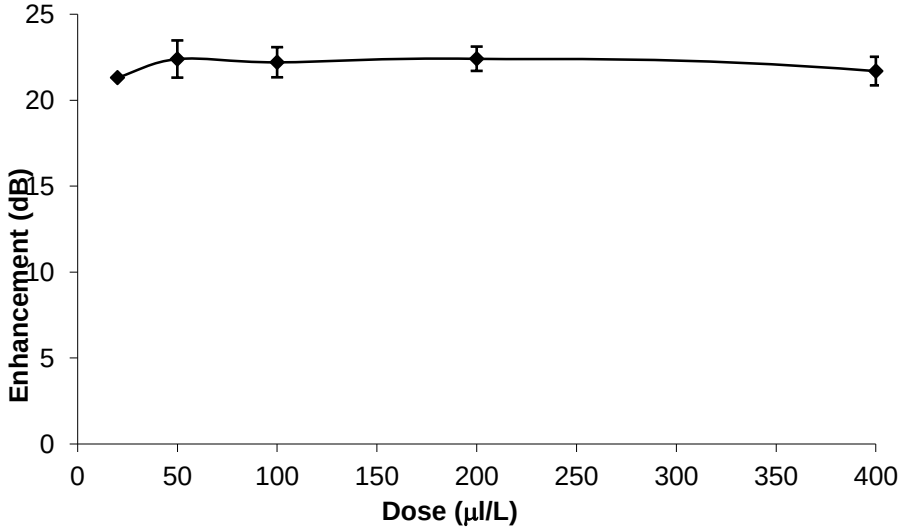

(a)

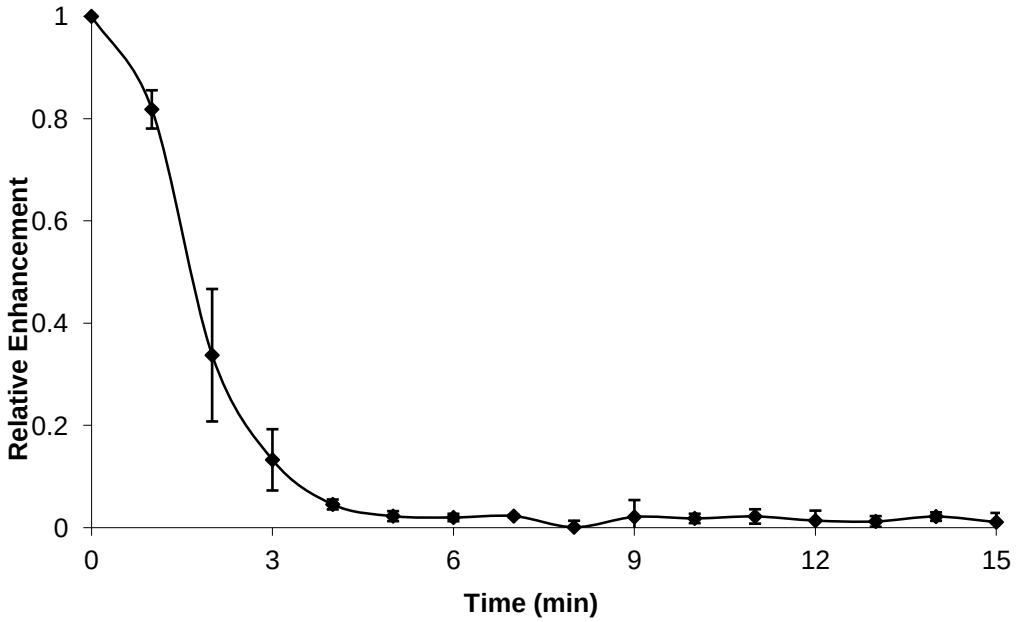

(b)

Figure 4.18: *In vitro* enhancement (a) and stability (b) of nanobubble SE61 fabricated standard procedure but collected 10ml just underneath the middle layer of microbubbles (n=3, error bar=SEAM)

4.3.2 The Effect of Total Surfactant Concentration on Nanobubble Population

The further study was to increase the nanobubble population. The first parameter investigated in this study was the effect of total surfactant concentration on size distribution. Dickinson et al. [16] showed that the concentration of the particles has some effect to the bubble size and its stability. The SOP in appendix A.2 was followed for separation of nano bubbles after the third wash, except that the amount of starting surfactant was varied. Figure 4.19 shows the mean diameter of nanobubbles when the total concentration of surfactant is varied at a percentage ratio of Span:TPGS constant at 80:20. The standard total concentration was 85.1 mM. This study compared the standard total concentration by decreasing the total concentration to 50 mM and increasing the total concentration to 100 mM. The mean diameter of nanobubbles was not statistically significant different in all conditions.

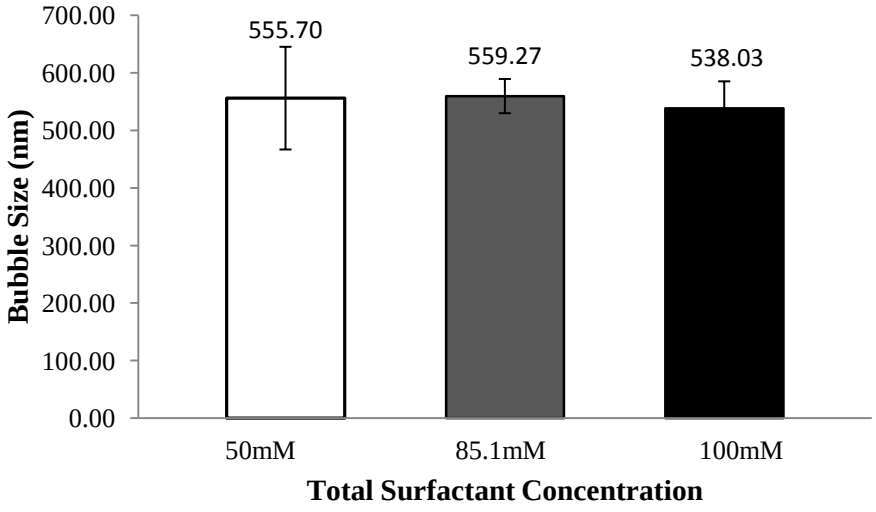

Figure 4.19: Bubble mean diameter when vary the total surfactant concentration at constant Span:TPGS ratio (n=3, error bar=SEAM)

Because there was no direct measurement of the number of nanobubbles, the amounts of fabricated nanobubbles were compared by means of turbidity measurement. The turbidity of the standard condition was set to one and other measurements were normalized by comparing them to this value. The results of the measurement are shown in Figure 4.20. The amount of nanobubble was highest at the standard total concentration of 85.1 mM. Decreasing and increasing resulted in decreased turbidity, which means a less fabricated nanobubbles population. Both decreases were statistically significant when compared with the standard conditions ($p=0.031$ for 50 mM and $p=0.002$ for 100 mM). This molar ratio and total molar concentration was found to be optimal for microbubble preparation in ST68 as well. [3]

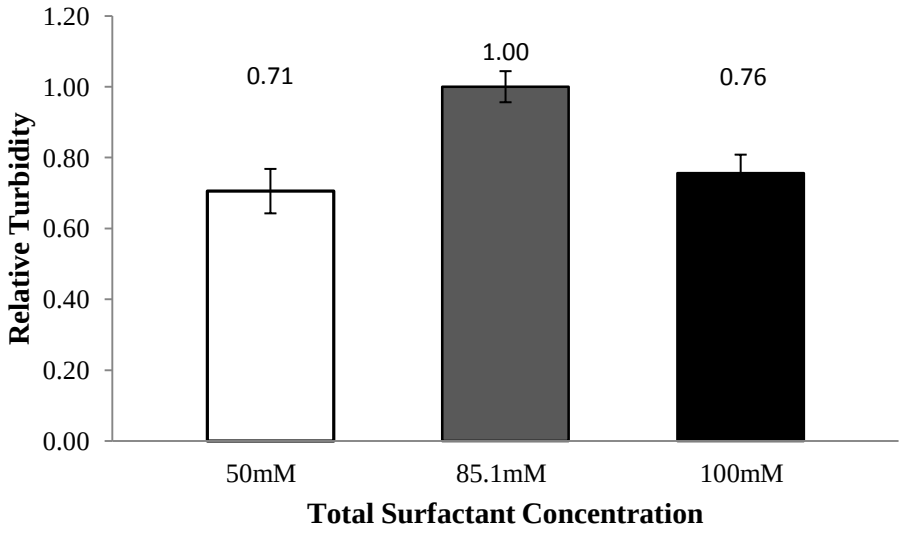

Figure 4.20: Relative turbidity when vary the total surfactant concentration (n=3, error bar=SEAM)

The reduced in nano population when decrease the total concentration may be explained by the stability of the bubbles. Dickinson et al. [16] showed that less particle

concentration lead to less stability. Since the nanobubbles has to be in the separation fennel at least three hours for three times in washing step, the less stable bubbles may not survive in this step. However, when increasing the total concentration, the nano population also decreased. This can be explained by size of particles. [17] The mean size particles of total concentration of 100 mM was around 200 nm, compared with around 60 nm for 85.1 mM. The relatively larger particle may produce larger bubbles, which was rise to the middle layer faster, resulting in decreasing in nanobubbles population.

4.3.3 The Effect of Sonication Power on Nanobubble Population

The next parameter in this study was sonication power. Brotchie et al. [67] showed that the power of sonication had an effect to the mean bubble size. Figure 4.21 shows the mean diameter of nanobubbles when sonication power was varied. The standard sonication power was 110 W. This study compared the standard sonication power by decreasing the sonication power to 80 W and increasing the sonication power to 140 W (the maximum power available). The mean diameter of nanobubbles was not statistically significant different in all conditions.

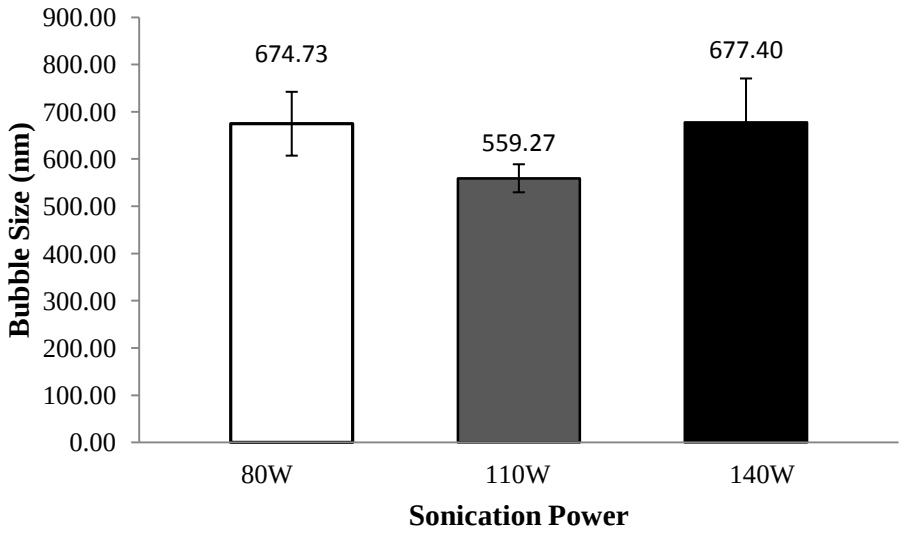

Figure 4.21: Bubble mean diameter when vary the sonication power (n=3, error bar=SEAM)

The results of the turbidity measurement when varying the sonication power are shown in Figure 4.22. The amount of nanobubbles was again highest at the standard sonication power of 110W. This decrease and increase in sonication power resulted in a decrease in turbidity, which means a smaller fabricated nanobubbles population. Both decreasing and increasing, however, was not statistically significant when compared with the standard conditions.

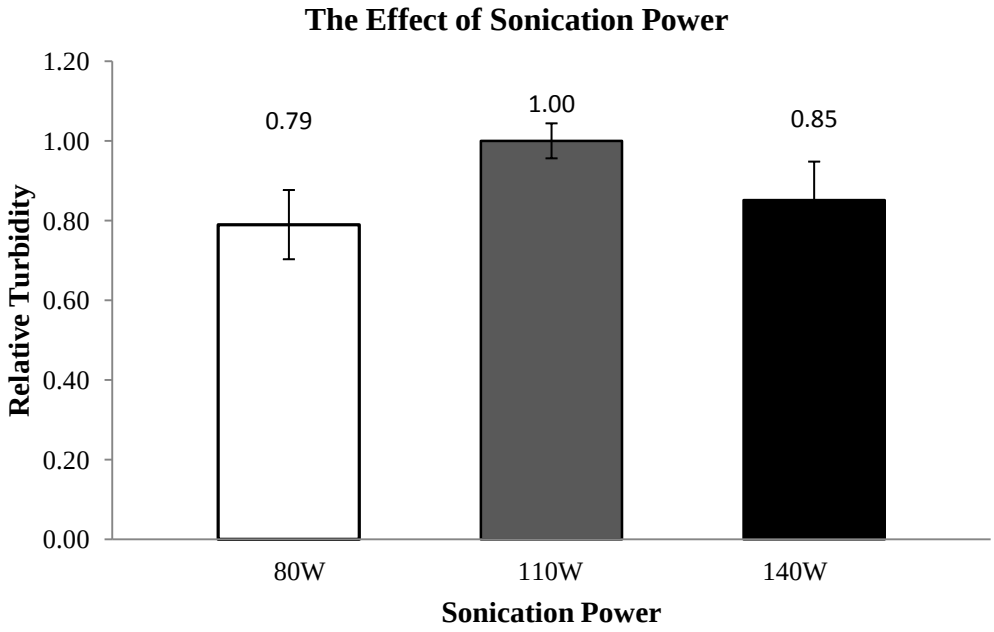

Figure 4.22: Relative turbidity when vary the sonication power (n=3, error bar=SEAM)

4.3.4 Conclusion on Nanobubbles

The nanobubbles nSE61 can be fabricated and collected separately from microbubbles if needed. These nanobubbles, however, gave less ultrasound enhancement and were less stable compared to microbubbles of SE61. There will be some benefit for less stability of nanobubbles under ultrasound because the nanobubbles will be used as drug carriers for the final goal of the study. Therefore, it should be beneficial for them to be less stable. By means of the turbidity measurement, the maximum amount of nanobubbles population was fabricated at the standard conditions.

4.4 *In vivo* Tumor Perfusion

Because a greater nanobubbles population of SE61 was successfully fabricated compared with ST68, specific aim 4 tested the hypothesis that among the two agents with different sized distributions, the agent with the smaller bubbles would be better in ultrasound imaging and tumor perfusion.

4.4.1 ST68 and SE61 Size Distribution

The agents were fabricated in the same conditions as the total concentration of surfactants at 85.1 mM and the ratio of Span 60 to Tween 80 and Span 60 to TPGS at the percentage ratio of 80:20. The amount of 1.5 g of NaCl, which is amount according to the standard procedure of a previous study, was added into the mixture of surfactants in 50 ml of PBS. Other studies have shown that the NaCl enhances the nano population, possibly due to charge stabilization since the bubbles can acquire a static negative charge during fabrication. [68] The mixture fabricated also followed the standard procedure. At the end of the third washing step, a middle layer was collected and mixed with cold PBS at the ratio of 1:1 for ST68. For SE61, the amount of 75 ml from the bottom layer was discarded after one hour at each washing step, and then the mixture of nano- and microbubbles was collected.

The number size distribution shows that ST68 is comprised of bubbles ranging from 955 nm to 2.67 μm with a mean diameter of 1.63 μm. For SE61, the size ranged from 342 nm to 900 nm with a mean diameter of 548 nm (Figure 4.23, ST68 in green and SE61 in red). This result confirmed the idea that the nanobubbles were produced more when changing from Tween 80 to TPGS.

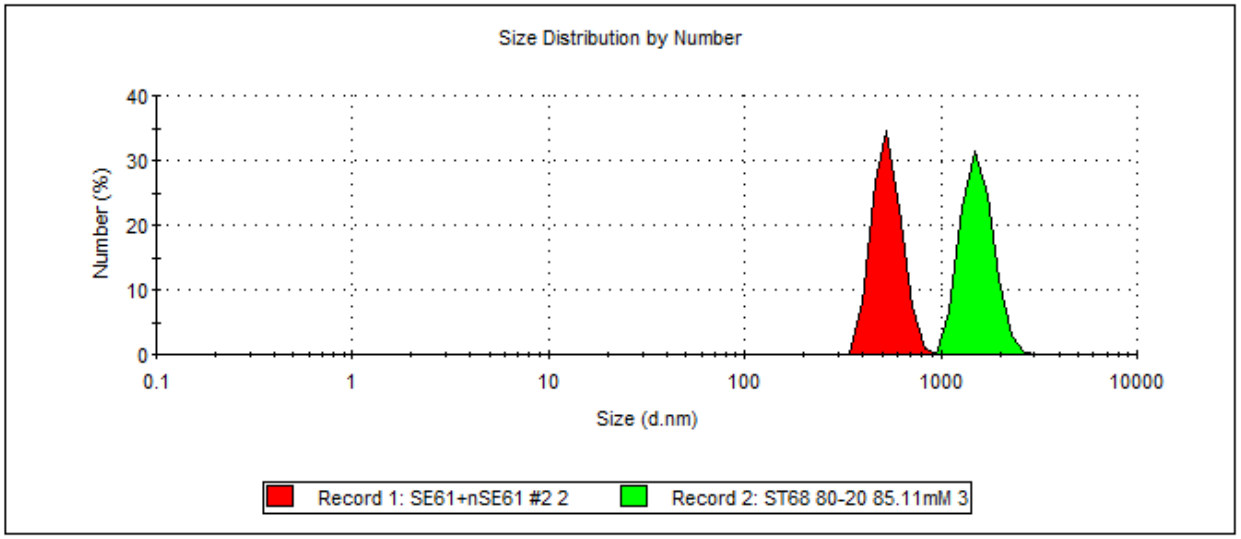

Figure 4.23: Size distribution of ST68 and SE61

4.4.2 *In-vitro* Ultrasound Enhancement and Stability Testing

Both agents gave a good ultrasound enhancement in *in-vitro* testing. The maximum enhancement for ST68 was 23.61 ± 0.97 dB and 23.38 ± 0.98 dB for SE61 (Figure 4.24a). Both agents also showed almost the same stability (Figure 4.24b). The half life of ST68 was 5.54 ± 0.43 min and 5.20 ± 0.20 min for SE61. There is no statistically significant difference between both agents in *in-vitro* ultrasound testing.

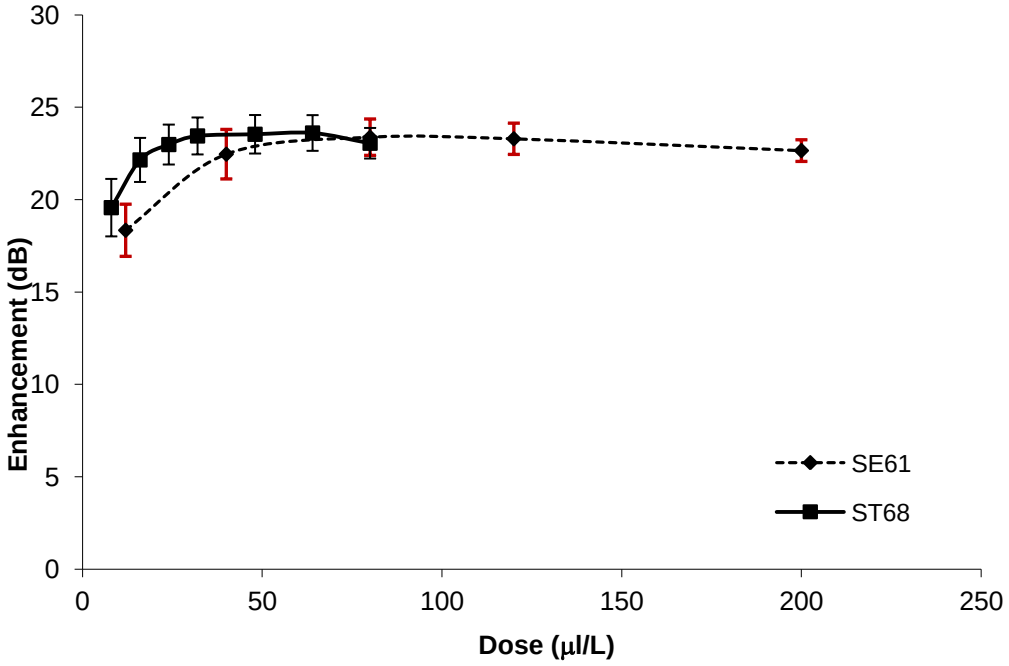

(a)

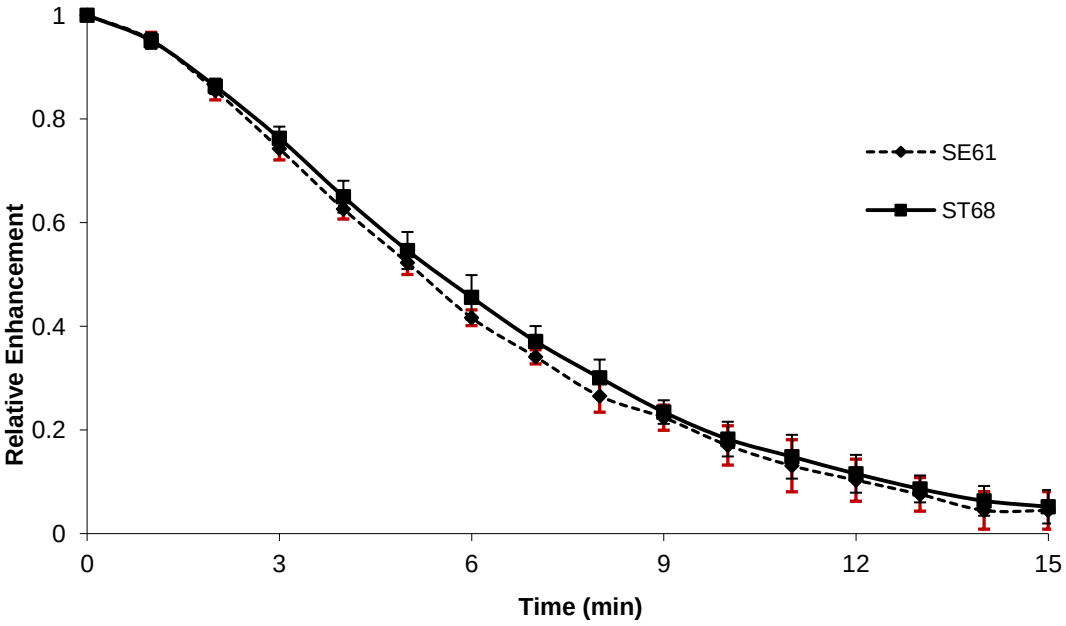

(b)

Figure 4.24 *In vitro* ultrasound enhancement (a) and stability (b) testing of ST68 and SE61 (n=3, error bar=SEAM)

4.4.3 Tumor Perfusion Imaging

The Power-Doppler images for both agents are shown in Figure 4.25. Each time frame is marked at the time of injection (a), SE61 arrival time (b), ST68 arrival time (c), SE61 maximum coverage time (d), ST68 maximum coverage time (e), and time after maximum coverage for both agents (f). B-mode images for Δ-projection are shown in Figure 4.26. Each time frame is marked at time of injection (a), SE61 arrival time (b), SE61 maximum arrival time (c), ST68 arrival time (d), ST68 maximum arrival time (e), SE61 maximum coverage time (f), and ST68 maximum coverage time (g). The tumor vessel can be clearly seen during the wash-in phase in B-mode but is hard to see in Power-Doppler.

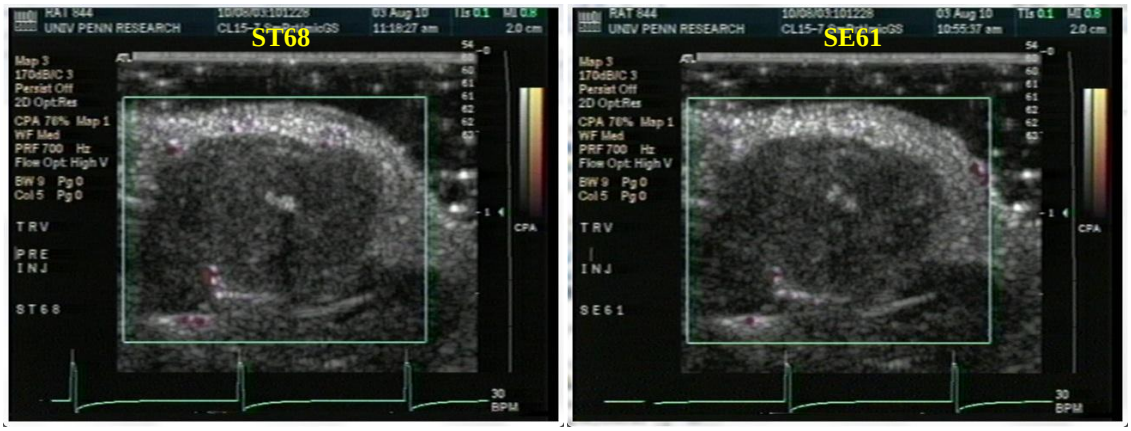

(a) 0, injection time

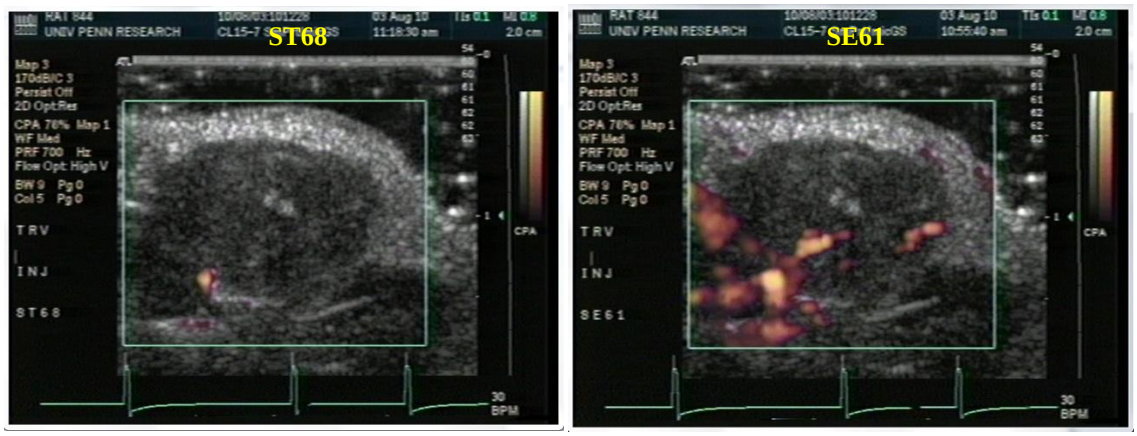

(b) 3.5s, SE61 arrival time

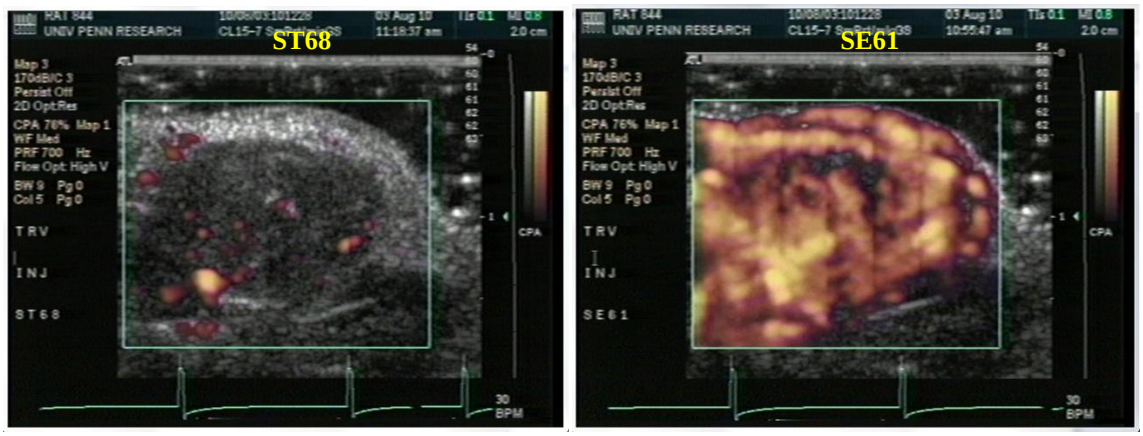

(c) 9.75s, ST68 arrival time

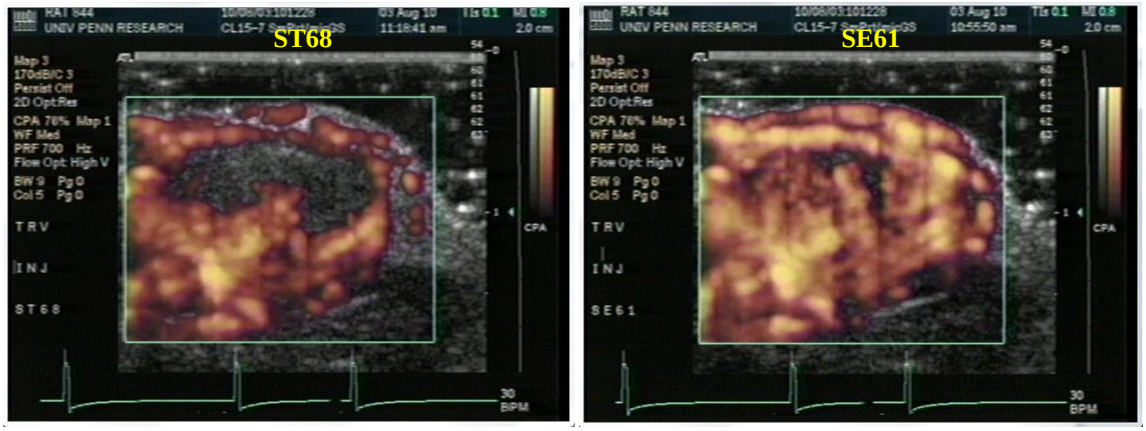

(d) 13.75s, SE61 maximum coverage time

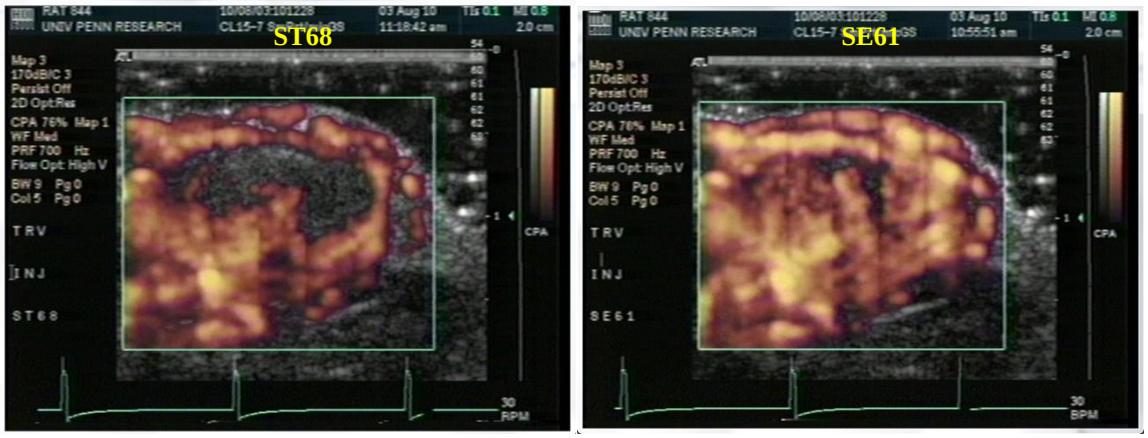

(e) 14.75s, ST68 maximum coverage time

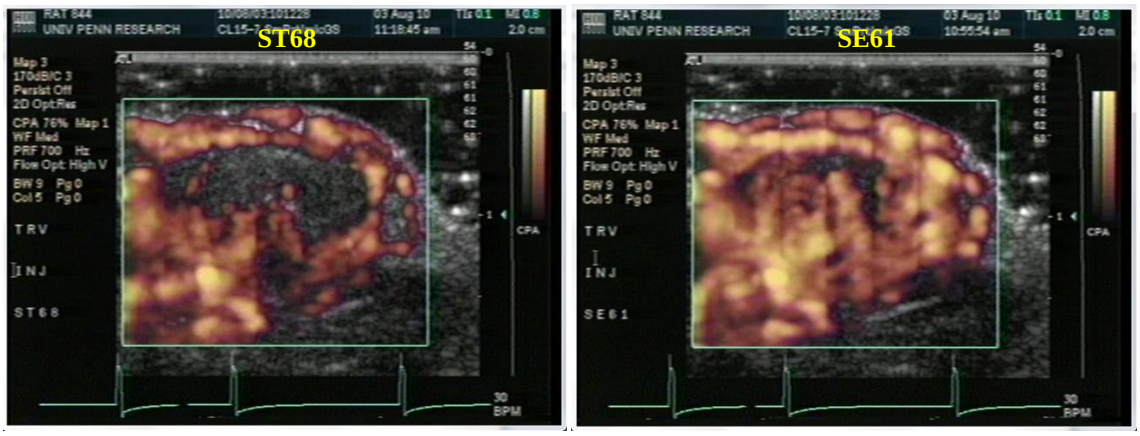

(f) 17.75s, time at after maximum coverage of both agents

Figure 4.25 Power Doppler Images of ST68 (left) and SE61 (right) at different time

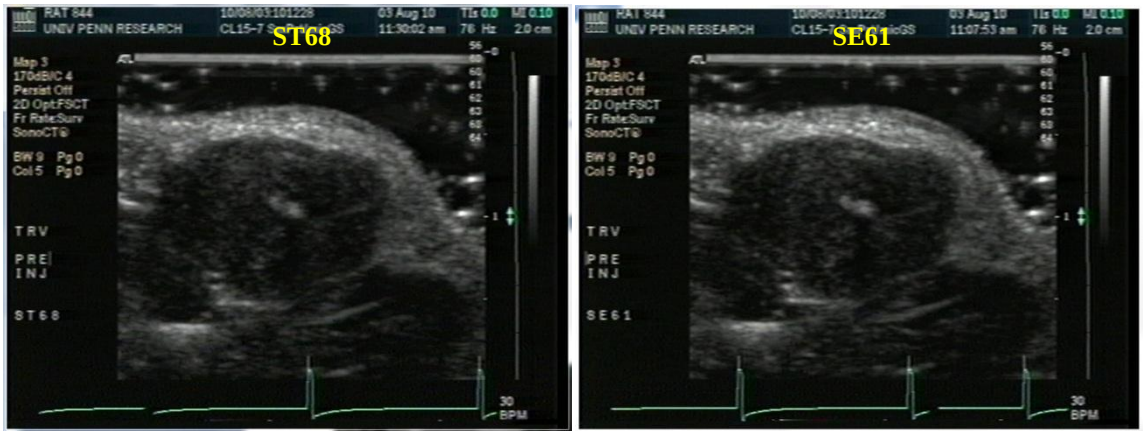

(a) 0, injection time

(b) 6.7s, SE61 arrival time

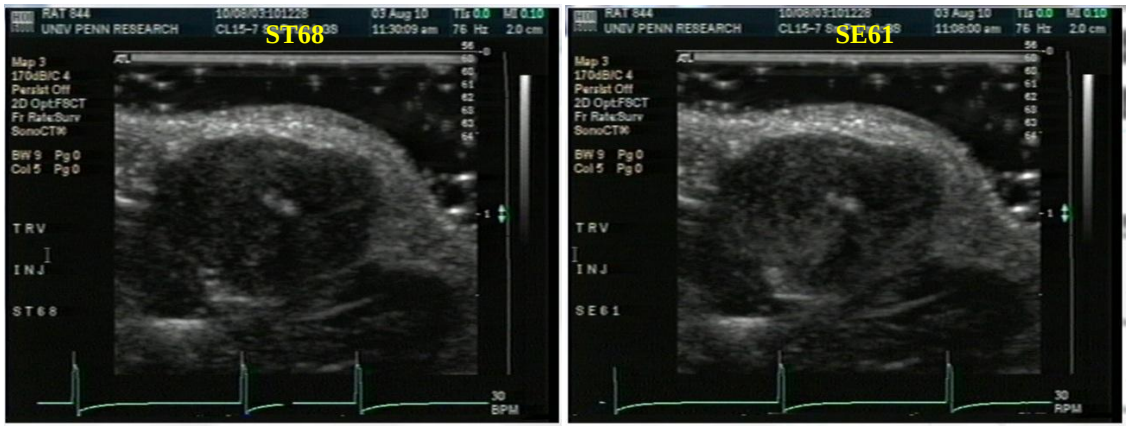

(c) 7.53s, SE61 maximum arrival time

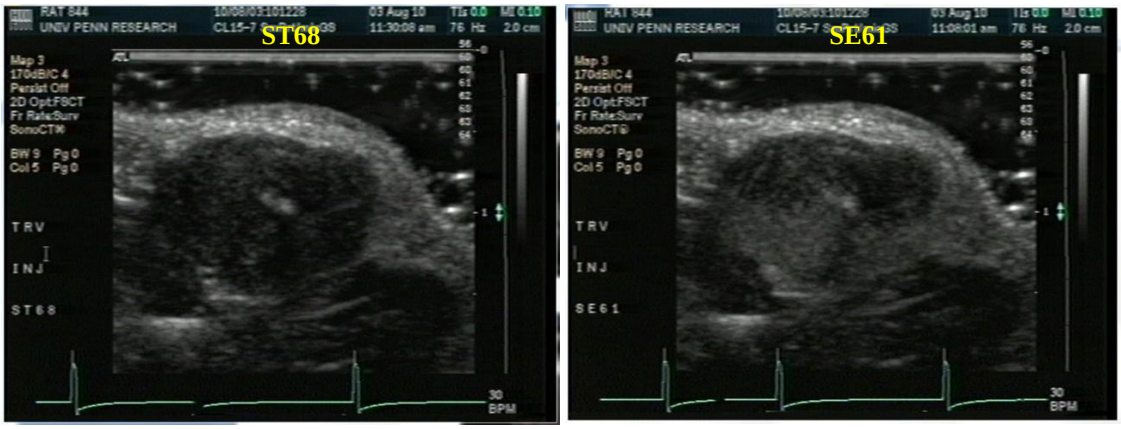

(d) 8.43s, ST68 arrival time

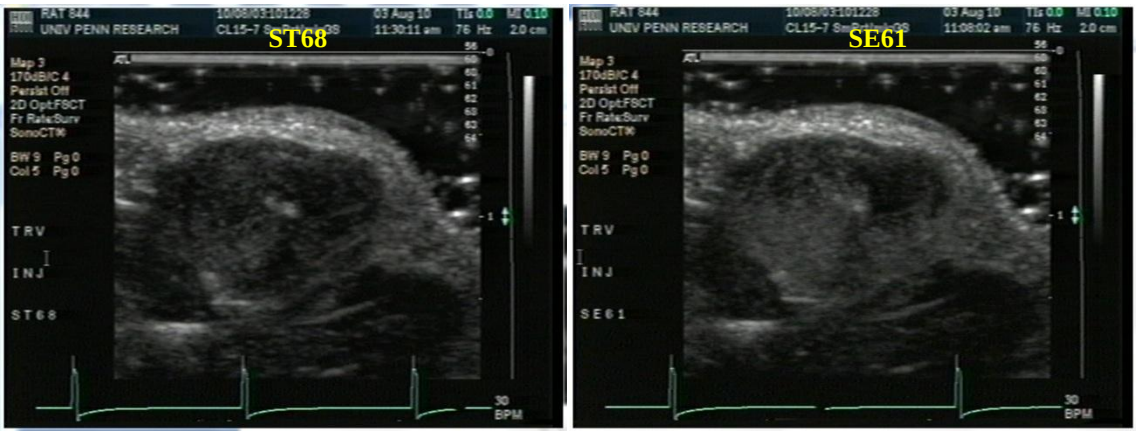

(e) 9.51s, ST68 maximum arrival time

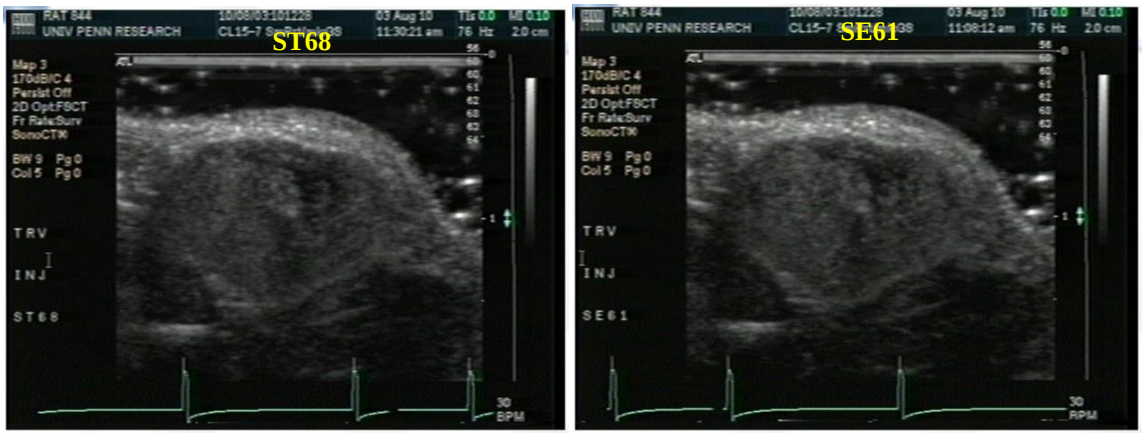

(f) 19.4s, SE61 maximum coverage time

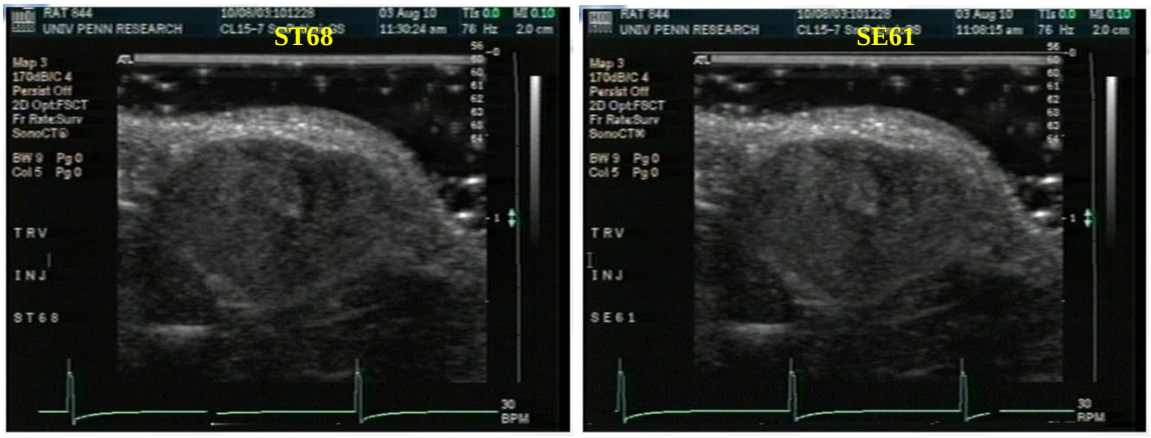

(g) 22.3s, ST68 maximum coverage time

Figure 4.26 B-mode images for Δ-projection of ST68 (left) and SE61 (right) at different time

4.4.4 Tumor Data Analysis

Data analyses for Power Doppler imaging are shown in Figure 4.27 and also summarized in Table 2.2. For the wash-in phase, SE61 reached the tumor earlier than ST68. Time to enhancement for SE61 was 6.50±0.88 seconds and 8.67±0.53 seconds for ST68 (p=0.036, n=6). However, in time to maximum coverage for both agents, there is no statistically significant difference (17.42±2.17 seconds for SE61 and 19.79±3.16 seconds for ST68), (Figure 4.27a). For the wash-out phase, there is a statistically significant difference for early clearance between both agents. Time to 67% coverage for SE61 was 76.83±14.47 second and for ST68 was 54.46±10.77 seconds (p=0.023, n=6). Time to 50% coverage for SE61 and ST68 were 98.58 ± 15.26 and 76.83±14.47 second, respectively (p=0.038, n=6). However, there was no statistically significant difference for late clearance (time to 33% coverage for SE61 is 118.25 ± 15.02 seconds and 100.42 ± 8.14 seconds for ST68 with p=0.057, n=6), (Figure 4.27b). It should be noted that all time to 67%, 50% and 33% coverage was time at maximum coverage to the time that the tumor coverage was at 67%, 50% and 33%, respectively.

For Power-Doppler imaging, there is no statistically significant difference between both agents in maximum coverage and area under curve (AUC). (Figure 4.27c and 4.27e) In contrast the perfusion ratio (arbitrary units) calculated by a first-pass kinetics gamma-variate function shows that there is statistically significant difference between both agents (63.30 ± 5.45 for SE61 and 42.03 ± 6.54 for ST68 with p = 0.027, n=6). (Figure 4.27d)

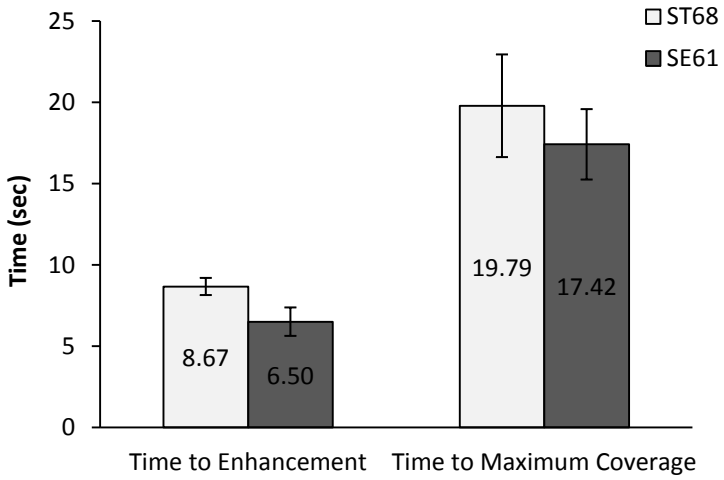

(a)

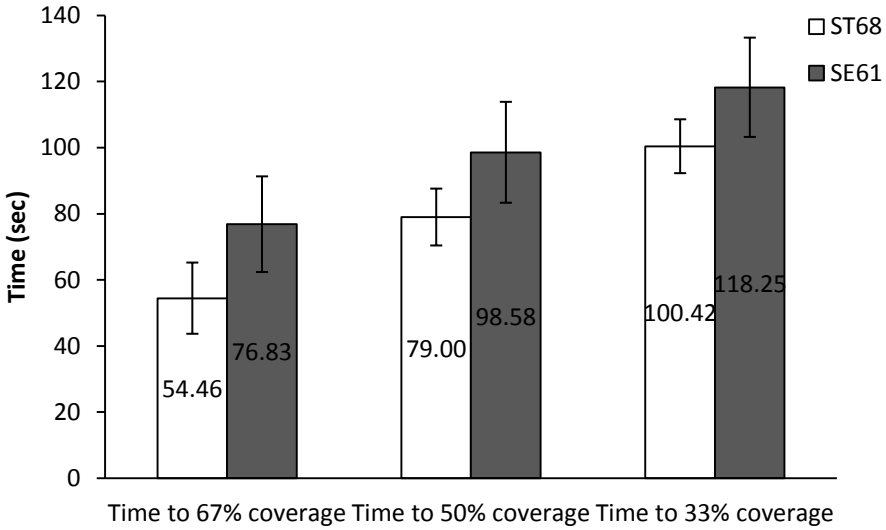

(b)

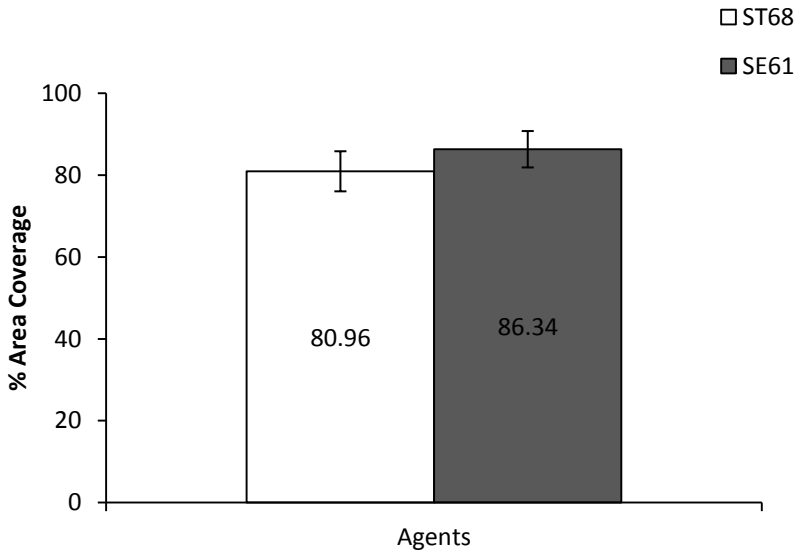
ST68
SE61
100
80
60
40
20
0
% Area Coverage
80.96
86.34
Agents

(c)

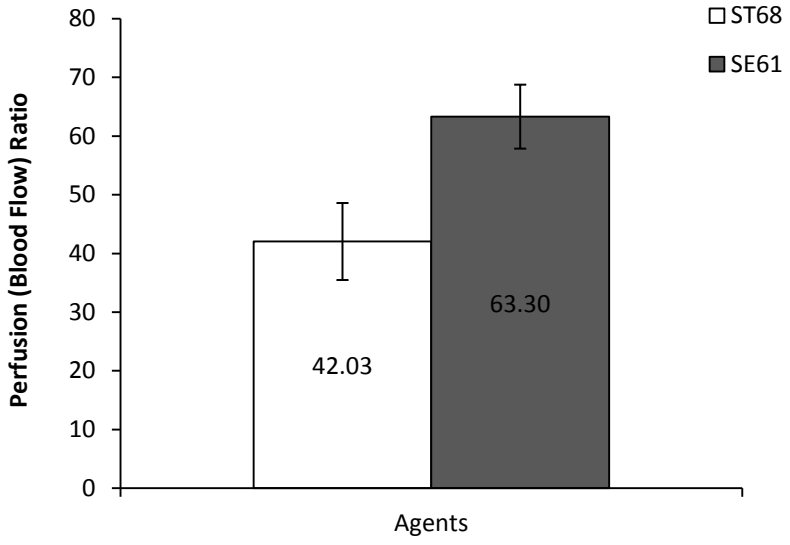
ST68
SE61
80
70
60
50
40
30
20
10
0
Perfusion (Blood Flow) Ratio
42.03
63.30
Agents

(d)

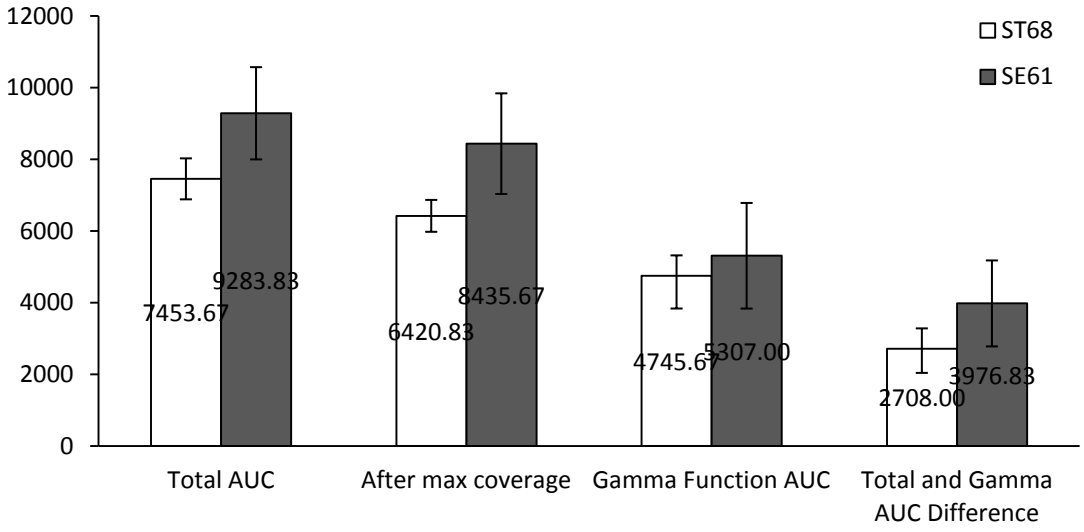

(e)

Figure 4.27 Quantitative analysis of Power Doppler imaging: (a) wash-in phase, (b) wash-out phase, (c) maximum area coverage, (d) tumor perfusion, and (e) area under curve (n=6, error bar=SEAM)

Table 4.2 Summary of quantitative analysis of Power Doppler imaging * ($p<0.05$, n=6)

Parameters		ST68	SE61
Wash-in Phase	Time to Enhancement	8.67±0.53s	6.50±0.88 s*
	Time to Maximum Coverage	19.79±3.16s	17.42±2.17s
Wash-out Phase	Time to 67% Coverage	54.46±10.77s	76.83±14.47s*
	Time to 50% Coverage	76.83±14.47s	98.58 ± 15.26s*
	Time to 33% Coverage	100.42 ± 8.14s	118.25 ± 15.02s
Percent Area Coverage		86.34 ± 4.45	80.96 ± 4.90
Perfusion (Blood Flow) Ratio		42.03 ± 6.54	63.30 ± 5.45*
Area under Curve	Total	9284 ± 1287	7454 ± 572
	After Max Coverage	8436 ± 1404	6421 ± 445
	Gamma Function	5307 ± 1474	4746 ± 911
	Difference of Total and Gamma Function	3977 ± 1200	2708 ± 671

There was an improvement in tumor perfusion with the SE61 which contained a higher proportion of nanobubbles compared to ST68. Residence time in the tumor was also greater. It should be noted that the difference between SE61 and ST68 in the early clearance phase was more pronounced than the late clearance in the wash-out phase. This should support the hypothesis that the small bubbles can exit through the 'leaky' vessel making it harder to exit the tumor. The study in the last specific aim showed that the smaller the bubble, the less stable it is. This might explain why the early clearance is more pronounced than the latter clearance.

Data analyses for Δ-projection imaging are shown in Figure 4.28. All time to enhancement, time to maximum coverage, and maximum arrival time (which means the time for the maximum amount of the agent to enter the tumor) were statistically significant different between both agents. (Figure 4.28a) For the maximum coverage, however, there is not statistically significant difference between both agents, which was in agreement with Power-Doppler imaging. (Figure 4.28b)

4.4.5 Conclusion on *in vivo* Tumor Perfusion

Both agents gave excellent improvement in image contrast of the tumors. However, the choice of mode of imaging makes a difference in the details of the image. Both of our agents showed a visible vascular structure in the tumor in B-mode which is superior to Power Doppler image. The agent with the higher nano population entered the tumor faster, perfused better, and took a longer time to clear out. From these results, SE61 will be a good candidate for using as an ultrasound triggered drug carrier.

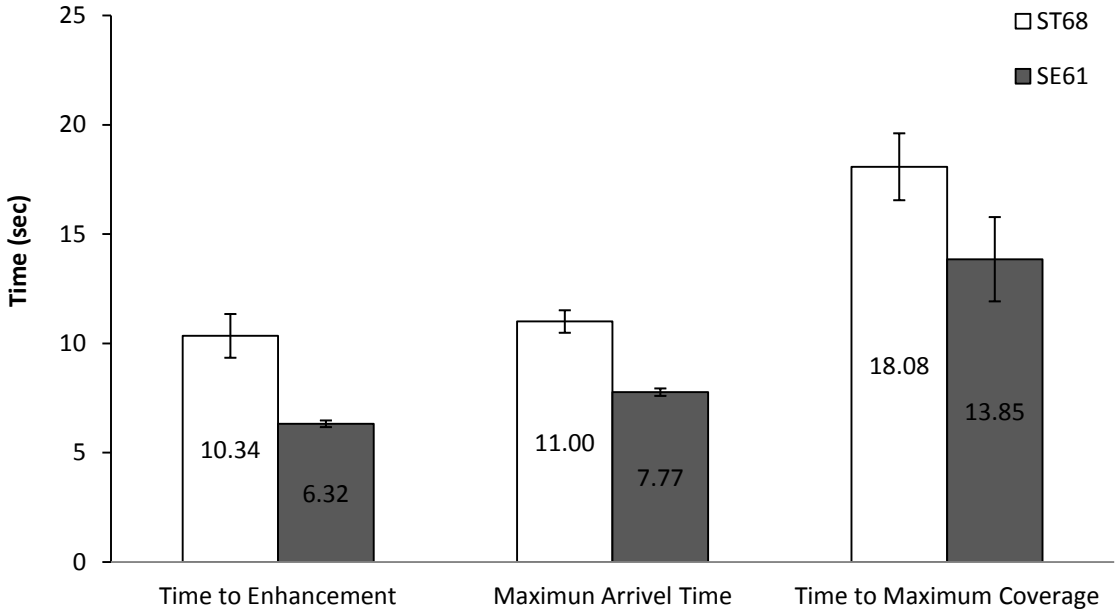

(a)

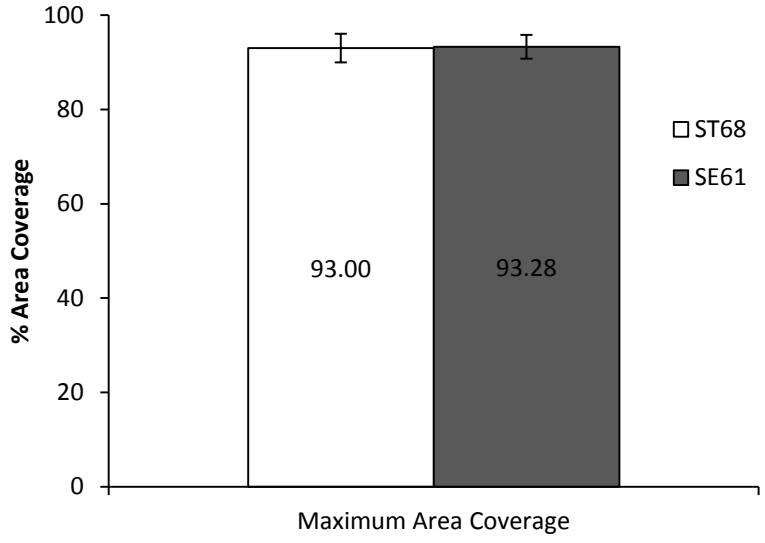

(b)

Figure 4.28 Quantitative analysis of Power Doppler imaging: (a) wash-in phase and (b) maximum area coverage, (d) tumor perfusion, and (e) area under curve (n=4, error bar=SEAM)

4.5 UCA as Carrier for Drug Delivery

The next study was to investigate the potential of the bubbles to act as drug carriers. Because the shell of the bubble was comprised of a hydrophobic portion, the hypothesis that the hydrophobic drug can be intercalated into the bubbles shell was tested. First, Nile Red was chosen as a hydrophobic drug model because its fluorescent property depends on its surrounding hydrophobicity, a so-called solvatochromic probe. This should be proof of principle that the hydrophobic drug can be intercalated into the hydrophobic shell of the bubbles. Second, a highly hydrophobic drug, Paclitaxel, was used to intercalate into the bubbles. The quantitative analysis was conducted to measure the amount of the Paclitaxel that could be intercalated into the bubbles and hence determine if the concentration would be high enough to warrant future study on the effectiveness of Paclitaxel loaded drug to cancer cell lines and *in vivo* testing.

4.5.1 Nile Red as a Hydrophobic Drug Model

The agent ST68 was first chosen for drug carrier study of Nile Red loaded microbubbles, since this agent is the most well characterized in previous work. Nile Red was added into the solution after the autoclave step and then heated until the solution boiled for 3-5 min. At this point, the solution color changed from milky white to pink or red depending on the amount of Nile Red that was added. This is due to Nile Red becoming dissolved into micelles with a resultant changed color in the non polar environment of the micelle. The solution was then left to cool down to room temperature. Microbubbles were then made by sonication at 110 W for 3 min in the presence of PFC.

The qualitative analysis of Nile Red intercalated in the bubbles can be tested by the fluorescent property of Nile Red. As mentioned before, Nile Red is strongly quenched in aqueous media and will fluoresce depending on the polarity of its environment. As hypothesized, the Nile Red should be intercalated into the hydrophobic shell of the bubbles. If the bubbles are observed under the fluorescent microscopy, the glowing shell of the bubbles against the dark in the solution should be seen. The glowing bubble shell under florescent can be seen in Figure 4.29. This image confirms the hypothesis.

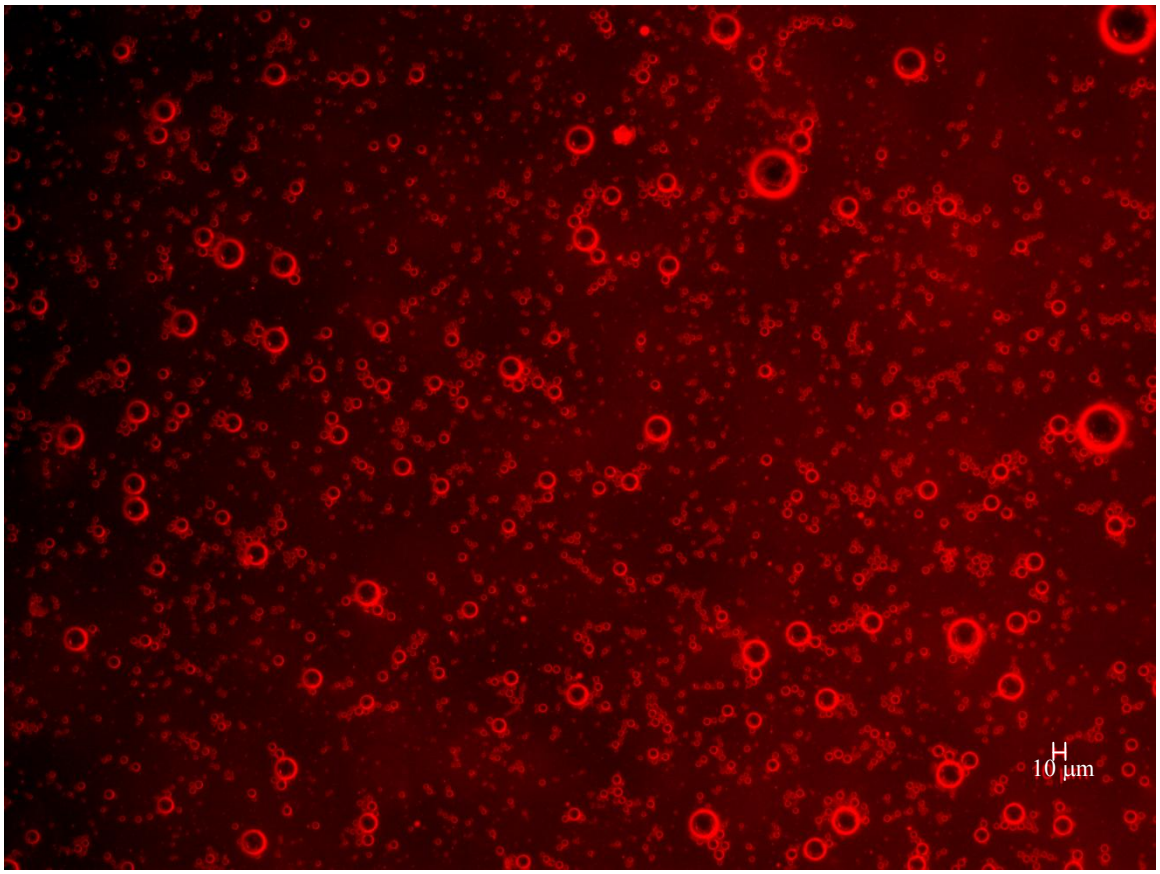

Figure 4.29 ST68 with Nile Red under fluorescent microscope (λ=620nm)

4.5.2. Paclitaxel Loaded UCA

The next goal of this study was try to intercalate Paclitaxel into the shell of the bubble. The amount of 10 mg of Paclitaxel was added into the solution after the sterilization step and then heated until the solution boiled for 30 min. The solution was then left to cool down to room temperature and follow the standard procedure for fabricating Paclitaxel loaded bubbles.

Both Paclitaxel loaded agents still gave a good ultrasound enhancement and no statistically significant difference in *in-vitro* testing compared with the control. (Figure 4.30a). Both Paclitaxel loaded agents show more stability when compared with the control but with no statistically significant difference (Figure 4.30b).

The quantitative measurement for the amount of Paclitaxel was done by HPLC. A calibration curve by area under peak is shown in Figure 4.31. The linear regression shows a very good agreement with raw data (R^2=0.9985)

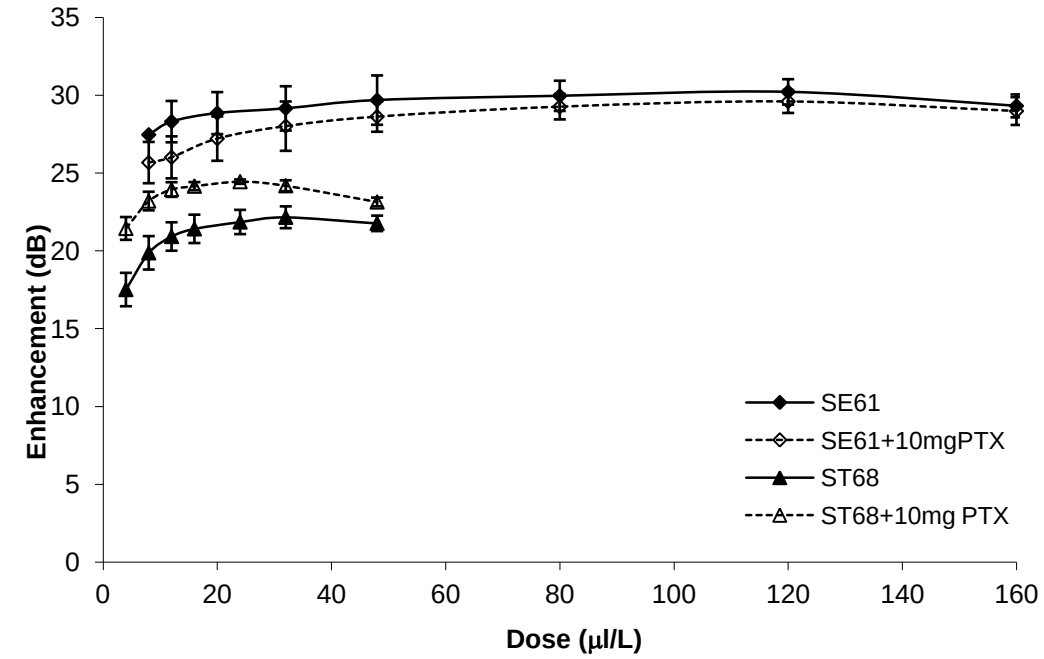

(a)

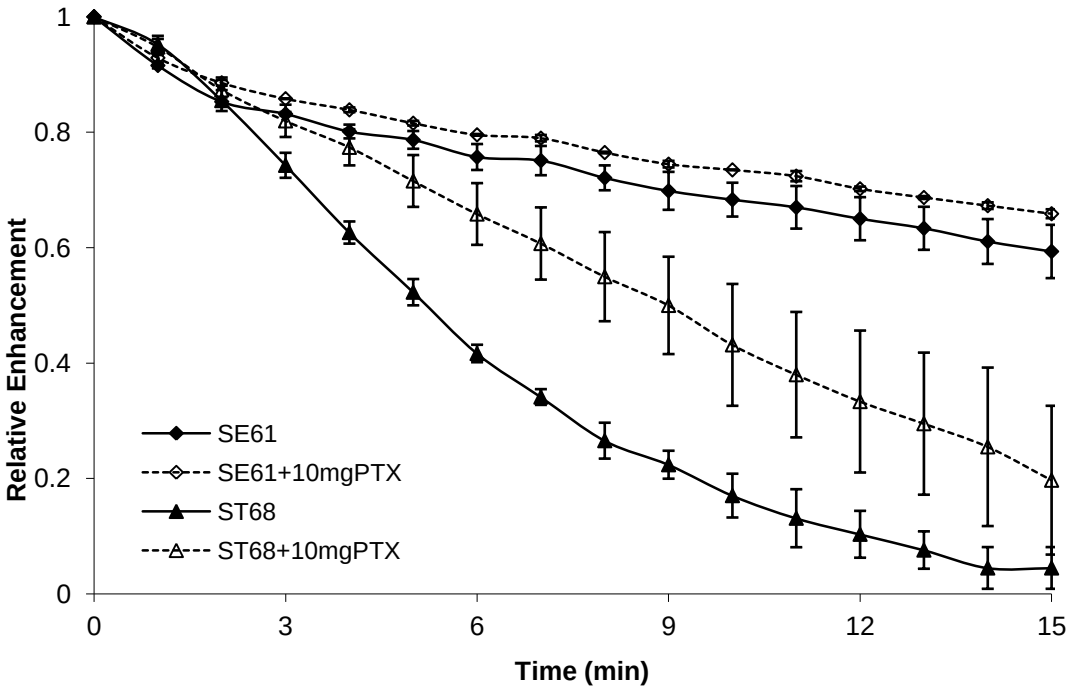

(b)

Figure 4.30 *In vitro* ultrasound enhancement (a) and stability (b) testing of ST68 and SE61 (n=3, error bar=SEAM)

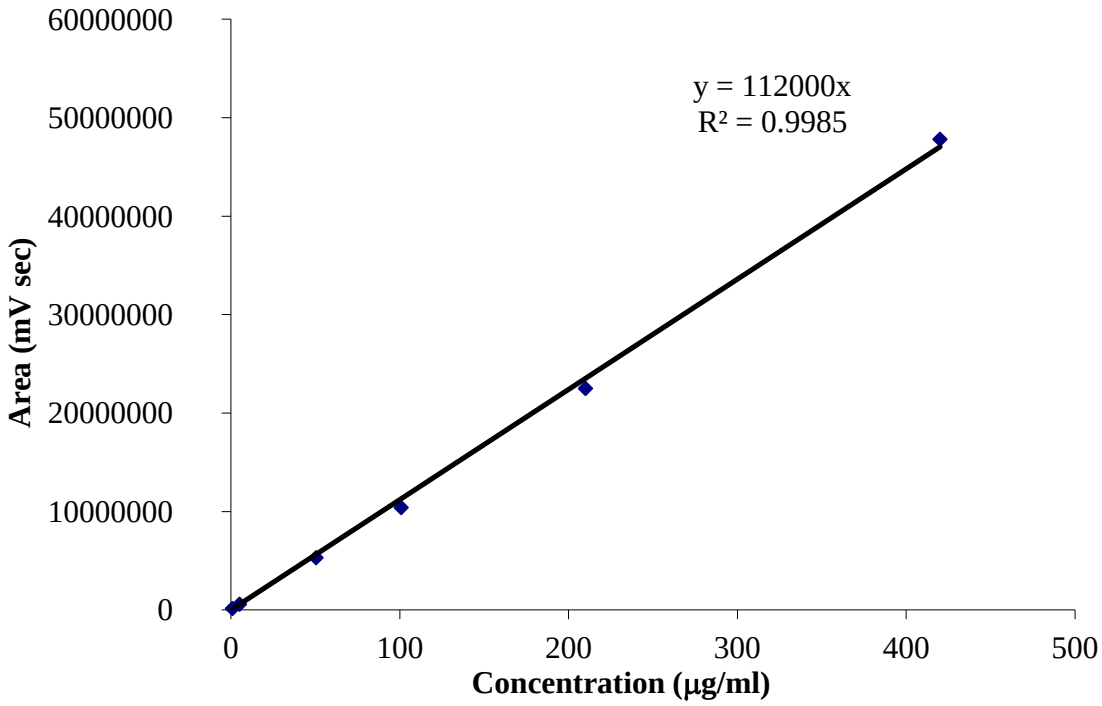

Figture 4.31 A calibration curve of Paclitaxel by HPLC with mobile phase of Acetoniltrile:DI water at percentage ratio of 60:40 at 1 ml/min by UV detector at 227 nm

The amount of Paclitaxel intercalated into the SE61 and ST68 is shown in Figure 4.32. The concentration of Paclitaxel in the solution was almost the same for both agents (3.79 μg/ml for SE61 and 3.77 μg/ml for ST68). This concentration was well above the suggested effective level of 0.043 μg/ml [69, 70].

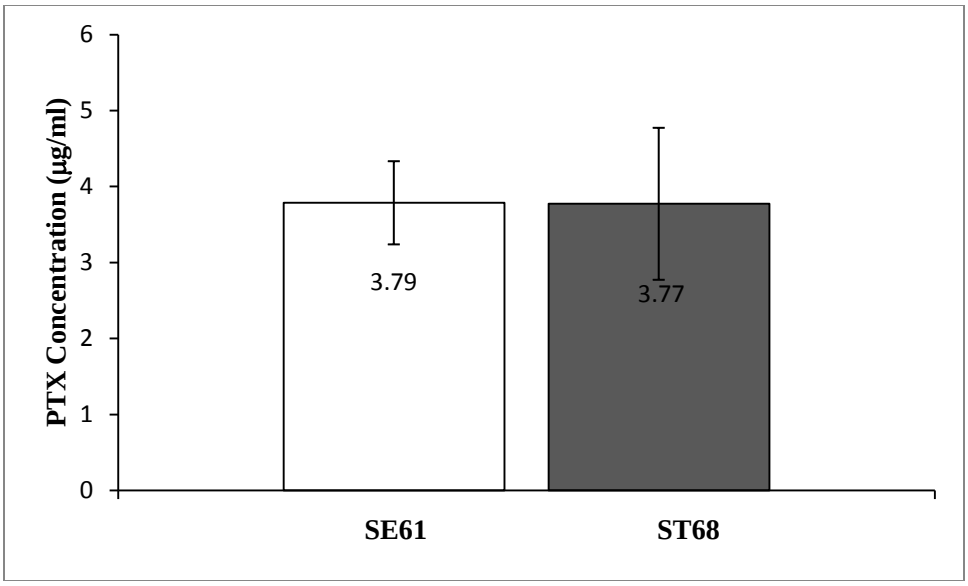

Figure 4.32 Paclitaxel concentration intercalated in SE61 and ST68 by HPLC with mobile phase of Acetoniltrile:DI water at percentage ratio of 60:40 at 1 ml/min by UV detector at 227 nm (n=3, error bar=SEAM)

4.5.3. Conclusion on UAC as Carrier for Drug Delivery

The hydrophobic drug can be intercalated into the microbubble shell. For Paclitaxel, the drug did not statistically alter the acoustic enhancement and the stability *in vitro* testing. For both agents, the amount of Paclitaxel loading was not different and the concentration was close to 100 times higher than the suggested effective concentration. [69, 70] The success of intercalating Paclitaxel into UCA can lead to further study of such alternative methods of cancer treatment by Paclitaxel with the goal of improving the efficiency of treatment and the reduction of undesirable side effects.

5. CONCLUSIONS AND FUTURE RECOMMENDATIONS

5.1 Conclusions and Contribution to Science

The objectives of this study were to test a new model, particle stabilized foam, in a surfactant-based UCA, and to fabricate a greater nanobubbles population UCA and put them to the test that the agent can perfuse in a tumor better than the rich microbubbles UCA. Not only imaging capability of the agents was tested, but also the ability to act as drug carriers was investigated.

The new agent, SE61, was developed by replacing the Tween 80 component in ST68. The new agent gives better ultrasound enhancement and stability for *in vitro* testing. The stability of the agents under ultrasound is influenced by the size of particles that we used to make the bubbles.

Not only does it have better acoustic properties, the new agent SE61 is also comprised of more nanobubbles using the same conditions used to fabricated the ST68.

In vivo tumor imaging for the two agents was conducted. Both agents provided an excellent improvement in imaging of vascular structure in the tumor. The choice of mode of imaging, however, makes a difference in the details of the image. The further imaging analysis and calculation showed that SE61 perfuses better and take longer to clear out of the tumor, possible as a result of the larger nano population.

The ability of the agents to act as drug carriers was also tested. The results show that it was possible to intercalate the hydrophobic drug into the shell of the agents. The highly hydrophobic cancer treatment drug Paclitaxel can be loaded into the agent with higher than the recommended concentration for the minimum effective level.

These results show the advance in tumor perfusion in ultrasound imaging. With the particle stabilized bubble model, this study can lead to an alternative way for advance drug delivery for cancer treatment.

5.2 Future Recommendations

For each specific aim, further study can lead to improvement and better understanding.

In specific aim 1, the contact angle of the particles between PBS and PFC should be measured. The measurement of contact angle may also help to explain the stability and size of the bubble. With the particle stabilized bubble model, it will be interesting to see if it possible to use drug particles to stabilized the bubble. Not only will this improve drug loading capacity, it also will be a new method for drug delivery.

For specific aim 2, Brotchie et al. found that one parameter that affected the size of the bubble when using a sonicator to form bubbles is the frequency of sonication. [69] It cannot be tested in this study because a sonicator that can change in frequency is not commercially available.

Finally, in specific aim 4, the results of this study show that it is possible to loading the drug into the agent. However, the effectiveness of drug loaded agent was not tested. *In vitro* and *in vivo* effectiveness should be further investigated.

For a long term goal, the hypothesis that the drug loaded surfactant-based UCA with ultrasound will be more effective still has to be tested. It is also a room for improvements in terms of targeting imaging and drug delivery. The addition of targeting ligands may allow development of agents with a greater affinity for these improvements.

List of References

1. American Cancer Society. Cancer Facts and Figures. 2009.

2. S.-S. Feng, S. Chien. Chemotherapeutic Engineering: application and further development of chemical engineering principles for chemotherapy of cancer and other diseases. Chemical Engineering Science 58 (2003) 4087-4114.

3. S. Singhal, C. C. Moser, and M. A. Wheatley, Surfactant-stabilized microbubbles as ultrasound contrast agents: Stability study of Span 60 and Tween 80 mixtures using a Langmuir Trough. Langmuir 9 (1993) 2426-2429.

4. M. A. Wheatley, S. Singhal. Structural studies on stabilized microbubbles: development of a novel contrast agent for diagnostic ultrasound. Reactive Polymers 25 (1995) 157-166.

5. F. Forsberg, Y. Wu, J. Liu, I. R. S. Makin, W. Wang, and M. A. Wheatley. Quantitative acoustic characterization of a new surfactant-based ultrasound contrast agent. Ultrasound in Med. & Biol. 23 (1997) 1201-1208.

6. F. Forsberg, R. Basude, J. Liu, J. Asessandro, W. T. Shi, N. M. Rawool, B. B. Goldberg, and M. A. Wheatley. Effect of filling gases on the backscatter from contrast microbubbles: Theory and *in vivo* measurement. Ultrasound in Med. & Biol. 25 (1999) 1203-1211.

7. R. Basude, J. W. Duckworth, and M. A. Wheatley. Influence of environmental conditions on a new surfactant-based contrast agent: ST68. Ultrasound in Med. & Biol. 26 (2000) 621-628.

8. R. Basude, M. A. Wheatley. Generation of ultraharmonics in surfactant base ultrasound contrast agents: use and advantages. Ultrasonics 39 (2001) 437-444.

9. B. E. Oeffinger, M. A. Wheatley. Development and characterization of nano-scale contrast agent. Ultrasonics 42 (2004) 343-347.

10. M. A. Wheatley, F. Forsberg, N. Dube, M. Patel, and B. E. Oeffinger. Surfactant-stabilized contrast agent on the nanoscale for diagnostic ultrasound imaging. Ultrasound in Med. & Biol. 32 (2006) 83-93.

11. T. G. Leighton. What is ultrasound?. Progress in Biophysics and Molecular Biology 93 (2007) 3–83.

12. F. Forsberg, D.A. Merton, J.B. Liu, L. Needleman, B.B. Goldberg. Clinical applications of ultrasound contrast agents. Ultrasonics 36 (1998) 695-701.

13. V. Sboros. Response of contrast agents to ultrasound. Advanced Drug Delivery 60 (2008) 1117–1136.

14. M. Bertolotto and O. Catalano. Contrast-enhanced ultrasound: Past, present, and future. Ultrasound Clin 4 (2009) 339–367.

15. N. Jong, F. J. T. Cate. New ultrasound contrast agent and technological innovations. Ultrasonics 34 (1996) 587-590.

16. E. Dickinson, R. Ettelaie, T. Kostakis, and B. S. Murray. Factor controlling the formation and stability of air bubbles stabilized by partially hydrophobic silica nanoparticles. Langmuir 20 (2004) 8517-8525.

17. S. Fujii, P. D. Iddon, A. J. Ryan, and S. P. Armes. Aqueous particulate foams stabilized solely with polymer latex particles. Langmuir 22 (2006) 7512-7520.

18. B. P. Binks, B. Duncumb, and R. Murakami. Effect of pH and salt concentration on the phase inversion of particle-stabilized foams. Langmuir 23 (2007) 9143-9146.

19. B. P. Binks and A. Desforges. Synergistic stabilization on emulsion by mixture of surface-active nanoparticles and surfactant. Langmuir 23 (2007) 1098-1106.

20. S. L. Kettelwell, A. Schmid, S. Fujii, D. Dupin, and S. P. Armes. Is latex surface charge an important parameter for foam stabilization?. Langmuir 23 (2007) 11381-11386.

21. B. P. Binks, M. Kirkland, and J. A. Rodrigues. Origin of stabilisation of aqueous foams in nanoparticles-surfactant mixtures. Soft Matter 4 (2008) 2373-2382.

22. M. D. Eisner, S. A. K. Jeelani, L. Bernhard, and E. J. Windhab. Stability of foams containing proteins, fat particles, and nonionic surfactants. Chem. Eng. Sci. 62 (2007) 1974-1987.

23. S. Zhang, Q. Lan, Q. Liu, J. Xu and D. Sun. Aqueous foams stabilized by Laponite and CTAB. Colloids and Surfaces A: Physicochemical Engineering 317 (2008) 406-413.

24. R. G. Algargova, D. S. Warhadpande, V. N. Paunov, and O.D. Velev. Foam Superstabilizatioon by polymer microrods. Langmuir 20 (2004) 10371-10374.

25. T. N. Hunter, R. J. Pugh, G. V. Franks, G. J. Jameson. The role of particles in stabilising foams and emulsions. Advances in Colloid and Interface Science 137 (2008) 57-81.

26. S. Cho, J. Kim, J. Chun, and J. Kim. Ultrasonic formation of nanobubbles and their zeta-potentials in aqueous electrolyte and surfactant solutions. Colloids and Surfaces A: Physicochem. Eng. Aspects 269 (2005) 28–34.

27. M. Matsumoto and K. Tanaka. Nano bubble—Size dependence of surface tension and inside pressure. Fluid Dynamics Research 40 (2008) 546-553.

28. R.J. Pugh. Foaming, foam films, antifoaming and defoamimg. Advance in Colloid and Interface Science 64 (1996) 67-142.

29. B. P. Binks. Particles as surfactants – similarities and differences. Current Opinion in Colloid & Interface Science, 7 (2002) 21-41.

30. U. T. Gonzenbach, A. R. Studart, E. Tvoort, L. J. Gauckler. Ultrastable particle-stabilized foams. Angew. Chem. Int. Ed. 45 (2006) 3526-3530.

31. J. C. Harris. Solubilization- a micellar phenomenon. The Journal of the American Oil Chemists' Society 35 (1958) 428-435.

32. E. Dickinson, R. Ettelaie, T. Kostakis, and B. S. Murray. Factors controlling the formation and stability of air bubbles stabilized by partially hydrophobic silica nanoparticles. Langmuir 20 (2004) 8517-8525.

33. M. Vignes-Adler and D. Weaire. New foams: fresh challenges and opportunities. Current Opinion in Colloids & and Interface Science 13 (2008) 141-149.

34. G. Kaptay. On the equation of the maximum capillary pressure induced by solid particles to stabilize emulsions and foams and on the emulsion stability diagrams. Colloids and Surfaces A: Physicochem. Eng. Aspects 282-283 (2006) 387-401.

35. T. S. Horozov. Foams and foam films stabilised by solid particles. Current Opinion in Colloid & Interface Science 13 (2008) 134-140.

36. A. Lawrie, A. F. Brisken, S. E. Francis, D. I. Tayler, J. Chamberlain, D. C. Crossman, D.C. Cumberland, C. M. Newman. Ultrasound enhances reporter gene expression after transfection of vascular cell in vitro. Circulation 99 (1999) 2617-2620.

37. D. M. Skyba, R.J. Price, A. Z. Linka, T. C. Skalak, S. Kaul. Direct in vivo visualization of intravascular destruction of microbubbles by ultrasound and its local effect on tissue. Circulation 98 (1998) 290-293.

38. R. K. Jain. Delivery of molecular medicine to solid tumors: lessons from in vivo imaging of gene expression and function. J. Control. Release 47 (1987) 3039-3051.

39. G. H. Sakorafas, E. Krespis, G. Pavlakis. Risk estimation for breast cancer development; a clinical perspective**.** Surgical Oncology 10 (2002) 183-192.

40. S. K. Hobbs, W. L. Monsky, F. Yuan, W.G. Roberts, L. Griffith, V. P. Torchilin, R. K. Jain. Regulation of transport pathways in tumor vessels: role of tumor type and microenvironment. Proc. Natl. Acad. Sci. USA 95 (1998) 4607-4612.

41. F. Yuan, M. Dellian, D. Fukumura, M. Leuning, D. D. Berk, V. P. Yochilin, R. K. Jain. Vascular permeability in human tumor xenograft: molecular size dependence and cutoff size. Cancer Res. 55 (1995) 3752-3756.

42. S. Unezaki, K. Maruyama, J.-I. Hosoda, I. Nagae, Y. Koyanagi, M. Nakata, O. Ishida, M. Iwatsuru, S. Tsuchiya. Direct measurement of the extravasation of polyethyleneglucol-coated liposomes into solid tumor tissue by in vivo fluorescence microscopy. Int. J. Pharm. 144 (1996) 11-17.

43. M. Gaumet, A. Vargas, R. Gurney, and F. Delie. Nanoparticles for drug delivery: The need for precision in reporting particle size parameters. European Journal of Pharmaceutics and Biopharmaceutics 69 (2008) 1-9.

44. M. Suzuki, K. Koshiyama, F. Shinohara, S. Mori, M. Ono, Y. Tomita, T. Yano, S. Fujikawa, G. Vassaux, and T. Komada. Nanobubbles enhanced drug susceptibility of cancer cells using ultrasound. Internal Congress Series 1284 (2005) 338-339.

45. Z. Gao, A. M. Kennedy, D. A. Christensen, N. Y. Rapoport. Drug-loaded nano/microbubbles for ultrasonography and targeted chemotherapy. Ultrasonics 48 (2008) 260-270.

46. N. C. Maiti, M. M. G. Krishna, P. J. Britto, and N. Periasamy. Fluorescence dynamics of dye probes in micelles. J. Phys. Chem. B 101 (1997) 11051-11060.

47. M. M. G. Krishna. Excited-state kinetics of the hydrophobic probe Nile Red in membranes and micelles. J. Phys. Chem. A 103 (1999) 3589-3595.

48. K. Nagy, S. Gokturk, L. Biczok. Effect of microenvironment on the fluorescence of 2-hydroxy-substituted Nile Red dye: A new fluorescent probe for the study of micelles. J. Phys. Chem. A 107 (2003) 8784-8790.

49. D. L. Sackett and J. Wolff. Nile Red as polarity-sensitive fluorescent probe of hydrophobic protein surfaces. Analytical Biochemistry 167 (1987) 228-234.

50. P. Greenspan and S. D. Fowler. Spectrofluorometic studies of the lipid probe, Nile Red. Journal of Lipid Research 26 (1985) 781-789.

51. A. B. Dahnikula, R. Panchagnula. Localized Paclitaxel delivery. International Journal of Pharmaceutics 183 (1999) 85-100.

52. A. K. Singla, A. Garg, D. Aggarwal. Paclitaxel and its formulations. International Journal of Pharmaceutics 235 (2002) 179-192.

53. M. S. Tartis, J. McCallan, A. F. H. Lum, R. LaBell, S. M. Stieger, T. O. Matsunaga, K.W. Ferrara. Therapeutic effects of Paclitaxel-containing ultrasound contrast agents. Ultrasound in Med. & Biol. 32 (2006) 1771-1780.

54. L. Mu and S. S. Feng. A novel controlled release formulation for the anticancer drug Paclitaxel (Taxel®): PLGA nanoparticles containing vitamin E TPGS. Journal of Controlled Release 86 (2003) 33-48.

55. L. Mu, P. H. Seow. Application of TPGS in polymeric nanoparticulate drug delivery system. Colloids and Surfaces B: Biointerfaces 47 (2006) 90-97.

56. John Eisenbrey. Ultrasound Sensitive Polymeric Drug Carriers for Treatment of Solid Tumors. PhD Thesis, Drexel University Department of Biomedical Engineering, Science & Health Systems; Philadelphia 2010.

57. C. Fonseca, S. Simoes, and R. Gaspar. Paclitaxel-loaded PLGA nanoparticles: preparation, physicochemical characterization and in vitro anti-tumoral activity. Journal of Controlled Release 83 (2002) 273-286.

58. F. Danhier, N. Lecouturier, B. Vroman, C. Jérôme, J. Marchand-Brynaert, O. Feron, and V. Préat. Paclitaxel-loaded PEGylated PLGA-based nanoparticles: In vitro and in vivo evaluation. Journal of Controlled Release 133 (2009) 11-17.

59. S. C. Kim, J. Yu, J. W. Lee, E. Park, and S. Chi. Sensitive HPLC method for quantitation of paclitaxel (Genexol®) in biological samples with application to preclinical pharmacokinetics and biodistribution. Journal of Pharmaceutical and Biomedical Analysis 39 (2005) 170-176.

60. C. M. Sehgal, T. W. Cary, P. H. Arger, and A. K. W. Wood. Delta-projection imaging on contrast-enhanced ultrasound to quantify tumor microvasculature and perfusion. Acad Radiol 16 (2009) 71–78

61. J. M. Thijssen and C. L. Korte. Modeling Ultrasound Contrast Measurement of Blood Flow and Perfusion in Biological Tissue. Ultrasound in Med. & Biol., 31 (2005) 279-285.

62. T. T. Rissanen, P. Korpisalo, H. Karvinen, T. Liimatainen, S. Laidinen, O. H. Grohn, S. Yla-Herttuala. High-Resolution Ultrasound Perfusion Imaging of Therapeutic Angiogennesis. JACC: Cardiovascular Imaging, 1 (2008) 83-91.

63. W. Wang, C. C. Moser and M. W. Wheatley. Langmuir Trough Study of Surfactant Mixtures Used in the Production of a New Ultrasound Contrast Agent Consisting of Stabilized Microbubbles. J. Phys. Chem. 100 (1996) 13815-13821.

64. L. Mu, T. A. Elbayoumi, and V. P. Torchilin. Mix micelle made of poly(ethylene glycol)-phosphatidylethanolamine conjugate and D-α-tocopheryl polyethylene glycol 1000 succinate as pharmaceutical nanocarriers for camptothecin. International Journal of Pharmaceutics 306 (2005) 142-149.

65. M. Sheu, S. Chen, L. Chen, and H. Ho. Influence of micelle solubilization by tocopheryl polyethylene glycol 1000 succinate (TPGS) on solubility enhancement and percutaneous pepetration of estradiol. Journal of Control Release 88 (2003) 355-368.

66. W. Ke, S. Lin, H. Ho, and M. Sheu. Physical characterizations of microemulsion system using tocopheryl polyethylene glycol 1000 succinate (TPGS) as a surfactant for the oral delivery of protein drug. Journal of Control Release 102 (2005) 489-507.

67. A. Brotcchie, F. Grieser, and M. Ashokkumar. Effect of power and frequency on bubble-size distribution in Acoustic Cavitation. Physical Review Letters 102 (2009) 084302(4).

68. Shweta Naidu Chitoor. Studies on a new ultrasound contrast agent: Strategies for increasing the population of nano bubbles and for encapsulation of Paclitaxel. Master Thesis, Drexel University Department of Biomedical Engineering, Science & Health Systems; Philadelphia 2011.

69. J. E. Liebmann, J. A. Cook, C. Lipschultz, D. Teague, J. Fisher, and J.B. Mitchell. Cytotoxic studies of Paclitaxel (Taxol ®) in human cell lines. Br. J. Cancer 68 (1993) 1104-1109.

70. S. Feng, L. Zhao, Z. Zhang, G. Bhakta, K. Y. Win, Y. Dong, and S. Chien. Chemotherapeutic engineering: Vitamin E TPGS-emulsified nanoparticles of biodegradable polymers realized sustainable Paclitaxel chemotherapy for 168h *in vivo*. Chemical Engineering Science 62 (2007) 6641 – 6648.

Appendix A: Standard Operating Procedures

A.1 Procedure for Fabrication of ST68 Contrast Agent

The standard procedure in this study is modified from previous standard procedure with no grinding step before autoclave.

1. 1.5g of sodium chloride, 1.48 g of Span 60, and 1ml of Tween 80 are added to 50mL of PBS, with a stirrer bar.
2. The beaker is covered with foil to which is attached a piece of autoclave tape and then stir.
3. The mixture is slowly heated with continuous stirring to bring to a boiling, and dissolve the solid Span.
4. The mixture is autoclaved with the stir bar in place for 35 min.
5. The mixture is allowed to cool to room temperature while rapidly stirring so that the Span comes out of solution as fine particles.
6. After the mixture has cooled to room temperature, it is prepared for sonication. (MAKE SURE TO REMOVE MAGNETIC STIRRER BAR)
7. The beaker is placed in an ice bath.
8. It is purged with sterile filtered (pore size 0.2 □m) gas of choice (usually PFC or SF_6) gas until bubbles cover the solution before sonication.
9. After it has been purged, the mixture is sonicated at between 110W for 3 minutes (Misonix Inc. CL4 tapped horn probe with 0.5” tip, Farmingdale, NY) with constant purging using a steady stream of gas of choice.

NOTE:

1. When *purging* with gas, the tip that supplies the gas WILL be in the solution. When *sonicating*, the tip supplying the gas will NOT be in the solution, only the sonication probe will be submerged.
2. During the sonication, the top of the beaker is covered with foil to trap the gas.

10. One sterile separation funnels are set up in that cold room to cool to 4^{o}C.
11. The contents of the beaker are poured into the separation funnels.
12. Wash three times with 50 ml PBS allowing 35 min of separation and discard the bottom layer.
13. At the end of the third wash, a middle layer (microbubbles) is collected.
14. The bubbles are either taken up into vacutainer tubes which are completely filled, or placed in glass vials, which are tightly capped only after the head space has been purged with the filling gas (usually PFC or SF_6). These vials are stored at 4^{o}C, characterized and used in 24 hr.

A.2 Procedure for Fabrication of SE61 Contrast Agent

The standard procedure for standard SE61 is slightly different form ST68.

1. 1.5g of sodium chloride, 1.464 g of Span 60, and 1.288 g of TPGS are added to 50mL of PBS, with a stirrer bar.
2. The beaker is covered with foil to which is attached a piece of autoclave tape and then stir.
3. After TPGS all dissolve, the mixture is slowly heated with continuous stirring to bring to a boiling, and dissolve the solid Span.

4. The mixture is autoclaved with the stir bar in place for 35 min.
5. The mixture is allowed to cool to room temperature while rapidly stirring so that the Span comes out of solution as fine particles.
6. After the mixture has cooled to room temperature, it is prepared for sonication.
7. The beaker is placed in an ice bath.
8. It is purged with sterile filtered (pore size 0.2 □m) gas of choice (usually PFC or SF_6) gas until bubbles cover the solution before sonication.
9. After it has been purged, the mixture is sonicated at between 110W for 3 minutes with constant purging using a steady stream of gas of choice.

For separate micron-sized and nano-sized SE61

10. Two sterile separation funnels are set up in that cold room to cool to 4^{o}C. (Using a 125 ml separation funnel yields good results)
11. The contents of the beaker are poured into one of the separation funnels (A), assisted by 50 ml cold PBS and the separation funnel is place in the fridge for one hour to allow for separation of the bubbles.
11. After one hour the lower 25 ml of solution is discarded and the next 50-75 ml of the solution is transfer to the second cold separation funnel (B).

    At this stage separation funnel A contains the majority of micron sized bubbles and funnel B contains the majority of nano sized bubbles.

Funnel A.

1) Wash twice with 50 ml PBS allowing one hour of separation and discard the bottom layer. At last wash, the middle layer containing predominantly micron sized bubbles is collected, and the lower portion is discarded.

Funnel B

1) Wash twice with 50 ml PBS allowing one hour of separation. Since there is no distinct layer for nanobubbles after the end of waiting period, 25ml of solution is discarded from the bottom of the separating funnel. The 10ml of nanobubbles is collected after the last discard.

For mixed micron-sized and nano-sized SE61

10. One sterile separation funnels are set up in that cold room to cool to 4^{o}C.
11. The contents of the beaker are poured into the separation funnels.
12. Wash three times with 50 ml PBS allowing one hour of separation. For the first and second washed, 50-75 ml of solution is discarded from the bottom of the separating funnel if no distinct layer is seen. For the third washed, 75 ml of solution is discarded.
15. A bottom layer (nanobubbles) and a middle layer (microbubbles) are collected all together.

The bubbles are either taken up into vacutainer tubes which are completely filled, or placed in glass vials, which are tightly capped only after the head space has been purged with the filling gas (usually PFC or SF_6). These vials are stored at 4^{o}C, characterized and used in 24 hr.

A.3 Procedures for *in vitro* Acoustic Characterization

The amount of 0.2 ml of the bubble is diluted to 10 ml in volume metric flask that made up the volume with cold (4^{o}C) of PBS. The following is the procedures for enhancement curve.

1. Add 50 ml of 37^{o}C membrane filtered 1X PBS (pH7.4) to the custom vessel with a stirrer bar.
2. This vessel is placed into another cubical tank with 20 gallons of 37^{o}C distilled water.
3. The stirrer is adjusted to level 3 and continue to stir throughout the measurement.
4. Create a new folder and subfolders for saving the results in the data folder
5. Lab VIEW 7.1 (National Instruments) software is used for acoustic testing
6. Click on the run button and choose a directory path, which was created in the step 4 to save the acquired data.
7. First running baseline, in the sample name folder write Baseline and click on Make baseline for the acquisition, then click acquire.
8. In the sample name type the dose of the bubble being injected.
9. Add the required dose of the diluted bubble to the custom vessel then click acquire.

10. Each dose after the previous acquisition, clean and replace the 37^{o}C PBS in the custom vessel.

11. Repeat with increasing doses until shadowing effect is seen. begins to affect enhancement

12. Export the data to the created folder and save them.

13. All doses are calculate back to the original concentration and reported as μl/L

The following is the procedures for stability curve.

1. Set number of time points to acquire 15 min of stability testing.

2. Click on the run button and choose a directory path, which was created to save the acquired data.

3. Click on capture waveform on set time interval.

4. Chose dose on the rise of enhancement curve and added this dose to the custom vessel filled 37^{o}C PBS.

5. Click acquire and export the data to the folder after 15 min.

A.4 Procedure for Size Distribution Measurement

1. Crate data file and open it.
2. Select measurement SOP by selecting Measure --> SOPs --> Size --> STXX then named the sample.
3. Add 1ml of diluted bubble from acoustic testing into a low volume disposable sizing tapered cuvette, and then place the cuvette in the slot of the instrument.
4. Click “Start” in protocol window.
5. The measurement is taken three times with 15 second between each reading. The sample is gentle turn upside down and back again for 5 times between reading to ensure that the bubbles are not floating and accumulate at the top of the solution.

A.5 Procedure for Concentration Measurement by HPLC

Method Setup

The conditions for running HPLC will be setup and save for future use. The previous method that already created also can be modified. The instruments no need to turn on for the setup.

1. Open Breeze Software, the click “View Method”, a top one on a left panel, and then choose LC for HPLC.

2. For Pump Setting, set flow rate for pump A and B in Flow tab, indicate mobile phases used in Solvents tab, and temperature in Temperature Control tab (This temperature should be the same as column temperature. If the condition running at room temperature, 30^{o}C is recommended to avoid the fluctuation of room temperature)

3. Set wavelength for UV detector. There are possible using two wavelengths simultaneously by checking Dual in Wavelength Mode. Then set wavelength in Channel 1 and 2 tab.

4. Click File, Save as and name a new method.

Equilibrate the system

1. Turn on Pump, Column heater, Injector, UV detector (it takes around 5 minutes for UV detector self calibration), and RI detector.

2. Open Breeze Software, then click "Manage Breeze", the bottom one on a left panel, then click System to see the software shows all instruments connected, if not, restart the software.

3. Purge the system; Pump, Injector and Detector, by click the middle icon on the left hand side of Flow indicator, then follow the screen.

3.1 The screen will first ask to prime the pumps with the mobile solution. To prime the pump, just draw 2-3ml for each pump. Open a reference valve locates above "Pump A" maker. Set flow rate and click next. After purging the pump, close the reference valve then click next for injector purging.

3.2 Set flow rate for injector purging. Attached the column at when the flow rate reaching the setting rate. (Attached the column at the bottom first to reduce the chance that air will go inside the column and damage the packing.) Also place the small amount of mobile phase for injector cleaning.

3.3 Purge the detectors.

Note: All flow rate setting should be 80-100% of actual flow rate in the Method, except for detectors purging, which 1ml/min is the maximum.

4. After purging the system, click Equilibrate System icon, a bottom left icon, then choose the method from the saved list and run until get a stable base line (between 2-6 hours depends on the conditions of the Method).

Note: It is important the mobile phase is HPLC grade and pass the 0.2□m filter in case of DI water and other solution. This is to avoid the system and column getting clot.

Analyze the sample

1. Place all 0.2□m filtered samples in the sample holder tray but placing one blank sample for the first sample to be analyzed. For some reason, our machine sometimes doesn't read the first sample correctly. **This is important!!!**

2. Set up a Sample Queue. For the first row, choose "Equilibrate" for function, choose the method and set 10 minutes for Run Time.

3. For the second row, choose "Inject Samples", choose the method, name blank for the first sample, then set Runtime and Injection Volume.

4. Then add all of samples into the sample queue. Make sure each sample is in the same vial number with the sample queue.

5. Click Run Sample icon, the second icon on the left, then name a sample set for your own reference.

Turn off the system

1. Set the flow rate to 0.1ml run the pump if pump already stopped.

2. Detach the column but detach the top of the column first then the bottom. Again this will reduce the chance that air will go into the column. Then stop the pump.

3. Turn off everything.

Analyze the data

1. Click “Find Data” on the left panel.
2. Choose Sample Set, Sample in Injection Tab, then choose the channel
3. Click Integrate icon to get Area Under Curve, Peak Height and Retention time for each peak. (Sometime this doesn’t work due to the peak is to low but a line can be drawn at the base of the peak to get all of these data.)

Appendix B: Tumor Perfusion Calculation by Gamma-Vatiate Function

For *in vivo* tumor perfusion, a first-pass kinetics gamma-variate function was used. Rissanen et al. [62] showed they can becalculated perfusion by: [Figure B.1]

$$Perfusion = \frac{\text{Blood flow}}{\text{tissue volume}} \qquad \text{Eq B.1}$$

and

$$Blood\ flow = \frac{Blood\ volume}{Mean\ transit\ time} \qquad \text{Eq B.2}$$

Because we want to compare perfusion of two agent for the same tumor, so that the tissue volume is constant that give us:

$$Perfusion \sim Blood\ flow = \frac{Blood\ volume}{Mean\ transit\ time} \qquad \text{Eq B.3}$$

which mean we can compare perfusion as a function of blood volume and mean transit time.

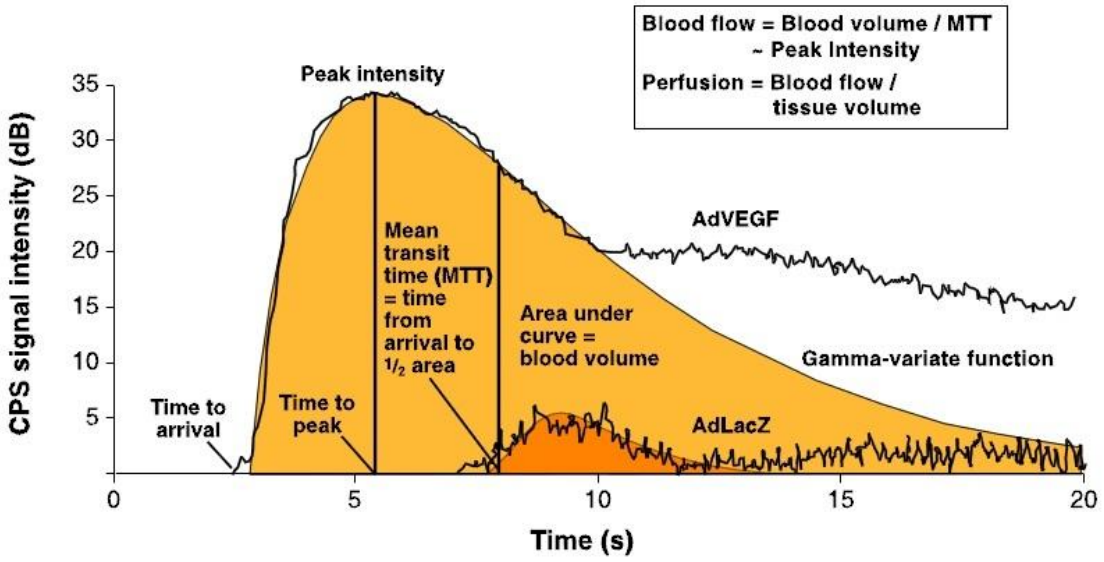

Figure B.1 First-pass kinetics gamma-variate function and intensity-time curve [62]

We can calculate blood volume and mean transit time by gamma-variate function. [61] In short, for first-pass kinetics gamma-variate function, we can plot the intensity of a signal by:

$$f(t) = P_{max}\left[\frac{e\alpha(t-t_1}{\beta-1}\right]^{\beta-1} exp[-\alpha(t-t_1)] \qquad \text{Eq B.4}$$

where $$t_1 = t_{max} - \frac{\beta-1}{\alpha} \qquad \text{Eq B.5}$$

$$\alpha = \frac{\beta}{t_{mtt}} \qquad \text{Eq B.6}$$

and $$t_{mtt} = t_{max}\frac{\beta}{\beta-1} \qquad \text{Eq B.7}$$

As you can see from equation B.4 to B.7, every parameters can be calculated by guessing only one parameter β, except P_{max} and t_{max} are the maximum signal and time at maximum signal, respectively. Both values are the values from the experiment. With f(t) best fit by guessing β, mean transit time (t_{mtt}) can be calculate from equation B.7 and blood volume is the area under curve of gamma-variate function, then the bloof flow can be calculate.

Vita

Boriphat Methachan was born in Lampang, Thailand, on August 20, 1974. He received his Bachelor of Engineering in Chemical Engineering from Mahidol University, Thailand in 1998. His senior project title was Improvement of Distillation Column and Temperature Control by DCS.

After he received his bachelor degree, he immediately pursued his first graduate degree with a scholarship from the Petroleum and Petrochemical College, Chulalongkorn University, Bangkok, Thailand. He worked under the supervision of Dr. Nantaya Yanumet in corroboration with Dr. Edgar A. O'Rear, III from the University of Oklahoma. His research was focused on applications for surfactants as in his work titled Formation of Hydrophobic Cotton Fabric by Admicellar Polymerization. He received his Master of Science in Petrochemical Technology in 2000.

During the end of his first mater degree, he received the prestigious Royal Thai Government Scholarship to continue his graduate study in Biomedical Engineering. In 2001, he was admitted into the Graduate School at Drexel University and received his degree of Master of Science in Biomedical Engineering in 2004. Immediately, he started his research under the guidance of Dr. Margaret Wheatley focused on surfactant-based ultrasound contrast agents.

After graduation from Drexel University, he will go back to Thailand and join a biomedical research group in the National Metal and Materials Technology Center (MTEC), Thailand.